Analysis of bulk behaviour of particles

based on their individual properties

by

Mozhdeh Mehrabi

Submitted in accordance with the requirements for the degree of

Doctor of Philosophy

The University of Leeds

School of Chemical and Process Engineering

May 2021

The candidate confirms that the work submitted is her own, except where work which has formed part of jointly authored publications has been included. The contribution of the candidate and the other authors to this work has been explicitly indicated below.

The candidate confirms that appropriate credit has been given within the thesis where reference has been made to the work of others. The work in Chapters 3 and 5 of the thesis has appeared in publication as follows:

Mehrabi, M., Hassanpour, A. and Bayly, A., 2021. An X-ray microtomography study of particle morphology and the packing behaviour of metal powders during filling, compaction and ball indentation processes. *Powder Technology*, *385*, pp.250-263.

I was responsible for collecting and analysing data and writing the paper. The contribution of the other authors was to the design and implementation of the research and supervising the project.

Acknowledgement

Throughout my incredible journey on this research, I received a lot of support and guidance from many people. First, I would like to express my sincerest appreciation to my main supervisor, Dr. Ali Hassanpour, who always kindly gave me direction and invaluable guidance throughout my project. I would also like to thank my co-supervisor Professor Andrew Bayly for his consultation.

My deepest appreciation is for my family for their continuous support, love, and motivation. So, thank you so much, Mitra, Marjan and, Amirali, thank you for your unconditional love. I also express profound gratitude from my deep heart to my favourite grandmother, love u Mamani. I am especially grateful and dedicate this thesis to my lovely mother Maryam Bokharaei who always shown me how to be strong woman and follow my dreams and my beloved father Mohsen Mehrabi who passed

away many years ago, but I am still attempting to follow his path and become like him.

You know how much I love both of you.

To My Dear Parents

Abstract

An in-depth understanding of bulk behaviour of particles based on their individual properties is a vital step for the powder handling industries, a good example is the selection of appropriate powder material and their flow consistency in additive manufacturing process which would have significant effects on the quality of the final products. Identification of the most reliable method to characterise powder flow behaviour in correlation to the conditions of powder spreading is still challenging. For instance, the low consolidation state of the powders within the process requires a characterisation technique which is capable of measurement for such conditions.

The aim of present study is to experimentally characterise powder properties and more importantly to determine the appropriate test method which could predict the powder spreading behaviour relevant to the additive manufacturing process.

In this research a variety of techniques are used to assess the powder flow behaviour of two different types of Ti6Al4V powders used in additive manufacturing, namely the spherical gas atomized (GA) and irregular hydride-dehydride (HDH) particles. The static and dynamic angle of repose, Hausner ratio and Carr Index, flowmeter, low stress and standard Schulze shear cells techniques have all indicated that the two powders behave under the free to easy flowing categories. However, GA powder (spherical) has slightly better flowability compare to HDH powder (irregular), presumably due to the difference in morphology of the particles.

The ball indentation method allows measurement at low stress level and it has been used in this study is to measure powder bed hardness at low consolidation stresses

(<0.5 kPa). The powder bed unconfined yield stress is then obtained by the low stress shear cell. The unconfined yield strength results from the ball indentation technique show a notable decrease of flowability for both powders at low stresses (less than 0.5 kPa), categorising them under the cohesive regime, in contrast to other techniques mentioned above.

Furthermore, the powder spreading experiments have been carried using an in-house spreader device and the results shows that under similar test conditions (gap size and spreading speed) the spread GA powder has a higher packing density compare to HDH powders. The irregular shape of powder HDH can lead to a looser rearrangement of particles and lessening the packing density.

Finally, the X-ray microtomography has been used to study the packing behaviour of powders during the process of filling, consolidation and ball indentation. The results reveal that the packing fraction for both GA and HDD powders increases from central zone towards the wall due to the lower coefficient of friction for particle-wall than that of particle-particle. Furthermore, it is found that the packing fraction slightly reduces under the indenter for the GA powder due to the dilation, while it does not change for HDH powder, suggesting it could be under a critically packed state. The study in this research has led to a better understanding of powder flow characteristics and its relevance to the spreading behaviour for the additive manufacturing.

Table of Content

List of Figures

List of Tables

Nomenclature

H	Hardness of material
Y	Yield stress
C	Constraint factor
ff_c	Flow function
σ_1	Consolidation stress
σ_c	Unconfined yield stress
F_{max}	Maximum indentation load
A	Projected area of the impression of the indenter
d_b	Ball diameter
h_c	Intercept of the tangent to the unloading curve
R	Particle radius
Ψ	Sphericity
AR	Aspect ratio
D_v	Volume equivalent sphere diameter
D_a	Area equivalent sphere diameter
V_p	Volume of particle
A_p	Surface area of particle
d_{min}	Smallest ferret dimension of particle
d_{max}	Largest ferret dimension of particle
L	Length of particle
W	Width of particle
T	Thickness of particle
ρ_B	Bulk density
ρ_T	Tapped density
HR	Hausner ratio
CI	Compressibility index
φ_e	Angle of internal friction
φ_x	Angle of wall friction
θ_p	Hopper angle

ff	Flow factor
$\sigma_{critical}$	Critical applied stress
D_{min}	Minimum orifice diameter
g	Gravitational acceleration
H_{min}	Minimum height of powder inside hopper
L_b	Length of powder bed
W_b	Width of powder bed
ρ_b	Packing bed density
$m_{powder\ bed}$	Mass of spread layer on the powder bed
$V_{Powder\ bed}$	Volume of spread layer on the powder bed
$PF_{density}$	Packing density fraction
CoF	Coefficient of sliding friction
α	Sliding angle
H_S	Height of tilted surface
L_S	Length of tilted surface

Chapter 1 Introduction

1.1. Introduction

In this chapter, the terms of additive manufacturing and powder flowability with the brief background of both terms have been highlighted. The aims of the project are described along with the structure of the thesis and project plans.

1.2. Additive manufacturing and powder flow

The classic Manufacturing process can be classified into five stages 1) Forming, 2) Moulding, 3) Machining, 4) Assembly, and 5) Finishing process (1). These processes are basically complex activities which require expensive equipments, economically inefficient for using the raw material and are very time consuming. Also, the capability of these methods to produce the complex component are very limited (2).

Additive manufacturing (AM) is a relatively new industrial production route to create 3D objects with precise shape by depositing material layer by layer and controlled by computer process. This technique is famous for reduced usage of materials compared to traditional manufacturing which often requires the removal of excessive material. Therefore, AM has become an alternative option to produce complex shape parts with great accuracy in geometry by using less raw material and produce minimal waste. The AM process to create a component is a layer basis approach that bonds layers of materials by using a heat source or chemical binder according to slides of its CAD file (3). This technique is recently expanded in a wide range of industries such as aerospace, medicine, and automotive (4). The ability of this method to create a complex shape with high accuracy is based on that a complex part can be made in one single process. In contrast, in the traditional manufacturing process which has

the limitation of the design of the products, complex shapes were produced separately, then assembled. Therefore, AM process optimised the production route and reducing the amount of energy, time, and labour work. Although to fully adopt this technique, characterisation of material is fully required for assurance of repeatability and consistency of the process. Since the performance and mechanical properties of built component influenced by material characteristics. The materials used for AM process can be categorised to sheets, wire, and powder. Recently the powder-based process in AM has grown significantly in industry and therefore, the single (size, shape, surface properties, etc.) and bulk (flow behaviour, packing fraction, etc.) behaviour of powders have become of great interest.

The term powder flowability requires further explanation. A simple definition of powder flowability is the ability of the powder or bulk solids to flow. Powder flowability is not a one-dimensional factor and cannot be expressed as a single value (5). It depends on the combination of physical (size, shape, and surface properties), chemical (density and composition), mechanical properties of the material (internal and wall friction), and properties of specific equipment used for processing the material (5). It is also affected by environmental conditions such as moisture, humidity, temperature, and time of storage (6). Consequently, powder flowability can be expressed as the ability of a specific powder to flow in a specific device in a controlled environment. However, the flowability of powder could be a prominent issue while dealing with fine powder (5).

In additive manufacturing, the term flowability which could be related to spreading is an important key factor since it can affect the final product quality or product development rate. However, there is still insufficient understanding of the powder spreading within the AM process which has a major impact on the quality of final products (7). The smoothness and uniform packing fraction of the bed have a significant influence on bonding between particles-

particles, layers, and mechanical properties of the final component (8). Therefore, the physical properties of the powder that can affect the flow, which could be associated with spreadability requires more attention and need full characterisation (such as its size and shape, surface texture and energy, size distribution, density, and compressibility, cohesive strength, and friction). These factors play an important role in providing quantitative knowledge of important properties on the behaviour of the bulk powder.

There are various well-known techniques available to evaluate powder flow behaviour such as angle of repose (9), tapped density (10), flowmeter (11), FT4 (12), and shear cell (13). However, there is no specific method established to simulate the motion of bulk powder during AM process (14, 3).

Another test method to characterise powder flowability was introduced by Hassanpour and Ghadiri (2007) to characterise the flow behaviour of powders, based on the indentation of powder bed under very low consolidation stresses (15). The indentation technique gives a measurement of resistance to plastic deformation under a specific force. They reported that the ball indentation results correlate very well with common flowability measurement technique by applying a "constraint factor" (C) which is the ratio of indentation hardness (H) to the yield stress (Y), (H/Y=C), which depends on single particle properties such as size, shape, roughness, and coefficient of friction (16). However, the hardness measurements could also be affected by the distribution of packing fraction of loose and consolidated powder bed at different compaction stresses, wall effects, and segregation of particles during filling and consolidation, which are yet to be studied in detail.

Ti6Al4V, also known as Ti64 is a titanium alloy with excellent properties such as high toughness, corrosion and creep resistance, high ratio of strength to weight, and biocompatibility which is the main reason to be used in the aerospace and biomedical

industry. It is the most popular titanium alloy in the international market (17). The TI6AL4V samples which were obtained by gas and hydrate-dehydrate processes with the 30-140 µm particle size range typically used in *the Electron Beam Melting* (*EBM*) process (which will describe in details in the next chapter) are characterised to discover the appropriate test method which could predict the flow behaviour in the additive manufacturing process the best and can be correlating with powder spreading, since there is no specific method established to simulate the motion of bulk power under spreading process (18).

1.3. Research aims and objectives and approaches

This work is motivated to reduce the material cost in additive manufacturing processes. Two samples of Ti6Al4V powders obtained by gas atomization (spherical) and hydrate-dehydrate processes (non- spherical) that consists of lower production costs were characterised for their single and bulk powder properties. Furthermore, Hydrate-dehydrate (HDH) powder is investigated in this work to understand the effects of using non-spherical powder in the EBM process.

Additionally, a range of powder flowability characterisation techniques such as density measurement, static and dynamic angle of repose, FT4 rheometer, ring shear cell, ball indentation, and flowmeter have been studied and compared. Then flow performance of both powders has been evaluated by using an in-house spreading rig to reveal any possible correlation between any specific flowability technique and the packing quality of the powder layer.

Therefore, the objectives of this research will be divided in three following sub section:

1.3.1. Physical particle properties

The objective of this phase is to determine the powder's physical properties of size and size distribution, particle shape, and density. Two samples of Ti6Al4V powders produced by different production routes with varying shapes and sizes are characterised using the X-ray microtomography technique.

1.3.2. Powder flowability characterisation

The objective of this phase is to determine and compare the flowability of both powders using different techniques such as measurement of the static and dynamic angle of repose, and measurement of powder compressibility using Hausner ratio and Carr index. To characterise flowability in the dynamic region; rotating drum, flowmeter, and FT4 rheometer have been studied. Also ring shear cell test was used to measure the shear strength of both powders to determine specific details of powder characteristics such as internal angle of friction, angle of wall friction, flow function, etc. which could be used in other methods like ball indention or flowmeter techniques to provide practical and effective reference values to optimise the design of the hopper in 3D printing. The ball indentation process also is used to determine the unconfined yield stress of both powders. In this phase, the effect of variation of particle properties and powder flow properties were correlated with results of bed packing fraction by using the in-house spreading rig.

1.3.3. X-ray microtomography study of ball indentation processes

A detailed study of the ball indentation technique is conducted using X-ray microtomography technique to visualize the ball indentation process for a better understanding of the packing behaviour of metal powders during filling, compaction, and ball indentation stages. To

develop better understanding of the effect of specific consolidation pressure and ball indentation on powder bed and to investigate how the packing density could change in different regions of the powder bed as a result of consolidation and indentation processes.

1.4. Thesis Structure

The dissertation is divided into six chapters. The description of each chapter is as follow:

Chapter one provides an overall *introduction* to the thesis and describes the importance of the work and objective of the dissertation.

Chapter two presents a *literature review* on additive manufacturing by explaining their different processes, materials, and pros and cons of this process. It also includes a general background of flowability and a wide range of techniques for powder flowability measurement regarding the AM process and the knowledge gap related to this research.

Chapter three gives detailed information about the *material and experimental methods* used throughout this thesis. It also includes the results on the shape analysis of test samples using X-ray microtomography.

Chapter four includes the *results* of the experiments that have been carried out as well as a discussion for powder flowability set of results and their correlation with powder spreading.

Chapter five includes the *results* of the detailed study of the ball indentation process by using x-ray microtomography.

Chapter six details the main *conclusions* of this work and outlines possible future work and studies for future research in this field.

Chapter 2   Literature Review

2.1. Introduction

The purpose of this chapter is to provide a comprehensive overview of the current scientific and technological state of the art of additive manufacturing. Also, in this Chapter, the term powder flowability have been highlighted along with various developed techniques for its evaluation.

2.2. General background of AM

AM is the process which was introduced in the 1980s and developed and expanded for direct production routes in many industries such as aerospace, medicine, and automotive (4). It is described by the American Society of Testing and Materials (ASTM) as "The process of joining materials to make objects from 3D model data, usually layer upon layer, as opposed to subtractive manufacturing methodologies"; (ASTM F2792-12a). There are several technologies where AM process can be classified and each technology has its own distinct process, which is described in the next section.

2.2.1. AM techniques

The current additive manufacturing process could be divided into three main categories as shown in Fig. 2.1 (19).

2.2.1.1. Laminated object manufacturing (LOM)

The simplest explanation in this process is that the adhesive-coated sheet material will be attached to each other. Sheets of material could be pre-coated by adhesive or immediately prior to the bonding process covered with adhesive, allowing them to attach to each other (19).
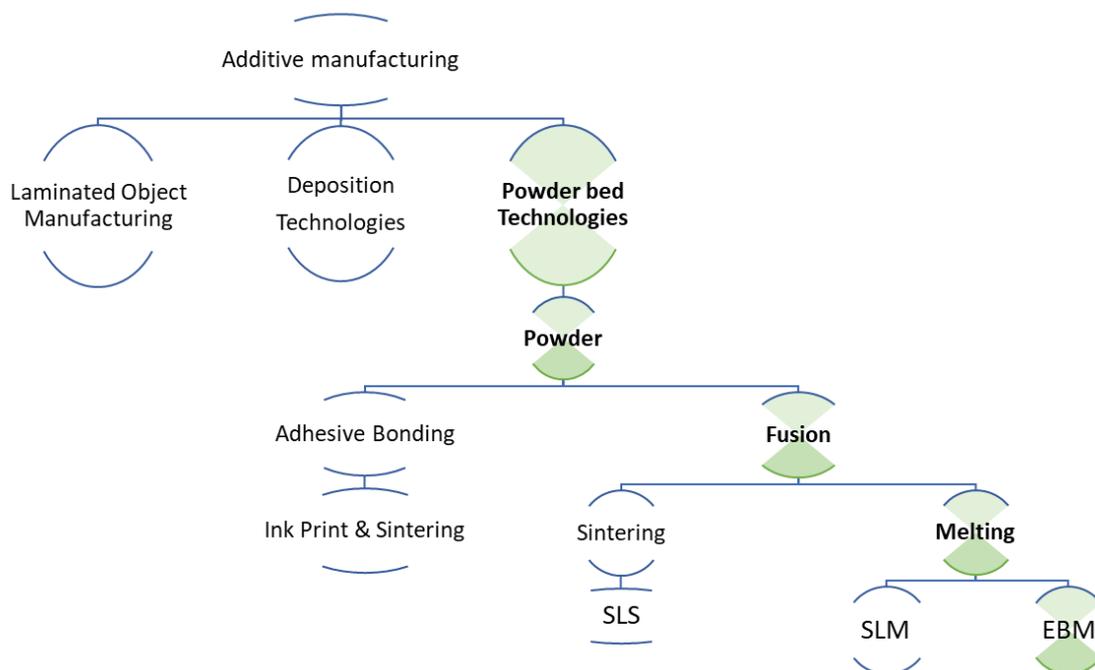
Figure 2. 1 Categorization of additive manufacturing technique

2.2.1.2. Directed energy deposition (DED):

Direct energy deposition is the process by which material (wire or powder form) is deposited through the moving arm nozzle around the fixed object and deposited layer by layer. Materials are bonded to each other through the precise temperature uses a focused energy

source acquired by laser or electron beam or use of chemical bonding agent upon deposition (Fig. 2.2) (20).

This method can be used with a wider variety of materials including polymers, ceramics, and metals.
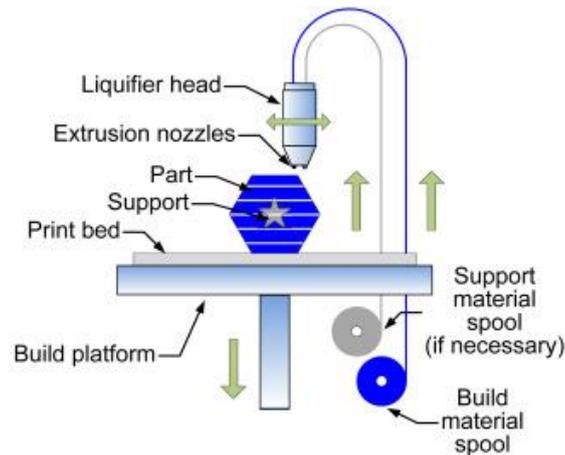
Figure 2. 2 Schematic diagram of Direct Energy Deposition (DED) (20)

2.2.1.3. Powder bed fusion (PBF)

Powder Bed Fusion (PBF) technology has two main classifications, i.e. powder bed-based and powder fed systems. Powder bed-based system (PBB) is also divided into selective laser sintering (SLS), selective laser melting (SLM), and electron beam melting (EBM) (21, 22). These systems use a powder spreader to form a fine layer of powder bed and a heat source such as laser or electron beam is used to melt or partially melt layers of material in a three-dimensional space. As the process completes, the excess powder is blasted away from the object.

Selective laser sintering (SLS)

The SLS process uses a high-power laser to fuse material and a specific method to control the heat source and process of adding a new layer over the previous one. It uses blade, roller or a combination of both (Fig. 2.3). First, the build platform which is the heat controller chamber is heated to just below the melting point of the material to minimize thermal distortion and to simplify the fusion process to the previous layer. Then each layer is built by a laser to sinter the material on the powder bed. This process benefits from requiring no additional support for the building structure as the sintered material forms the part and the remaining un-sintered powder remains in place to support the structure. The excessive powders can be cleaned away and recycled once the part of structure has been built. This method can be used for a wider variety of materials, including plastics, metals, the combination of metals, combination of metals and polymers, and combination of metals and ceramics (23).
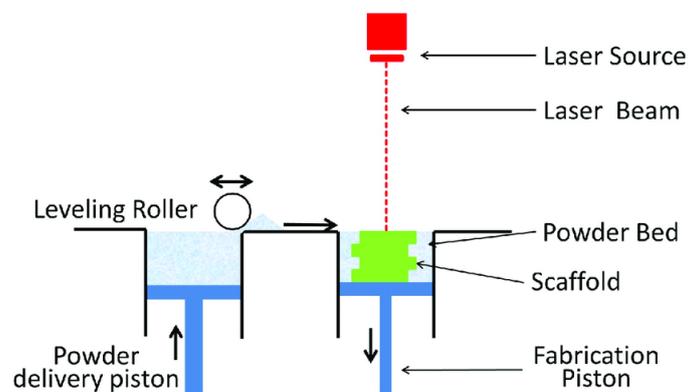
Figure 2. 3 Schematic diagram of SLS process (23)

Selective laser melting (SLM)

The SLM process is the same as SLS with the only difference being the use of focused laser beam to achieve the full melt on the molecular level to create a homogenous part. It ideally

works for pure material as there is only one melting point for each element. However, alloys also generate great results (24).

Electron beam melting (EBM)

The EBM process is quite similar to SLM process which is explained in the previous part. This technique consists of powder hoppers, blade, build stage, and heat source (Fig. 2.4). First, the powders spread by blade or rake and a thin layer of powder (usually around 50-200 μ) depending on process condition, then an energy source (beam) scan and melt area selectively layer by layer according to the 3D CAD file of component, to reach to 100% material density (26, 27, 28).

 In this process, an electron beam is used to melt the powders as a heat source with a high voltage between 30 to 60 kV (19). This process is operated in a high vacuum chamber, as opposed to SLM and SLS, to minimize or eliminate environmental interaction such as oxidation for reactive material such as Ti6Al4V which have a high attraction to oxygen and nitrogen. The EBM technology has lately been considered to be the right option for the production route of metallic materials to be processed for fully dense components with improvements to their performance such as structural complexity, thermal behaviour, and required mechanical properties. It also has the ability to process a wide variety of alloyed metal powders. Additionally, due to high energy input (electron beam) and fast scan speed this method generates a faster build rate compared to other methods (25).
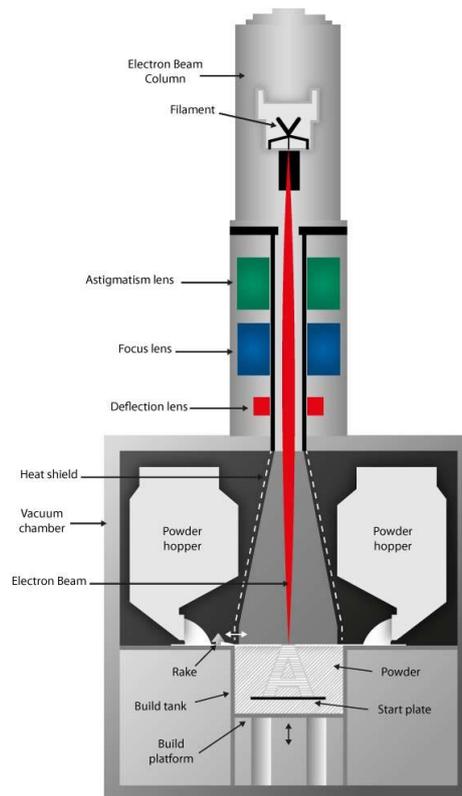
Figure 2. 4 Electron Beam Melting (EBM) mechanism (image credit: arcam.com)

Spreading the powder during AM process by using a certain device, plays an important role in the generation of good quality powder beds. The spreading procedure has a significant impact on the quality of the final products. It is highly critical that each powder layer has uniform thickness and density as a high porosity or non-uniform layers could lead to weaker bonds between layers and poor mechanical properties of final products. Also, the properties of these powder layers will be different from bulk powder as a result of a process condition, wall effect, etc.

So far, most AM process used one of the following spreaders to achieve a desire layer thickness (Figs. 2.5 and 2.6):

A blade is moving across the powder surface to spread the powder. Usually, the length of the blade is as long as the powder bed.

A roller is rotated on the powder bed surface and pick up the powders and redistribute them. Compare to the blade, the roller gives the gentler compaction of the powder (3).
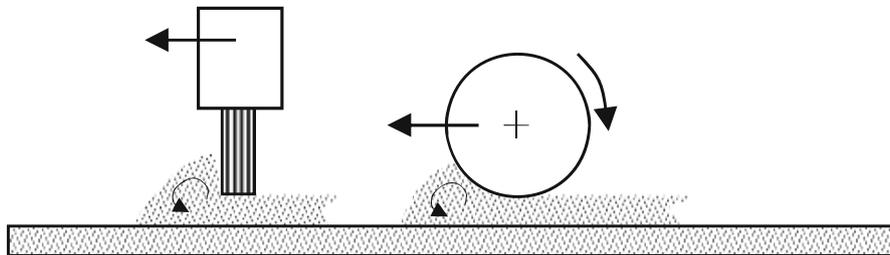
Figure 2. 5 Spreading systems; Roller and Blade (3)

However, (Roy et al., 2014) introduced the combination of both blade and roller to get the better dispersion of powder. So, first a thin layer of powder is spread by blade then a counter rotating and vibrating roller passes through the surface. Vibration of the roller breaks the agglomerates and increases the packing of powders which makes a thin uniform layer of powder (29).
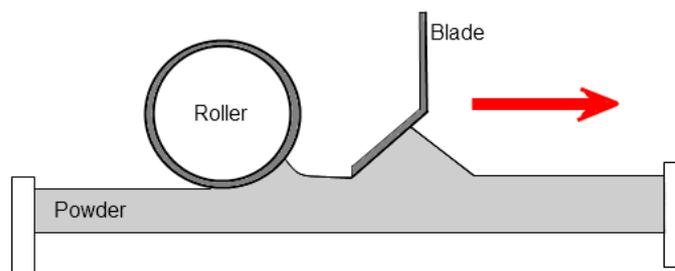
Figure 2. 6 Using the blade and rotating and vibrating roller (29)

The effect of surface compactness and layer smoothness of different poly-Ether Ether Ketone (PEEK) in different spreading process was validated by Berretta et al. (2014) (30). Also, Ziegelmeier et al. (2015) also demonstrated that the final part surface quality is depended to

the roughness of powder bed and there has been a strong connection between powder volume fraction and the porosity of powder bed (31).

Recently, Shaheen et al. (2019) presented in their research by using the discrete particle method (DPM) that counter-clockwise rotating roller as a spreading tool improves the powder layer quality compared to spreading with a blade (32).

2.2.2. Additive manufacturing materials

It is possible to use any material to create an object by using layer by layer method. Although, the final quality of the components is largely depended on the materials. The most used materials in AM are polymers, ceramics, and metals. These materials are often produced and used in form of powder or wire. However, there is other material used in AM such as food items and glass where their usages are not widespread.

2.2.2.1. Thermoplastics

Thermoplastic polymers are the most popular and cheapest class of additive manufacturing materials. Acrylonitrile butadiene styrene (ABS), polylactic acid (PLA), Polyamide (Nylon) and polycarbonate (PC) each offer distinct advantages in different applications. Water-soluble polyvinyl alcohol (PVA) is also typically used to create temporary support structures, which are later dissolved away (33). They are mainly efficient for low-volume manufacturing and minimise waste.

2.2.2.2. Ceramics

A variety of ceramics have also been used on powder bed selective laser processing (SLS, SLM), including zirconia, alumina and tricalcium phosphate. Also, glass products can be made

by using an alternate layer of powdered glass and adhesive then baked together before use (34).

2.2.2.3. Metal

A range of metals and metal alloys are used in additive manufacturing, from precious metals like gold and silver to strategic metals like stainless steel and titanium. One of the most popular metal alloys in the world is "Ti6Al4V". It contains 90% titanium, 6% aluminium, and 4%vanadium which apparent in the name, although the material can contain small amounts of other components, such as of oxygen, hydrogen and nitrogen (17).

Titanium alloy (Ti6Al4V)

There are mainly two methods for titanium production. Traditionally Kroll process® is producing titanium sponge by chlorination of TiO_2 ore at high temperatures in the presence of carbon and then reacting the resulting $TiCl_4$ with magnesium. Another method to produce pure titanium is Armstrong process® where $TiCl_4$ is injected to liquid sodium, producing NaCl and Ti powders. Post processing actions such as ball drying and ball milling following to provide particle size distribution for powder metallurgy process (36).

The Ti-6Al-4V alloy is widely used in AM process in order to fabricate the component in biomedical, aerospace and automotive for its excellent properties: 1) high toughness; 2) corrosion and creep resistance; 4) relative low elastic constant (roughly around 110MPa compare to Stainless steel with young's Modulus of 200 MPa) (37); 5) high ratio of strength to weight which is the main reason to be used in aerospace and biomedical industry, where high strength and low weight is always vital (3).

There are various approaches to produce Ti6Al4V such as gas atomisation (GA), hydration-dehydration process (HDH), plasma rotating electrode process (PREP) and plasma atomisation (PA) (38, 39).

- The Gas Atomisation (GA) process; where pure or pre-alloyed titanium molten in vacuum, the melt is poured into the nozzle and atomised by stream of high-pressure inert argon gas (which preferable over helium due to economic purpose) (Fig. 2.7)(40).
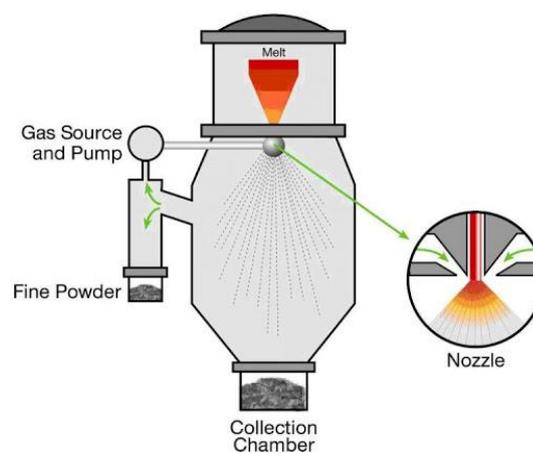
Figure 2. 7 Schematic diagram of Gas Atomisation (image credit: maschinetech.com)

- The Hydride- De-Hydride (HDH) process; which is mostly chemical method where raw material in the form of solid scrap, billet or machined turnings are cleaned from impurities then hydrogenated in atmospheric hydrogen pressure and the temperature of 400°C to produce brittle material. That brittleness helps the process to not require a high energy for milling. Then, milled hydride titanium is dihydride by increasing the temperature to 700°C in vacuumed chamber (Fig. 2.8) (19, 41, 42).

Hydride

Hydrogen atmosphere at ~650°C

Brittle hydride ⇨Crush Mill

Produce fine hydride powder

De-hydride

- High vacuum heating
- ~ 350°C

Final powder

- Low level of metallic impurities
- Required size distribution
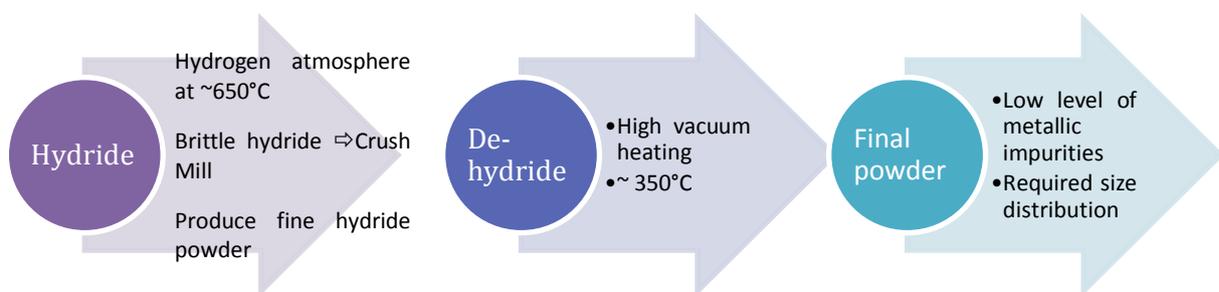
Figure 2. 8 Schematic diagram of HDH process (41)

- The Plasma Electrode Process (PREP); is a centrifugal atomisation method where the titanium metal made into electrode rod as a feedstock and melted by plasma torch. Then the liquid melt is spun off from the high-speed electrode surface to form the droplets because of centrifugal force and then solidified to powders (40).

- The Plasma Atomisation (PA) process where pre-alloy titanium in the form of a wire is fed into a hot zone (around 10,000 K) heated by plasma torches. The wire is melted and broken into droplets that would cool rapidly and collected. A typical cooling rate is in the range of 10–1000C/s (Fig. 2.9) (40).

18
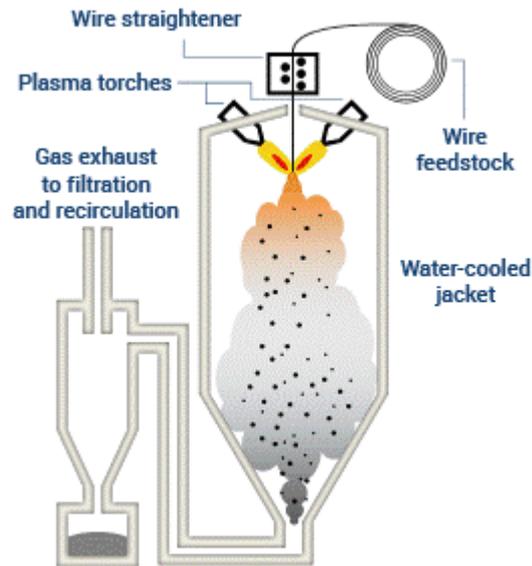
Figure 2. 9 Schematic diagram of Plasma Atomization (PA) (image credit: advancedpowders.com)

All the above production processes produce spherically shaped particles such as Ti6Al4V powders in Fig. 2.10a, b and c except for the HDH process that produces angular shaped particles presented in Fig. 2.10d.
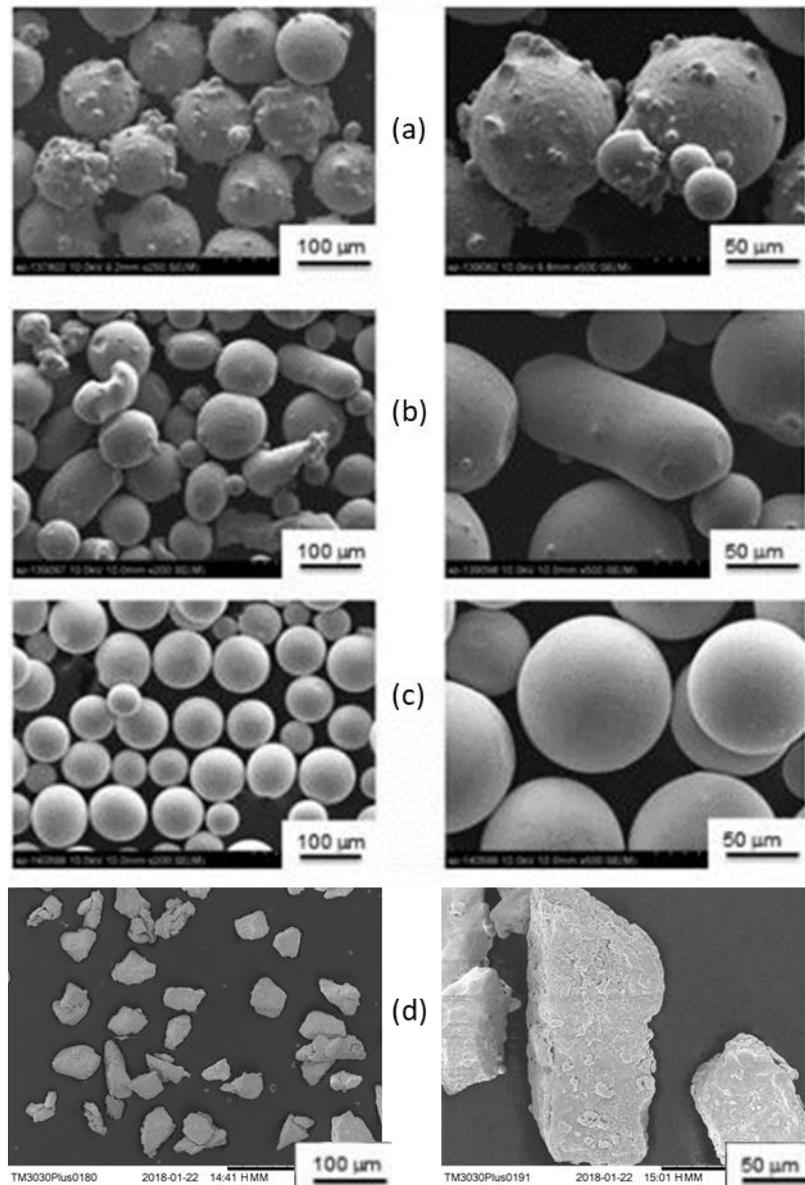
Figure 2. 10 Spherical Ti6Al4V particles produced by (a) GA process, (b) PA process (c) PREP process (40) and (d) HDH process

Based different manufacturing techniques, powders can have different characteristics such as shape, size and surface properties which can influence spread powder bed quality and later the built part properties.

2.2.3. Advantages and disadvantages of AM

There are few major advantages and disadvantage of additive manufacturing process compare to conventional manufacturing process which should be consider (1):

2.2.3.1. Efficiency in material use

One of the major differences between additive and traditional manufacturing is based on their process. In AM unlike the conventional route, products are created by building the parts layer by layer therefore, it only uses the material necessary for creation, ensuring minimal wastage of material. Also, the left-over material is often reused for next production processes. On the other hand, conventional manufacturing is based on subtracting large amount of material which usually cannot be used and become a waste. In this way, additive manufacturing process compared to conventional production reduces the cost of material and waste.

2.2.3.2. Efficiency in the use of resources

Additive manufacturing does not require several steps and technology to facilitate it. On the other hand, conventional manufacturing often requires supplementary resources such as cutting tools, coolant, fixtures, and different machine such as turning, milling, and drilling to create a finished metal part. In contrast, additive manufacturing is a single device which can handle creation of variety parts. As a result, there is less labour work compare to conventional method due to completely automated route.

2.2.3.3. Part complexity

Part complexity is one of the important factors which could be achieved by additive manufacturing route. Parts that have complex features or customized products can be manufactured in a single piece. While convectional manufacturing parts are produced separately and assembled into a single piece.

2.2.3.4. Flexibility in production

A final advantage of additive manufacturing to conventional route is customisation. In conventional manufacturing, the large number of identical products create a small room for customisation while AM with ability to print any configuration object, offers to produce the similar product unique to each other with customisable feature.

Additive manufacturing, however, cannot fully compete with conventional manufacturing, especially in the domain of mass production, primarily because of the following:

2.2.3.5. Limitations in size

In additive manufacturing process, parts can only be created one at the time and, due to small print chamber there is a restriction to the size of component. Therefore, to create the bigger product, the small parts need to be printed separately then assembled. This can increase the costs and time, preventing economics of scale.

2.2.3.6. Presence of imperfections

The parts produced through the additive manufacturing often have rough surfaces and lower quality compared to conventional manufacturing method. This may be as a results of inhomogeneous powder layer which require post processing such as polishing, machining and sanding. So, the speed of manufacturing can be slowed by post processing and surface preparation (19).

2.2.3.7. Cost

For small production, additive manufacturing equipment do not usually require an expensive set up, however, compared to conventional process, it is still an expensive investment. Additionally, high quality additive manufacturing machines can range from $300,000 to $1.5 million (42) plus material cost which is varied for different feed stock and running cost for machine such as specific gas requiring for inert environment still make this process much more expensive compared to conventional process.

Recently, there is a huge investment to improve the additive manufacturing short-comes through the researchers at universities, government research laboratories, and a variety of industries.

2.2.4. Summary

As AM technique has recently become a potential production process, the development of process parameters to build desirable final parts such as minimal porosity, low surface roughness, and high strength become important. These objects directed the researcher to

focus on the characterisation of input material and use a different technique to characterise different powders to predict the behaviour of AM process.

Powder bulk properties are influential factors that affect the quality of the final product; hence a thorough understanding of these factors is crucial in AM. Better flowability of powder is vital but a complex parameter that can reinforce the overall quality of the AM part. To produce homogeneous layers, it is imperative to make use of powders with high flowability, which consequently reduces excessive voids and discontinuities in the final part (43, 44). Therefore, the generation of a very thin layer of powder bed in AM process from a reservoir or hopper at relatively low consolidation normal (around 103Pa) and shear stresses (around 102 pa) (45) is a complex process. To characterise the flow and packing behaviour of powders in AM process, it is essential the testing device operates as closely as possible to the process conditions especially with a view on the stress states in the powder (14).

Therefore, the term powder flowability and few techniques are presented in the next section and discussed regarding to AM process, where the powders move dynamically over the powder bed with effects of aeration caused by the speed of spreading device.

2.3. General background of powder flowability

Figure 2. 11 Powder flowability (image Credit: Stable Micro Systems Ltd)

Powder flow term is an observation, and it is a description of how bulk material (powder) will flow in specific environment. The powders which are produced for industrial applications can have different flow behaviour problems resulting from a combination of physical properties of the material and equipment design. Therefore, it is important to characterise the physical properties relevant to powder flow as a function of consolidation stress. Regarding AM, powder spreading is a vital step of EBM process. The more homogenous powder layer means a uniform packing density where powders rearrange to maximum particle contact and minimum voids that makes powder melting more stable and as a result denser final product (4). However, there is still insufficient understanding of powder flow or spreading in additive manufacturing powder bed-based system in general (3).

There are several techniques available for assessing the flow behaviour of the powder such as uniaxial test, shear cell e.g., Jenike or the Schulze ring shear tester etc. However, these tests are not capable of handling measurements of low consolidation stress less than 1 kPa and require relatively large amounts of powders.

As stated before, a study of the flowability or the flow properties of a bulk solid must be done to design correctly the handling equipment to avoid or minimize operation problems. According Prescott and Barnum (5), flowability is not an inherent property. Generally, powder flowability is defined as the ability of the powder to flow freely under specific set of conditions such as:

- Chemical composition of the particles

- Particle size distribution

- Particle shape and type

- Surface's properties

- Temperature

- Moisture content

- Vibration

- Equipment design

However, it is not currently possible to determine numerically the flow properties of bulk solids considering all that parameters (6). Thus, experimental suitable testing methods must be developed and performed to:

- Investigate the possibility to describe the flowability with testing methods.

- Characterise the flow behaviour of different kind of powders at different conditions.

The principles of the flowability of bulk solids which can be experimentally determined and some of the suitable testing methods used to characterise the flow behaviour of powders are described in this section. A wide range of techniques for bulk powder flow measurements and a comprehensive review are available in the literature. Therefore, some techniques and their

comparison are presented in this chapter for evaluation of powder flowability in regard to AM.

2.3.1. Qualitative flowability measurement methods

2.3.1.1. Tapped density

This method which was introduced by (Hausner 1967) is one of the most commonly used measurement techniques to qualify flowability (46). It is the ratio of the tapped density (mass per volume after mechanically tapped) over the apparent density (mass per volume of free fall) powder. The change in volume and ability of powder to move after tapping is related to inter particle friction and cohesiveness of the material which has direct impression of powder flowability. Carr index (47) is the ratio of the difference between the tapped and bulk densities to tapped density. Essentially the lower Hausner ratio (HR) and Carr index (CI) indicate that the powder is more free flow and less cohesive.
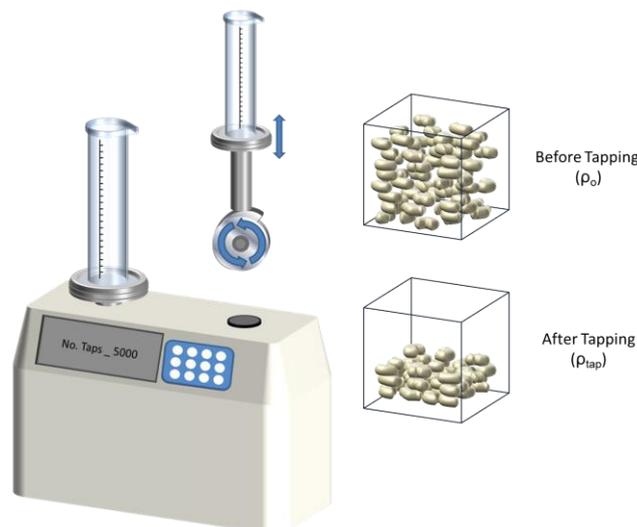
Figure 2. 12 Illustration of tapped density measurement (image credit: Freeman technology)

There are loads of literature investigating and characterizing the powder flowability by using the tapped density. For instance, (Podczeck, 2012) investigated the correlation between die filling performance and Carr index (48). (Emery, 2008) used the Hausner ratio and Carr index to characterise API and Respitose powder under different moisture contact (49). Also, (Traina et al, 2013) find the flowability of powders and granular material by dynamic tapped density measurement (50). Leadbearter et al. (1968) have detailed study of iron powders with measurement of tapped density which associated some drawbacks to the method. It reported that the cup capacity, number of tapping and the filling method have a huge impact on the density value (51). Also, it has been proved by Abdullah et al. (1999) that density is highly dependent on the number of tapings and could be different if using different testers (Hosakawa or Copley) (52). There are few researches on AM powder using HR as an indicator of flowability measurement (53, 54). Tang et al. studied the apparent and tapped densities to characterise flowability of Ti6Al4V powder from virgin to 16 times reused powder. They concluded that the flowability of the powder based on Hausner ratio unexpectedly improved with increasing reuse times due to the absence of satellite particles and the removal of moisture.

This process is easy, reproducible, relatively quick, and simple to calculate. However, it cannot be used for solo technique to determine the flowability of powder as flowability also, depends on other factors such as shape, size, adhesion, and moisture content (55). This method is also very operator dependent. In addition, it is apparent that density measurement technique is far away from the spreading situation in AM, where small amount of powder dynamically spread over the powder bed with very small compression force and no tapping applied during the process (3). Although, there can also be found research results in literature supporting a

contrary view that HR could be good indicator for compaction ability and deposition of powder layer in SLS process (56).

2.3.1.2. Angle of repose

Among various method of flowability test the angle of repose is a simple, direct and dynamic method for measuring powder flow. In this test, the powder is poured freely through the specific funnel size to make a pile of powder settled under the gravity. The slope angle of the conical pile of powder on to the free surface (horizontal base) is the angle of repose and is considered as a measure for powder flowability (57). Despite of its high user dependency (58), the stress state and dynamic movement of the powder can be considered quite close to AM process condition.
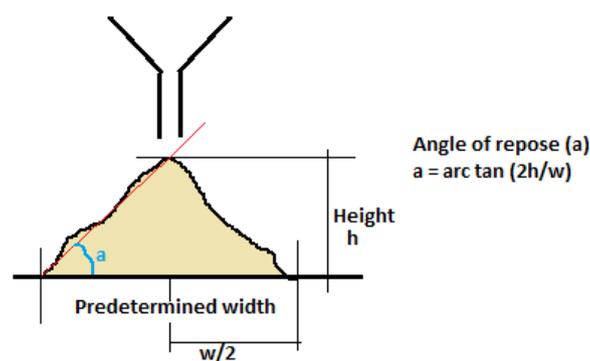
Figure 2. 13 Illustration of angle of repose technique (image credit: Wikipedia)

Xu et al. investigated the effect of milling time on Ti6Al4V HDH powder flowability by using both angle of repose and density measurements. They obtained that the ball milling efficiently improved the flowability of HDH powders due to a change in particles shape (59). Although Sun et al. (43) concluded that this technique is not useful to characterise flowability and could not link the AOR to the process performance of powder in AM due to simplicity of

method. However, due to simple sample preparation, quick performance and repeatability, this technique is usually used for quality control and comparison of different bulk powder.

2.3.1.3. Flowmeter

Flow rate can be measured based on the time taken for specific powder to flow through a funnel or vessel. There are several commercially available techniques such as Hall flowmeter, Flodex flowmeter and Vibrating capillary method to study flow rate and flowability of given powder (60, 61).
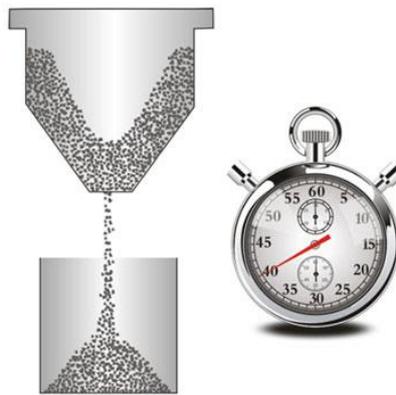
Figure 2. 14 Illustration of powder flowrate measurement (image credit: bettersizeinstruments.com)

Powder flowrate or Hall flowrate is the most frequently used method to measure flowability for free flow powders (62, 63). The time required to discharge the certain amount of bulk powder through the calibrated orifice size can be used to measure flowability of powder. This method is very cheap and simple and can be used widely for AM powders. However, Schulze defined some drawbacks of this method such as operator dependency (type of filling) and the effect of aeration of the powder on flowrate. Due to this drawbacks he concludes that flowmeter technique is only simple comparative test which is not suitable for quantitative

measurement on powder flow (58). Liu et al. studied three types of Ti6Al4Vproduced by electrode induction melting gas atomization (EIGA), plasma rotating electrode process (PREP), and plasma atomization (PA) and compared their flowability by using the hall flowmeter and concluded that the Ti6Al4V powder produced by PA process has the best flowability, followed by EIGA and PREP Ti6Al4V powder (38). They correlate flowability results with particle shape and microstructure characterisation. However, Sun et al. established in their study that this method only, cannot distinguish the differences between the titanium powders concerning their behaviour in EBM process (43). Although, this technique can be used to determine some powder characteristics which could be used in EBM process specially to design the hopper in EBM machine.

2.3.1.4. Rotating drum (Avalanche angle)

Another method which is developed by Kaye et.al (1995) to indicate powder flowability in industry is the dynamic angle of repose or avalanche method (64). This technique typically consists of a rotating, transparent drum filled with a certain amount of powder and a camera in front of a backlight. The camera records pictures of the powder free surface and the cross-sectional area of powder inside the drum during rotation. The pictures can be analysed for powder avalanche angle and surface fractal of powder, which associated with powder flowability and inter particle forces (65). This methodology has been used by Krantz et al. (14) to assess polyurethane and polyester epoxy powders and he found a good correlation between the angle of repose and the avalanche angle, as both methods subject the powders to similar stress states.
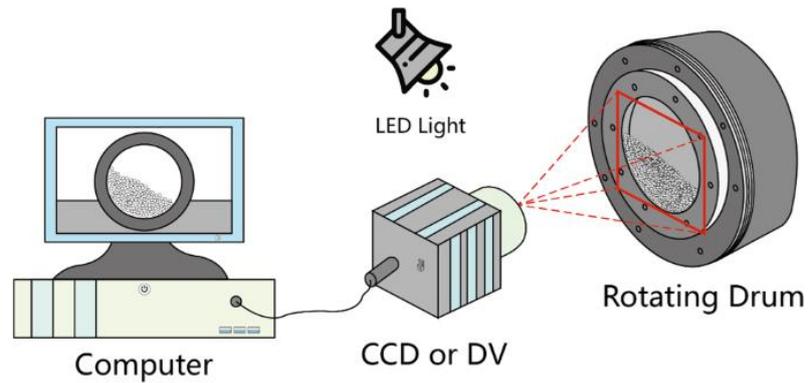
Figure 2. 15 Illustration of rotating drum (66)

Regarding AM process, the behaviour of powder under dynamic condition such as avalanche method is a better indicator of flowability, which is much closer to the powder-bed based additive manufacturing process such as SLS, EBM processes than the other techniques. However, for cohesive powders this technique could be inaccurate due to an increased friction of particle-wall and caused poor visibility of light detection. The cohesive powders also provide less stable avalanche and result which make the analysis more difficult. Spierings et al. (3) have detailed study of Fe and Ni based powders which is usually used for SLM process both using avalanche angle and optically valuation by five experienced people and found very good correlation between the powder avalanche angle, surface fractal with optical evaluation of powder flowability to assess a homogeneous powder layer quality in AM. Gu et al. (67) used this method to characterise flowability of three different Ti6Al4V powders from different powder suppliers and found the correlation between the powder characteristics and part properties after SLM process. However, they rotated the drum manually three times, which does not give any indication about the accuracy of the angle.

2.3.2. Quantitative flowability measurement methods

2.3.2.1. Uniaxial compression

Jenike (1965) was first to introduce a quantitative measurement of flow for bulk solid. Uniaxial compression test is a widely used technique to measure the flowability of powder while a known amount of stress applied on it. Generally, the cylinder is partially filled by certain amount of powder and then vertically loaded under desired stress called consolidation stress σ_1. Under consolidation stress, particles will rearrange and reduce the voids inside the bulk. The more the volume of the sample decreases, the more cohesive and compressible the powder is. After consolidation, the supporting wall will be removed and the bulk solids subjected to the vertical stress, which make the specimen fail. The necessary stress cause failure of the bulk solid is called Unconfined yield strength σ_c as shown in figure 16.
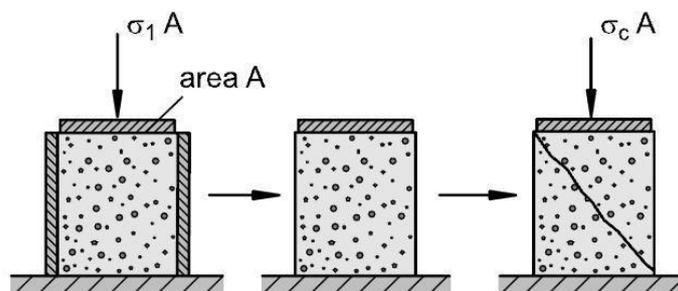
Figure 2. 16 Principal behind uniaxial compression test (69)

The Jenike flow index/flow function (ff_c) is the ratio of the consolidation stress to the unconfined yield stress as follow:

$$ff_c = \frac{\sigma_1}{\sigma_c}$$ Equation 2.1

The flowability of the powder can be classified according to the ff_c values of flow function. Cohesive powders have relatively higher unconfined yield strength due to their inter-particle forces, which adhere particles together and need a greater stress to break them. While for free-flowing powders, the tensile stress is relatively weaker, and results into a greater flow function (68).

Uniaxial technique is simple, relatively fast, and reliable measurement to find the unconfined yield stress and flow function of powders. However, this technique does not provide any information regarding internal and wall friction. Also, there are some disadvantage about this method such as maintaining the free flow powder during the initial state after the supporting wall will be removed and flowability measurement is very difficult for low consolidation stress which is a specific condition for AM process.

2.3.2.2. Schulze ring shear cell test

Shear cell is well known measurement technique to determine flowability at moderate or high stress condition with good reproducibility. This method gives a good insight into powder properties such as powder flowability, compressive strength, powder compressibility, consolidation time ''caking'', internal and wall friction, and bulk density (69).
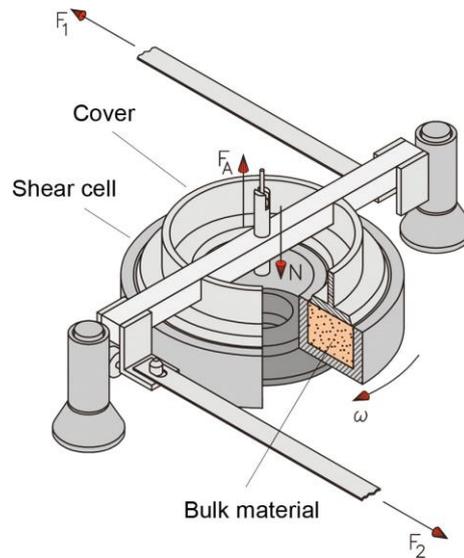
Figure 2. 17 Illustration of Schulze ring shear cell test (58)

Despite of flow function being the conventional method used in academia, shear cell is limited to static stability and high compressibility, therefore it is not a decent technique for measuring powder at low stress, flowing at high shear rate which is the situation in AM process.

However, this technique provides powder characteristics that could be utilised in other flowability techniques such as ball indention or flowmeter to provide practical and effective reference values for hopper design optimisation in 3D printing (70).

2.3.2.3. FT4 powder rheometer

In last decade, Freeman Technology (Tewkesbury, UK) have developed the FT4 powder rheometer to characterise the flow properties such as flow energy, aerated flow energy, shear properties, compressibility, permeability and bulk density in dynamic regime of shear strain rate.

The flow resistance is characterised by flow energy; the summation of rotational and translational work required to drive a rotating impeller a certain distance into the powder bed. It has shown an ability to differentiate the flowability of powders that otherwise exhibit similar behaviour under shear testing (71). The energy calculated is mostly dependent on the inter-particle forces and not affected by other factors such as compressibility and it also could measure the cohesiveness of the powder under very low stress condition (72). From this technique various parameters can be obtained as follow:

Basic Flowability Energy (BFE): The energy (mJ) required to displace a conditioned powder during downward testing in the seventh test.

Normalized Basic Flowability Energy (NBFE): The NBFE is equal to the ratio of BFE to the sample mass. The normalized basic flowability energy (NBFE) accounts for the differences in sample mass, and therefore allows for general comparison of powders.

Specific Energy (SE): The energy per gram required to displace conditioned powder during upwards testing. As the specific energy is measured on the upward traverse, it gives an indication of how the powder will flow in a loosely packed and unconfined state.

Stability Index (SI): The Stability Index (SI) represents a factor by which the measured flow energy changes during repeated testing and is equal to ratio of flow energy of the test seven to the first test. Agglomeration and segregation of the samples can be assessed by a stability index.

Flow Rate Index (FRI): It corresponds to the ratio of flow energy of the eleventh test to the eighth test. It used to characterise the sensitivity of a powder to flow rate change.

Conditioned Bulk Density (CBD): The conditioned bulk density (g/ml) corresponds to the density of a sample inside the vessel of FT4 after the pre-conditioning step.

As portrayed from Fig. 2.18, there are numbers of other tests that can be measured with FT4 rheometer. FT4 also have ability to do the torsional shear and permeability measurement by using different pistons at low consolidation stress for a wide range of powders.
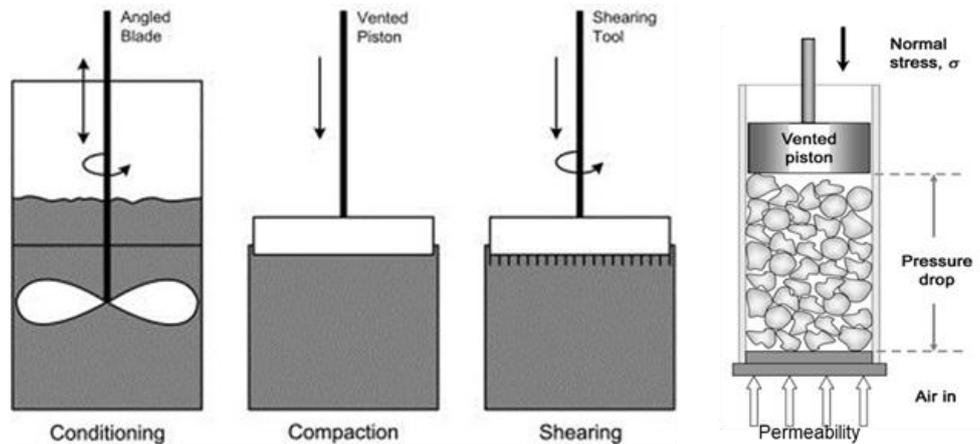
Figure 2. 18 Illustration of FT4 rheometer (image credit: Freeman technology)

However, according to Dihoru et al. (2003), the flow properties measuring by FT4 is dependent on the vessel size and impeller geometry and give the different results based on their alterations (73). Also, Sogaard et al. (2012) observed the large variation of results for cohesive powder due to packing state, so to reproducing the initial state of powder is still challenging (74). Clayton reported the measurement of dynamic flow properties of virgin, blended and used Ti6Al4V powders by using the FT4 and concluded that this method is very helpful in optimising lifecycle management right through from virgin powder to final waste (75). Therefore, they assumed that the used powder would not flow as freely as the virgin material and consequently is less likely to successfully perform in the process. Also, Wei et al. analysed raw (irregular shape before atomization) and spherical powder of Ti6Al4V and compare their flow properties by using FT4. They concluded that flowability, compressibility

and shear performance of spherical powders improved as with those raw powders indicating that the spheroidization showed enhanced flowability (70).

2.3.2.4. Ball indentation

Ball indentation is another method to measure the powder flowability based on resistance of bulk powder to plastic deformation (76). In this method, the relatively small amount of powder is subjected to low stress and the resistance of bulk powder to plastic deformation and hardness of powder can be calculated. The hardness of powder bed can be measured as:

$$H = \frac{F_{max}}{A}$$ Equation 2.2

where F_{max} is maximum indentation load and A is the projected area that indenter has impression on sample which can be obtain by following equation;

$$A = \pi(d_b h_c - h_c^2)$$ Equation 2.3

where d_b is the indenter diameter and h_c is the intercept of the tangent to the unloading curve. However, for bulk solid of powders, during the plastic deformation under load of indenter, the material around the indenter deform elastically and cannot flow easily and causes the increase in local yield stress. This may cause the hardness of powder become greater than the plastic yield stress and their ratio called Constraint factor (77);

$$C = \frac{H}{Y}$$ Equation 2.4

where C is constraint factor, H is hardness and Y is yield stress.

The procedure is relatively simple, the low friction die fill with quite small amount of sample and pre-consolidate at different pressure. Then the sample subjected to spherical indenter and depth-load cycle will be recorded. The spherical indenter is better option rather than conical or cylindrical due to not having sharp edge to be equivalent in size to any individual particle. The loading will be increased to reach to the optimum load and then unloading to zero with the same rate. The elastic deformation of powder bed will be recovered during unloading process as can be seen in Fig. 2.19.
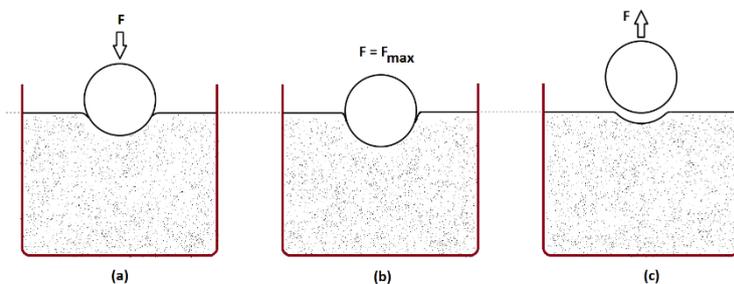
Figure 2. 19 Schematic of ball indentation (a) loading, (b) maximum loading and (c) unloading (76)

Hassanpour and Ghadiri (2007) found a very good correlation between the hardness and unconfined yield stress for cohesive powder of α-lactose monohydrate and magnesium carbonate, however, for glass beads the results were diverted from linear trend. Weng et al. (2008) observed that the hardness of bulk solids and yield stress will be increased by increasing the pre-consolidation stress, they also found that constraint factor is varied with single particle physical properties as well such as particle shape, roughness and mechanical properties such as indenter geometry and friction (78). Consequently, ball indentation has been successfully applied for assessing powder flowability for the following materials: lactose, starch and Avicel (16), glass beads, Respitose SV003 and Fluid Catalytic Cracking (FCC)

equilibrium catalyst (commonly used in the petroleum industry) (68) and calcium carbonate (Durcal 15) and limestone (79). They reported that the ball indentation results correlate very well with common flowability measurement technique.

This technique has also not been used for any free flowable powders, which is usually utilised in additive manufacturing. However, the hardness measurements using this technique could also be affected by the distribution of packing fraction of loose and consolidated powder bed at different compaction stresses, wall effects and segregation of particles during filling and consolidation, which are yet to be studied in detail. This will require a 3-dimensional imaging technique to get an insight into the process of filling, compaction, and indentation. The best this method for this purpose is the use of x-ray and computed tomographic techniques to provide a 3-dimensional information of the power bed.

X-ray microtomography (XMT)

X-ray microtomography (XMT) is a non-destructive, relatively fast and accurate method which can reveal detailed information of the internal 3D structure of objects. Recently, it has been utilised for dimensional measurement and porosity analysis of internal structure of complicated components in AM process (80). In recent years there have been various research works analysing the metal powder feedstock using high resolution micro CT from single particle characterisation (81- 82) to study the effect of the grade of metal powder on porosity and quality of final components (83).

It could also be said that this is a main method for high-quality and detailed analysis of single particle physical properties such as sphericity, surface area, volume and aspect ratio, which all have significant effects on the quality of powder bed. Chawanji et al. (2012) compared the packing efficiency of two different milk powders under specific load and attributed their

different behaviour to the particle properties. They found that the packing efficiency is higher for powder containing surface fat which acts like lubricant and reduce particle-particle friction and leading to closer packing (84).

Also, XMT has been used extensively to study particle behaviour during die compaction. Particularly McDonald et al. (85) worked intensively on the effect of different punch shapes (flat, angled and rounded) on the rearrangement and movement of 0.5 mm glass spheres during compaction by using XMT. The study focused on the shape of different punches on localised density around the indenter and but the effect of size and shape of particles on the packing density was not the subject of the study. Later, they studied the particle movement during compaction by using blended aluminium and tin powders with size distribution of 38-45 and 125-140 μm, respectively. They reconstructed the tomographic images with voxel size of 27 μm and but could only track the local pixels of tin particles at different stage of compaction, presumably due to the small size of aluminium particles. They reported a dimensional displacement maps around the compaction punch and found the localised density fraction (86). The in-situ shear deformation of aluminium powder during compaction and the formation of shear crack have also been demonstrated (87), however, individual particles in the whole powder bed were not visualized and the quantitative analysis of radial and axial packing fraction for the entire bed and the wall effects for specific applications such as ball indentation were not reported.

Numerical modelling of powder packing density and die compaction during ball indentation have also been studied and provide great insight of the process (88, 89). Although the shear zone of powder around the ball indenter to find the shear stress and the effect of constraint factor in confined powder bed have been numerically studied, the effect of wall, localise packing fraction for loose or at low stress compaction and the effect of indenter size on

confinement region have been not been experimentally reported during the ball indentation process.

2.3.2.5. Sevilla powder tester (SPT)

Sevilla Powder tester is an automated powder characterisation technique to measure the uniaxial tensile strength of a relatively small amount of fine powder.
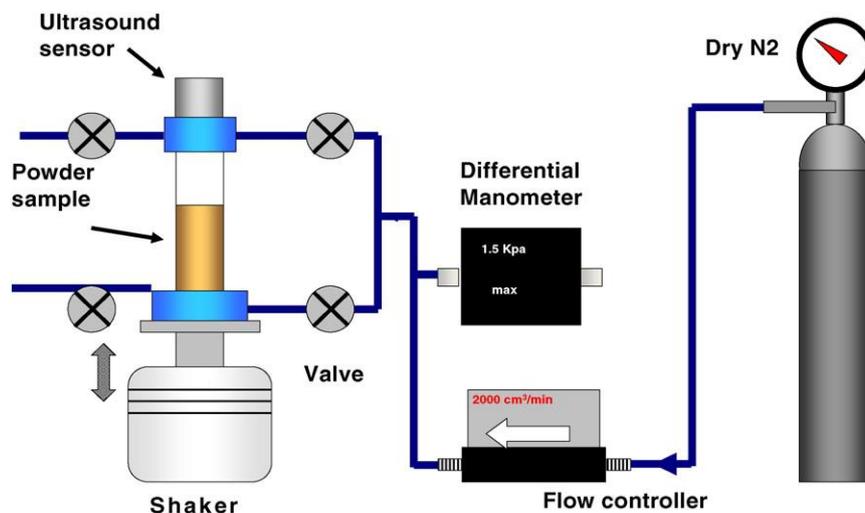
Figure 2. 20 Sevilla powder tester (79)

As can be seen in Fig. 2.20 it consists of porous base, vertical cylinder, electromagnetic shaker and pressure transducer. First, the certain amount of powder placed inside the cylinder on a porous base which the pores are much smaller than the particle size. It is very important to uniform powders by using the controlled gas flow (dry Nitrogen) through the sample to erase the memory effect of historical stress. Also, by using dry Nitrogen, the particle adhesion effect could be minimized (90) and make the powder bed into a freely bubbling regime.

For very cohesive powder, it is essential to use the shaker to break up any channels and agglomeration that block the fluidizing gas. After stationary state, the gas flow suddenly stops,

and powder bed is subjected to the opposite direction flow, which puts the powder bed under compressive load. In order to measure the consolidation stress at the bottom of powder bed, the weight of sample should be divided by the area of the bed. The uniaxial tensile yield stress is measured by reversing the flow to the upward direction and increase it slowly to put the powder bed under tensile stress and the total pressure drop is measured. Although this technique is fully automated, and it requires a relatively small volume of powder (typically 50 ml) to perform the test (91), it is not commercially available and not suitable for all powders, because the samples need to be fluidised (88).

2.3.2.6. Raining bed method

There is another method for directly measuring the tensile yield stress which is called Raining Bed Method. This technique was first introduced by Buysman and Peersman (1967) and then developed later by Seville and Clift (1984) and Formisani et al. (2002) (92, 93, 94). This technique consists of a ring shear cell with compactor for powder sample. In this technique first, the air flow through the powder removes any historical stress during production or storage and then the direction of air flow will change to compact the powder bed greater than gravity force then the whole setting rotating 180 degree.

The powder bed will be held by pulling force of air flow, then the air flow force decrease gradually and then at the point of air flow equal to weight of powder, if the powder is free flowing, it will fall like rain. In contrast for cohesion powder the tensile stress and inter-particle friction resist of falling, even when the air flow pressure is smaller than gravity force. Despite the fact that this technique is reproducible and characterises the tensile stress directly and at low levels of stress, it has not been validated by other techniques and further study is needed.

2.3.2.7. SSSpin tester

Another quasi-static system to measure the flowability is the SSSpin Tester. It worked based on centrifugal force both for consolidation of bulk solid and yield strength. At first powder become compacted by using centrifugal force, then the same force uses to determine yield strength of powder. The latest instrument provides the pressure range of (0.05kPa to 72 kPa). The SSSpin Tester is capable for testing yield strength and flowability for a variety of pharmaceutical, catalysts, cosmetics and ceramics (95). It is very fast, repeatable procedure and provides consistent data. Unfortunately, this technique is also not commercially available.

2.3.2.8. Couette device

Tardos et al. (2003) developed the Couette device which the powder is sheared between two concentric vertical cylinders with different rotational rates (96). The instrument consists of inner and outer cylinder of different size and sensors to determine the normal stress in both horizontal and vertical direction and torque of inner cylinder at given powder bed height. They characterise several powders at three regimes of static, quasi-static and dynamic regimes. The results shown that the shear stress increases with strain rate for dynamic and quasi-static regimes. The drawback of technique is that the device requires a large amount of sample. A schematic representation of device is shown in Fig. 2.21 with details of shear gap, computer-controlled camera to capture the image of the powder flow and its rotating and stationary cylinders.
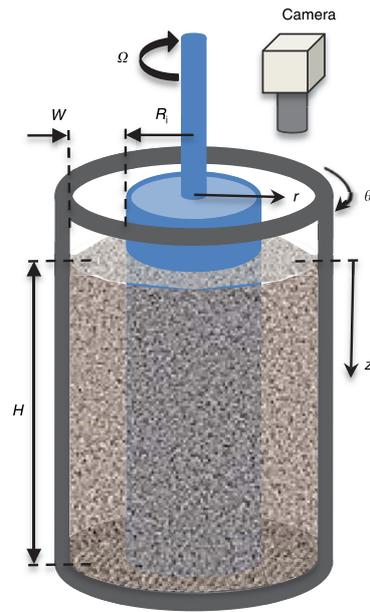
Figure 2. 21 Illustration of Couette device (87)

2.4. Conclusion of literature review

Powder properties are influential factors that affect the quality of the final product; hence a thorough understanding of these factors is crucial in AM (Fig. 2.22).
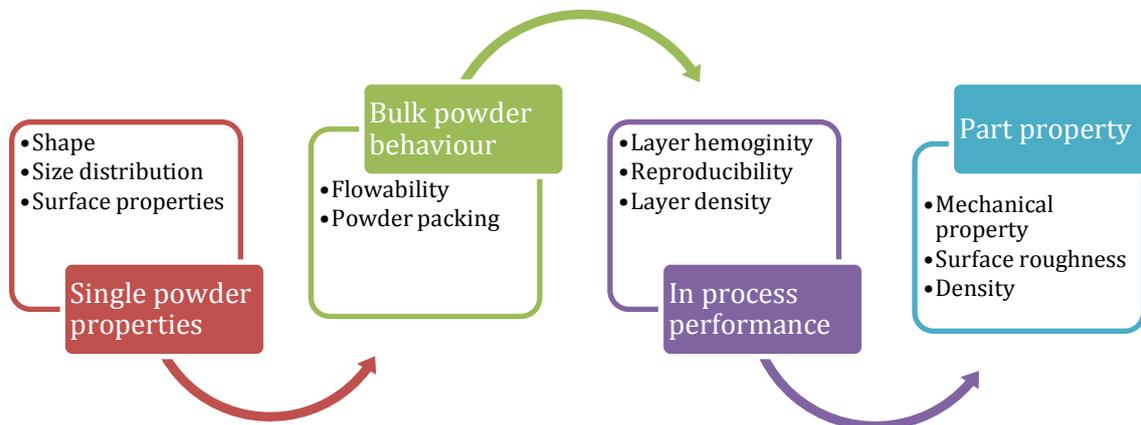
Figure 2. 22 Influencing parameters and their analysing method on metal powder for AM process (97)

A wide-ranging overview on different methods for powder flow measurement is given in literature and their pro and cons have been discussed. Despite of well establishment of characterisation of powder flowability on quasi static regime, there is still insufficient understanding of powder flow failure in the dynamic regime. An increasingly important sector dealing with powders operated at high strain rates is AM. There is currently great effort being put into relating the spreading performance in AM to various flow testers. However, a different approach is needed to describe the behaviour of spreading of thin powder layers for the increased demand of powder spreading in additive manufacturing (32).

A comparison of the common powder flowability techniques based on suitability for AM technique is summarized in Table 1 in terms of:

1. Possibility for measuring flowability near to powder bed base AM techniques

2. Requirement of relatively small quantities of testing powder

3. Quantifying variation of shear stress

4. Reproducibility

5. Possibility of measuring time consolidation

6. Aeration of powder regarding to free surface

7. Simplicity

8. Compacting force measurement

		1	2	3	4	5	6	7	8	
Static Measurements	**Angle of Repose**	(×)	×	×	✓	×	✓	✓	×	No consolidation stress, no quantitative measurement. But simple, reproducible and cost effective.
Quasi-static Measurements	**Shear Cell**	×	✓	✓	✓	✓	×	×	✓	Reproducible state, major consolidation and unconfined yield stress can be determined.
	Ball Indentation	(×)	✓	✓	✓	✓	×	×	✓	It is able to measure flowability at low consolidation stress, small amount of sample.
	SSSpin Tester	(✓)	✓	✓	✓	×	×	✓	✓	Fast, repeatable, small amount of sample, small consolidation stress.
	Raining Bed	(✓)	×	×	✓	✓	×	(×)	×	Reproducible, measuring tensile stress directly at low level of stress.
	Sevilla Tester	(✓)	×	×	✓	✓	×	(×)	✓	Tensile strength can be measures. Pre-consolidation is available, time consuming.
Semi-Dynamic	**Tapped Density**	(×)	×	×	✓	×	✓	✓	×	Very simple, give qualitative result.
Dynamic Measurements	**FT4**	✓	×	✓	✓	✓	✓	×	×	Characterise the flow energy, shear properties, compressibility, permeability and bulk density.
	Couette Device	(✓)	×	✓	✓	✓	×	✓	×	Measuring the shear stress at different strain rate, require large amount of sample.
	Hall Flowmeter	✓	×	×	✓	×	✓	✓	×	Qualitative result, with no consolidation state but it is simple.
	Rotating Drum	✓	×	×	✓	×	×	✓	×	Qualitative result, with no consolidation state, suitable for AM powder characterisation.

Table 2. 1 Comparison of common powder flowability techniques

✓   There are evidence in literature that the method meets the condition
x   There are evidence in literature that the method does NOT meets the condition
(✓)   There is not enough evidence in literature that the method meets the condition
(x)   There is not enough evidence in literature that the method does NOT meets the condition

2.5. Knowledge gap

Understanding the behaviour of powders upon packing is essential in the production of AM parts. Less dense components with higher porosity may be created as a result of utilizing powders will lower true densities (98). In order to reduce the porosity of the layer, spherical and smooth particles are beneficial as they have higher particle density and enhanced flowability (99). Better flowability of powder is a crucial but complex parameter that can reinforce the overall quality of the AM part. For the production of homogeneous layers, it is imperative utilise powders of high flowability, that consequently reduces excessive voids and discontinuities in the final part (100, 101). Therefore, generation of a very thin layer of powder bed in AM process from a reservoir or hopper at relatively low consolidation normal (around 10^3Pa) and shear stresses (around 10^2 pa) (45) is a complex process. To characterise flow and packing behaviour of powders in AM process, it is essential the testing device operates as closely as possible to the process conditions especially with a view on the stress states in the powder (14).

Despite the large research to characterise the powder properties, there is a wide gap in the literature on the effects and correlation of particle properties on powder flowability and improvements of powder layers in AM industry.

Chapter 3 Materials and Methods

3.1. Introduction

The materials and morphological analysis by using XMT of two different types of Ti6Al4V powders used in the EBM process, namely the spherical gas atomized (GA) and irregular hydride-dehydride (HDH) particles are presented in this chapter. In addition, the list of methodologies used in this work to characterise powder flowability is presented in this chapter.

3.2. Material

In this work two grades of Ti6Al4V powders obtain from different manufacturing processes, (i) Hydride-dehydride (HDH), irregular shape particles with size distribution of 25-120 μm (Fig. 3.1a) and (ii) Gas Atomised (GA), nearly spherical particles with size distribution of 25-130 μm (Fig. 3.1b), have been investigated to compare their packing behaviour. Both Ti6Al4V powders were supplied by GKN Ltd. UK.
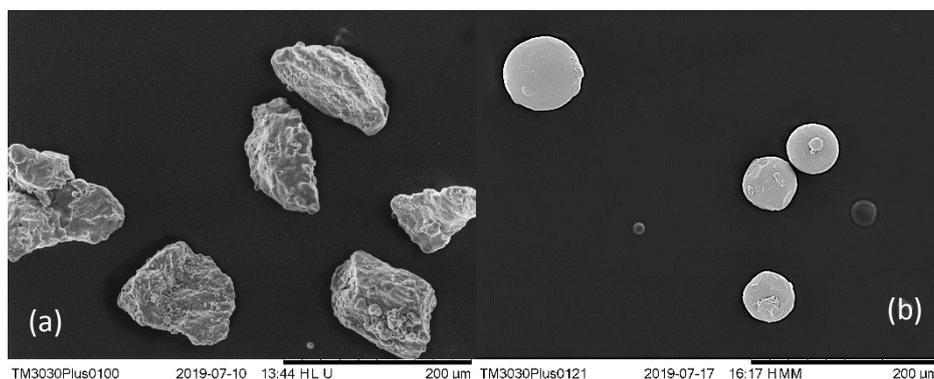
Figure 3. 1 SEM images of (a) Hydride-dehydride (HDH) and (b) Gas atomization (GA) of Ti6Al4V samples

The particle size distributions of both powders were measured with laser diffraction technique (dry method) using the Mastersizer 3000 Particle Size Analyzer (Malvern Panalytical, UK). In order to obtain accurate measurements, an average particle size distribution of ten measurements was taken to ensure powder was fully dispersed and stable.
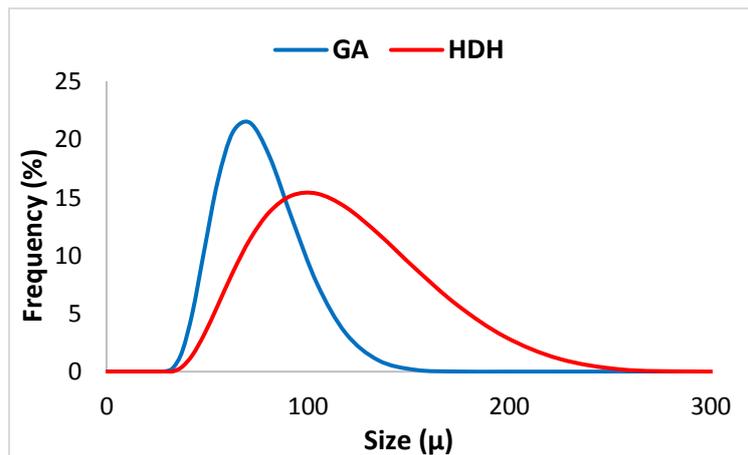
Figure 3. 2 Size distribution of GA and HDH powders measured by laser diffraction

Chemical compositions of both powders were determined using the Energy Dispersive X-ray (EDX) to identify the element of each sample. The intensity of backscattering of electrons (BSE) are related to the weight percentage of each atomic number of the element which is determine the elemental composition of each sample as well as obtain element map (Fig. 3.3). This study has been carried out by Dr Jabba Gardy at the University of Leeds.
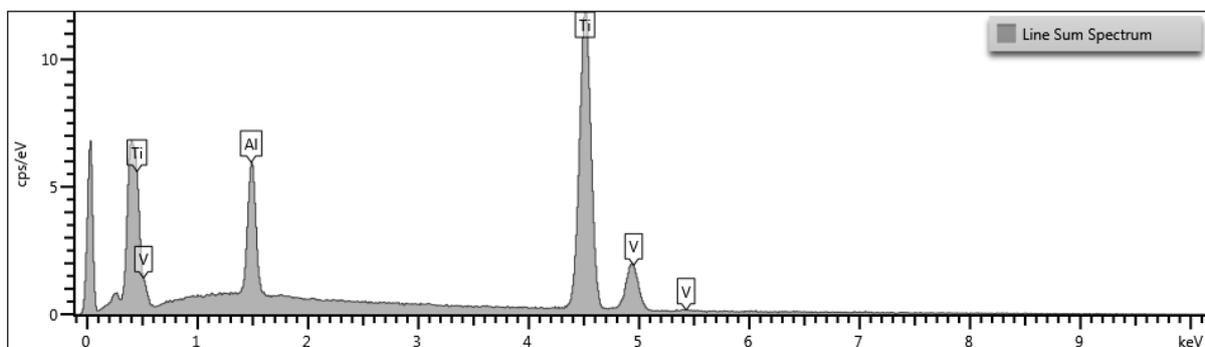
Figure 3. 3 The elemental composition of the Sample 1 according to the X-ray intensity and specific wavelengths

In Fig. 3.4, the BSE image of GA powders with line profile analysis are presented. Different colours represent the identification of different chemical composition of titanium, aluminium, and vanadium.
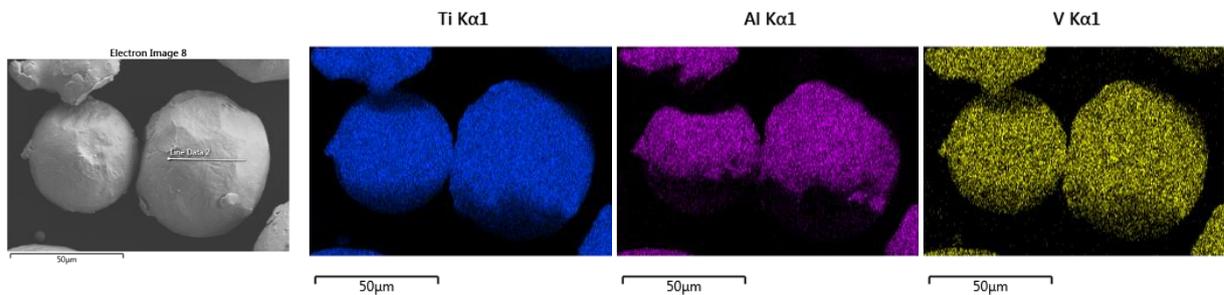
Figure 3. 4 BSE image of Sample 1 with line profile analysis.

The chemical compositions of both samples are presented in (Table 3.1).

Element	GA Wt%	HDH Wt%
Ti	89.6	89.35
Al	6.23	6.57
V	4.17	4.07
Total	100	100

Table 3. 1 The elemental composition of the samples GA and HDH measured by using XRD

Pycnomatic ATC (Thermo Scientific™) system also was used to measure the true density of the powders according to the ASTM B923 standard. The powder was weighed and poured inside a calibrated cup. Helium gas was used as a displacement medium, to penetrate between powder particles. The difference in pressure before and after the gas expansion was

measured to calculate the volume of the powder. Each powder sample was measured 20 times to ensure the accuracy of the measurement. Results were presented in Table 3.2.

Powder	True Density (g/ml)
GA	4.44
HDH	4.47

Table 3. 2 True density of both samples measured by Pycnomatic

3.2.1. Shape characterisation

XMT is a non-destructive, relatively fast and accurate method for high-quality and detailed analysis of single particle physical properties such as sphericity, surface area, volume and aspect ratio, which all have significant effect on the quality of powder bed. Shape characterisation of particles has been historically studied by G3 morphology, QuicPic, electron microscopy and more recently XMT (102, 103). The relationship between particle shape and flow characteristics has not been extensively studied, and studies are mostly limited to flow of spherical/ spheroidal particles (104) and it is great importance to predict the flow behaviour of irregularly shaped particles.

Bumiller et al. (2002) suggesting that particle shape might have significant effects on powder flow properties by using shear cell for assessing the flow properties of glass sphere, calcium carbonate crystal and plate shape talc powder; three dissimilar materials in morphology but similar particle sizes (105). Podczeck and Mia (1996) investigated shear properties of 8 different powders with different size and shape and they concluded the particle size and shape have great influence on powder flow factor and internal angle of friction (106). Yu et al. (2011) presented in their work that both particle size and shape play an important role in

determining the powder flow behaviour by studied numerically the bulk powder flow of twenty-three powder with various particle size and shape distribution (107). All these researches concluded that both particle size and shape play important role on shear parameters, flowability but did not differentiate between effect of particle size and the effect of particle shape.

In this research, the XMT (MicroXCT, Xradia Versa 410) at the University of Leeds was used for particle shape analysis. The device shown in Fig. (3.5), it consists of X-ray generator, a Sample stage and charge-coupled detector.
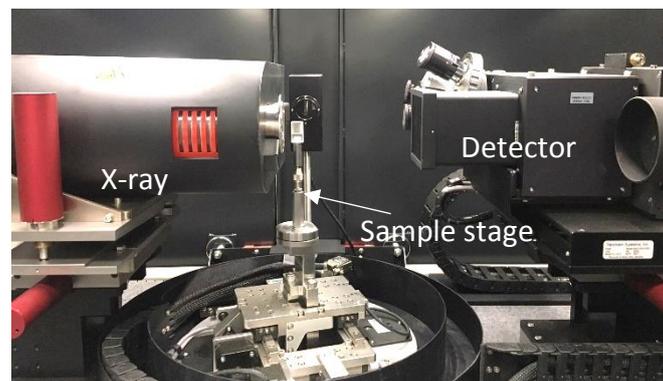
Figure 3. 5 Inside the Micro XCT, Xradia Versa 410

During the experiment X-ray with photon power of 140 kV and current setting of 70 μA were used to acquire series of projection images as sample was rotating. The acquisition conditions and parameters of XMT has been presented in Table (3.3).

X-ray Device	Voltage (kV)	Current (μA)	Filter	Exposure time (s)	Number of projections	Voxel size (μm)
Zeiss Xradia Versa	140	70	HE2	12	1600	7.4

Table 3. 3 Acquisition conditions and parameters of XMT

To separate particles in order to calculate their equivalent diameter, volume, sphericity and other shape parameters, the "*watershed segmentation*" from the Avizo® software has been used. This concept was initially introduced by Digabel and Lantuejoul (1978) and since then it has been used in several applications such as medical, soil and powders (108, 109, 110). Fig (3.6) illustrate the concept of "watershed segmentation". The binary image indicates two particles in contact with known radius (Fig. 3.6a). In Fig. 3.6b two distance local "minima" can be identified and therefore the "watershed line" can be placed between the particles in contact (Fig. 3.6c) from which the "catchment basins" can be used to separate particles.

(a)

Local minima

(b)

Watershed line

segmentation

Catchment basin

around the particle

(c)
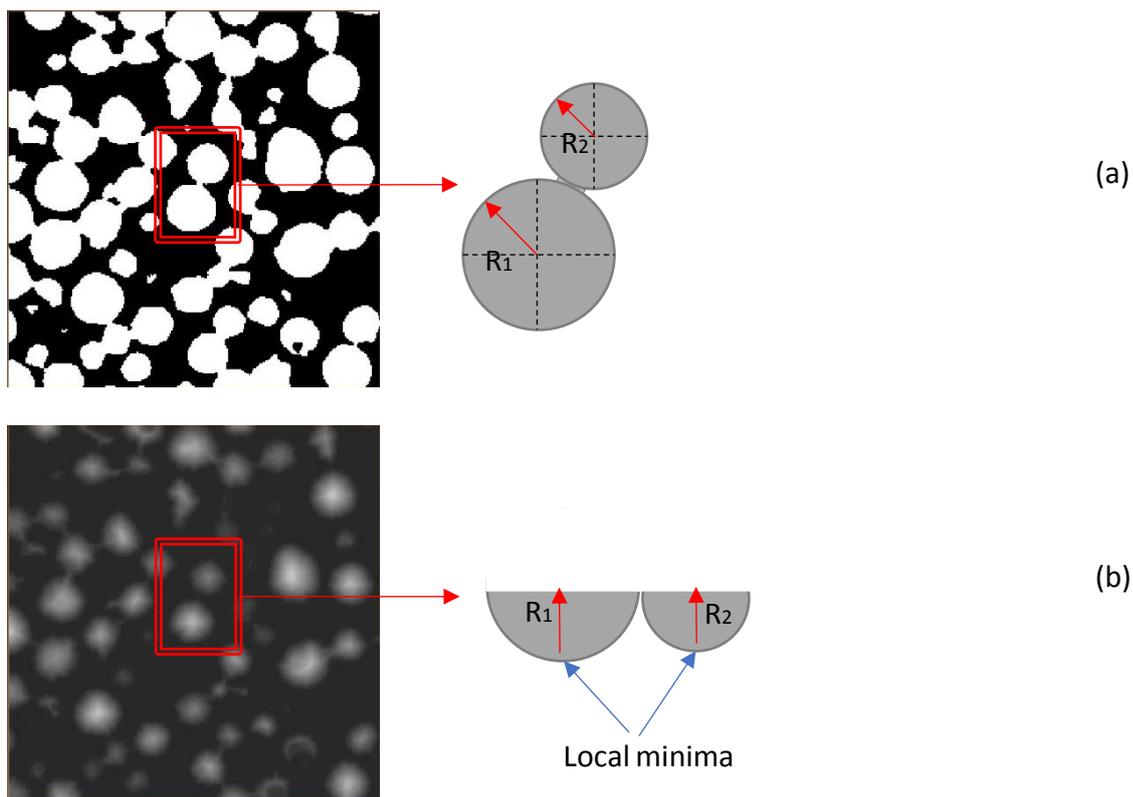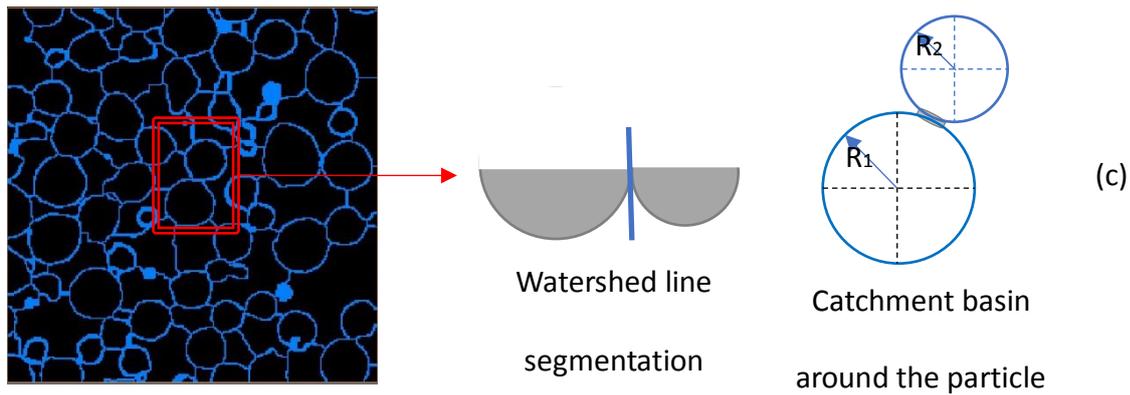
Figure 3. 6 Illustration of watershed segmentation

In this research, to improve the quality of segmentation the "marker-controlled watershed" method was used. This method has been applied by Miller et al. for several applications (111, 112). The "marker control watershed" is for modification of vicinity of local minima to improve the precision of defining catchment basin and segmentation.

The first step of this method for separation is to construct the binary image of particles by choosing the binarization range which indicates particles in contact (Fig. 3.7b). The second step is "distance transformation" to define the minima for individual particles, i.e. the bright voxel representing the particle grain, from which the particle boundaries could be identified (3.7c). Then the distance transformed image is processed by the "H-maxima" (defining a filter limit for minima) to modify number of local minima to minimise/eliminate over segmentation (3.7d). The next step involves watershed segmentation, where the whole image is considered as topographic surfaces according to the method described earlier (Fig. 3.6) to identify the "catchment basins" (Fig. 3.7e) from which particles can be separated and labelled for further analysis (Fig. 3.7f). This works reasonably well for round particles (111) while for highly irregular shapes there could be more than one minima for each object which makes the separation of wide size distribution particles very challenging (110).
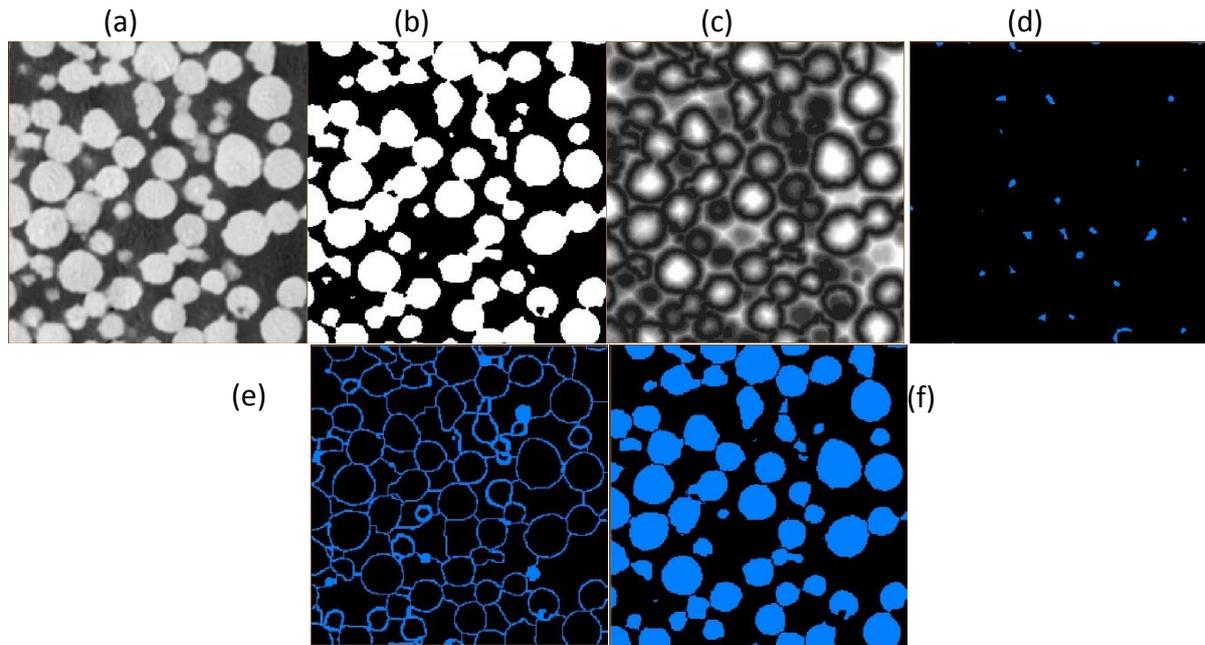
Figure 3. 7 Steps of digital separation of particles. (a) Original greyscale image of powder GA, (b) initial binary images of attached particles, (c) distance transformation, (d) H-maxima transformation, (e) image after watershed segmentation line, (f) separated particles

Wang et al. (111) established that the best results for "marker-based watershed" segmentation is obtained for particles with the particle diameter to voxel size ratio of bigger than 30 which is not the case for particles used in this study. However, there is a potential to separate the GA powders while there is an error for irregular shape particles, i.e. the HDH sample in this work, making the method unsuitable for the separation which detects several local minima for each individual particle, leading to over-segmented images (113, 114). In this case for irregular shape particles, Nadimi and Fonseca (133) introduced in-house imaging processing codes employed to segment the images to identify individual grains. They firstly binaries the images using Otsu's thresholding and subsequently apply an iterative watershed algorithm to overcome the challenges posed by the large diversity and complexity of the shapes.

In this work, in another sets of measurements the particles were placed in cotton filled sample holder to make sure they are separated and not touching each other. Then the results for both methods were compared. For GA powders there has been an excellent agreement between the d_{50} of particle obtained by the two methods, indicating the "marker-controlled watershed" is feasible to separate the particles (Fig. 3.8). However, for HDH, the results of the two methods were not comparable, making the "marker-controlled watershed" method unsuitable for individual separated particle analysis.
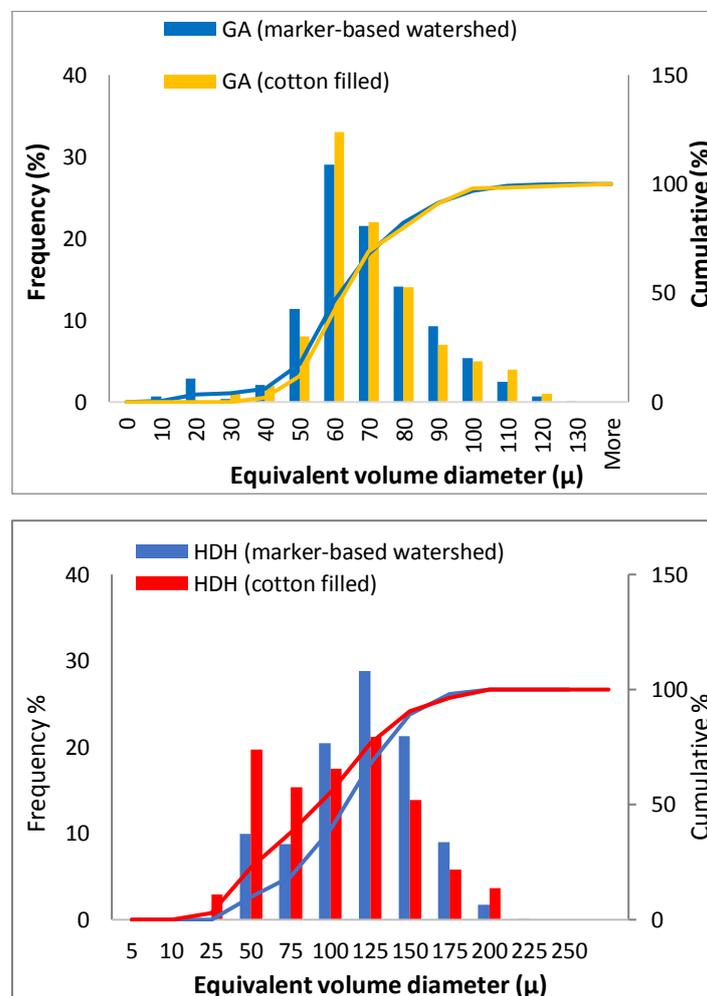
Figure 3. 8 Comparison of the cotton filled and marker-based watershed segmentation methods to characterise of particle size distribution

After segmentation, individual particles (more than 20,000 particles) for both samples were analysed for their shape factors such as "sphericity" (Ψ), "aspect ratio" (AR) and "equivalent diameters" (based on both volume and surface area). At glance, it can be observed that GA particle has more roundness and its surface is smoother as compared to the HDH particle which shows an irregular elongated shape with a high degree of surface roughness (Fig. 3.9). Further detailed quantitative shape analyses of the powders are given in the following section.
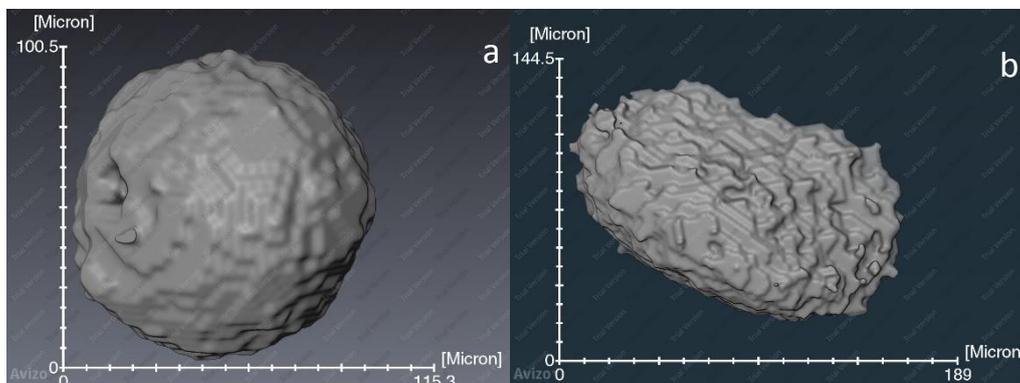
Figure 3. 9 Close up images of reconstructed particles (a) GA and (b) HDH

Based on the XMT image, a triangular mesh from the Marching Cube method which is the algorithm to divide the input volume into a discrete set of cubes can be reconstructed to provide the volume and the surface area of the particle (115). Once the triangular mesh surface of the particle is reconstructed, the equivalent diameter is based on physical properties of particles such as their volume or surface area can be determined. For non-porous particles, the equivalent spherical diameter is the measurement which is commonly used (116). This can be a reported as the "volume equivalent sphere diameter" (D_v), the diameter of sphere with same volume as the particle volume, or the "area equivalent sphere

diameter" (D_a), the diameter of a sphere with the same surface of particle. The results for GA and HDH powders based on both diameters are presented in Fig. 3.10. As would be expected for non-spherical particles there is a difference between the distributions based on the two diameter definitions. As well as overall particle shape, there is a contribution from surface pores and satellite particles in the case of GA powders and the surface roughness of HDH particles.
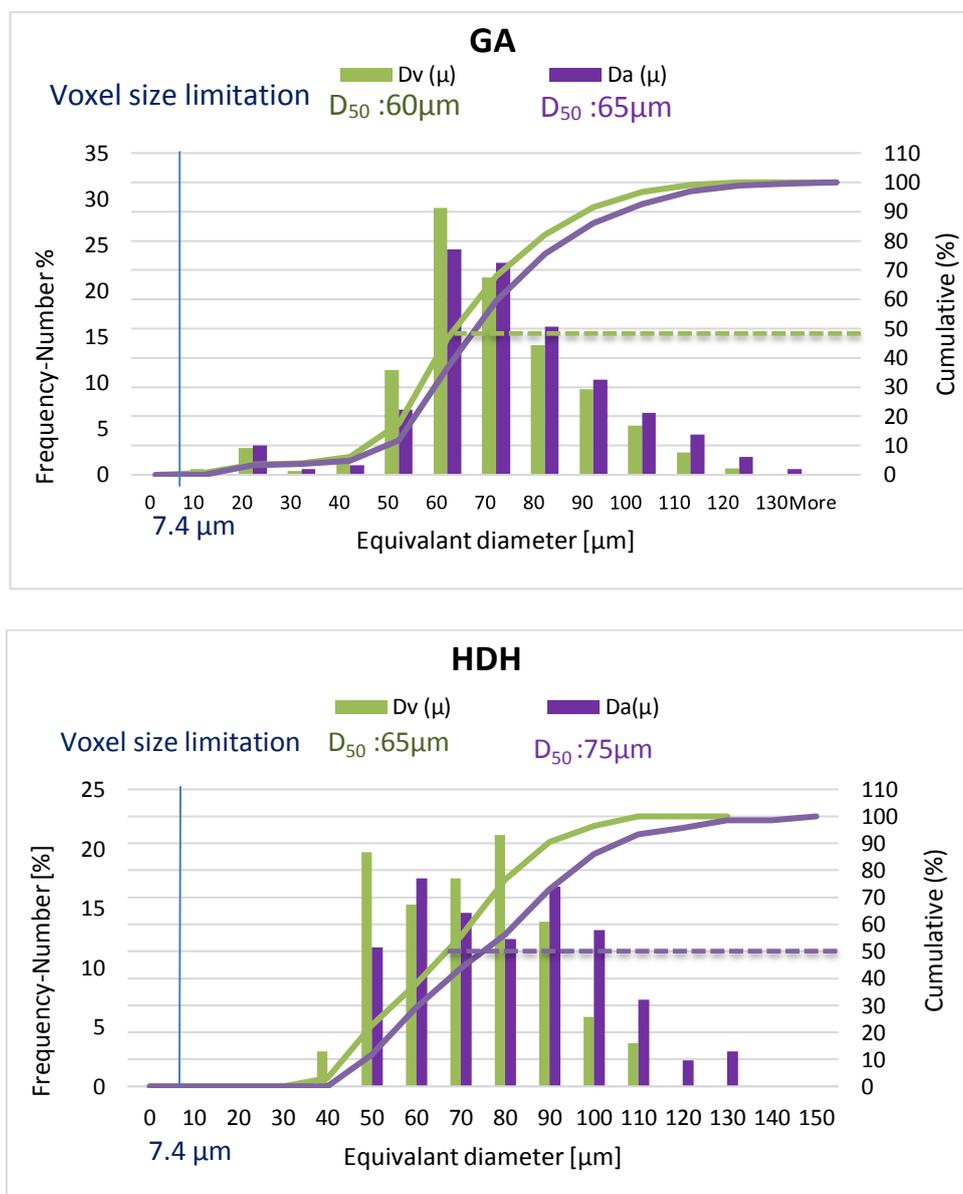
Figure 3. 10 Comparison of equivalent diameter extracted from Volume and surface area of 20,000 individual particles

Sphericity (Eq. 3.1) was measured by the ratio of surface area of a sphere with same volume as the given particle to the surface area of the particle using the correlation shown below:

$$\psi = \frac{\pi^{1/3}(6V_p)^{2/3}}{A_p}$$

Equation 3.1

Where V_p is volume of given particle and A_p is its area.
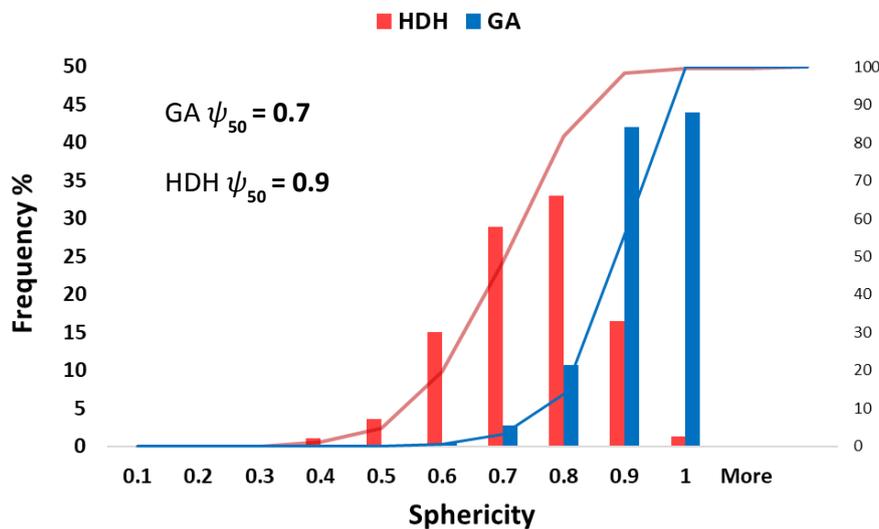
Figure 3. 11 Sphericity of GA and HDH samples

As can be seen from Fig. 3.11, majority of GA powders have nearly spherical shape unlike the HDH powders. Some GA particles have satellites (e.g., in Fig 3.12a) with the sphericity in range of 0.8 to 09. In addition, there are occasional concave shape (e.g., Fig.3.12b) as well as nearly spherical but hollow (e.g., Fig. 3.12c-3.12d) GA particles with sphericity ranging 0.6 to 0.8. Liu et al (2019) characterised different 2D shape factor and size of Ti6Al4V by shape analyser and scanning electron microscope and found the average roundness of Gas atomized (GA)

particles are 81%, the average elongation is 84%, and there are 52% of powders without satellites (117).
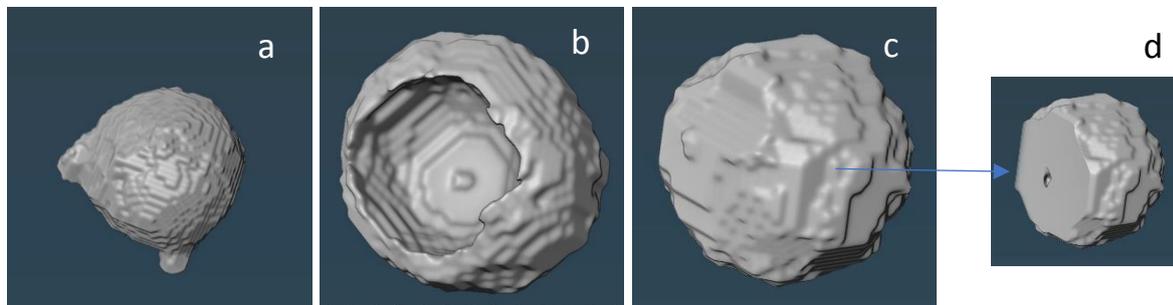
Figure 3. 12 Different shapes of GA particles (a) particle with satellite, (b) concave particle, (c) porous particle (d) cross section of particle c

For instance, the particle in Fig. 3.12c is nearly spherical but because it is porous, its equivalent volume diameter used in the numerator of Equation 3.1 would be underestimated as the particle volume (V_p) is given by the software as the total volume of voxels (excluding the pores). This will result in a smaller sphericity (0.85) while for similar particle (similar dimension) without the pore, its sphericity shown to be 0.98 (Fig. 3.13).
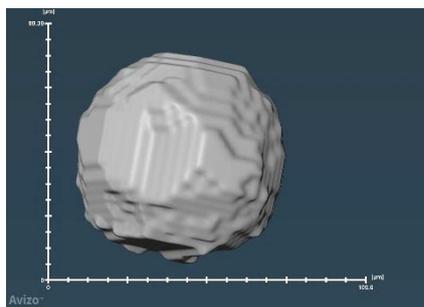
Length (µm)	Thickness (µm)	Width (µm)	sphericity
83.34	75.12	72.63	0.98

Figure 3. 13 Particle GA with dimensions and its sphericity

Recently, a new open-source software is presented to perform shape characterisation of three-dimensional non-spherical particles such as form, roundness, and surface roughness (134). However, particles with simplified geometries are required to run within the software.

The aspect ratio of a particle is the ratio of its smallest feret's dimension (d_{min}) to the largest feret's orthogonal (d_{max}) as given below:

$$AR = \frac{d_{min}}{d_{max}}$$

Equation 3.2

Where the largest and smallest feret's diameter is defined as the longest and shortest closest possible distance between two parallel tangent lines around the particle and named d_{max} and d_{min} respectively.
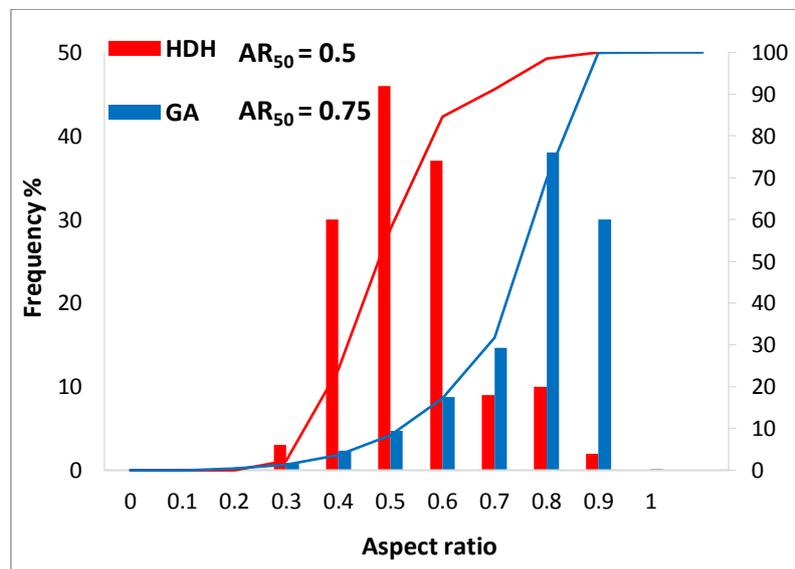
Figure 3. 14 Aspect ratio of GA and HDH samples

It is qualitatively obvious by the SEM images that HDH particles are more elongated as compare to GA particles, which is also confirmed quantitatively, from their aspect ratio results in Fig. 3.14.

Except some irregular GA particles, owing to the process of gas atomization (e.g. in Fig. 3.15a-3.15b) which have aspect ratio in the range of 0.4 to 0.7, the aspect ratio for the majority of GA powders (68%) is within the range of 0.8 to 0.9 with few occasional satellites (Fig. 3.15c-3.15d).
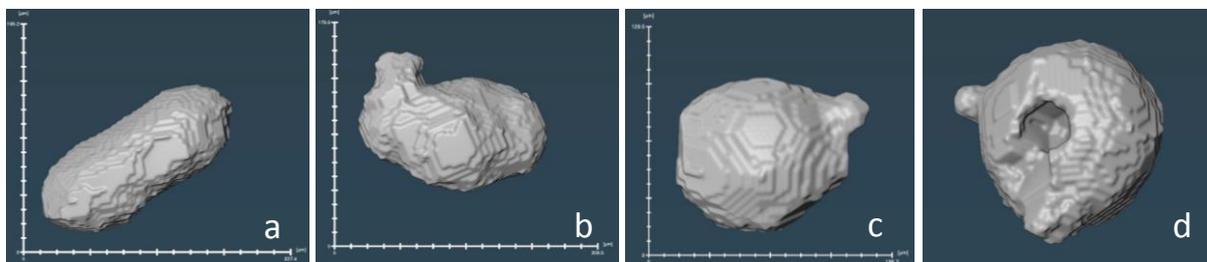
Figure 3. 15 GA particles with 0.4 to 0.8 range of aspect ratio (AR); (a) AR= 0.43 (b) AR= 0.57 (c) AR= 0.70 (d) AR= 0.83

For comparison, few hollow (with blind/ enclosed pore) and concave particles are presented in Fig. 3.16. For hollow particles despite their "envelope" spherical shape, the sphericity ranges of from 0.70 to 0.85 depending on their pore sizes. Bigger porosity results in smaller "true" sphericity. However, such particles have high aspect ratio which is not necessarily indicative of their true shape. Hence, care must be taken when comparing particle shapes based on the above parameters.

For concave particles the aspect ratio could not be a good shape indicator. There are particles with high aspect ratio that have a small sphericity due to existence of their concave hole.

Some particles have smaller equivalent diameters (D_v) than their three-dimension axes (length (L), width (W), thickness (T)), which can be found for both hollow and concave shape particles.

Pores and shape of local internal porosity could result in defects in AM built parts which are known as the most critical flaws in regard to the mechanical strength and component toughness (118).

Hollow Particles

Ψ: 0.72	Ψ: 0.85	Ψ: 0.78	Ψ: 0.89
AR: 0.86	AR: 0.91	AR: 0.88	AR: 0.90
Dv (μ): 103.6	Dv (μ): 80.4	Dv (μ): 70.6	Dv (μ): 88.2
L(μ):123.9, W(μ):107.1, T(μ):110.2	L(μ):90.4, W(μ):81.6, T(μ):82.7	L(μ):83.6, W(μ):73.8, T(μ):75.6	L(μ):99.9, W(μ):90.0, T(μ):92.5

Ψ: 0.72	Ψ: 0.86	Ψ: 0.78	Ψ: 0.80
AR: 0.84	AR: 0.87	AR: 0.78	AR: 0.88
Dv (μ): 93.7	Dv (μ): 94.9	Dv (μ): 104.6	Dv (μ): 93.0
L(μ):115.2, W(μ):97.2, T(μ):98.3	L(μ):108.7, W(μ):93.8, T(μ):97.0	L(μ):115.0, W(μ):105.9, T(μ):108.1	L(μ):110.1, W(μ):96.7, T(μ):98.1

Concave Particles

Ψ: 0.70	Ψ: 0.66	Ψ: 0.64	Ψ: 0.64
AR: 0.79	AR: 0.70	AR: 0.68	AR: 0.86
Dv (μ): 95.2	Dv (μ): 68.8	Dv (μ): 86.5	Dv (μ): 77.7
L(μ):117.3, W(μ):113.3, T(μ):98.2	L(μ):100.7, W(μ):70.9, T(μ):73.5	L(μ):135.9, W(μ):92.0, T(μ):91.2	L(μ):98.2, W(μ):84.6, T(μ):87.1

Ψ: 0.79	Ψ: 0.68	Ψ: 0.77	Ψ: 0.89
AR: 0.85	AR: 0.81	AR: 0.85	AR: 0.91
Dv (μ): 90.2	Dv (μ): 93.1	Dv (μ): 76.5	Dv (μ): 101.0
L(μ):111.0, W(μ):94.6, T(μ):93.5	L(μ):124.1, W(μ):100.9, T(μ):103.3	L(μ):91.6, W(μ):77.9, T(μ):80.8	L(μ):111.7, W(μ):101.3, T(μ):106.8

Figure 3. 16 Comparison of hollow and concave particles for their sphericity, aspect ratio, porosity and diameters

3.3. Experimental equipment

3.3.1. Tapped density

Measuring the tapped density can be used to analyse the flowability of powder as well. The Hausner ratio and Compressibility Index (47) as mentioned before are two flow indicators can be derived from bulk and tapped density.

First, to find the tapped density, the powder was weighted (100 gr) and loaded into a 250ml graduated measuring cylinder were initial volume of powder was recorded. Then the cylinder was placed on a tapped density tester JV 2000 equipment (Copley Sci., UK) and was subjected to tapping. An impact load of 5Hz was used to settle the powder by mechanically raising the cylinder and allowing it to drop at a specific distance of 3 +/- 0.2 mm under its own weight for 30 minutes until there were no change in volume.

Then tapped volume collected and tapped density "ρ_T" were measured. Bulk and tapped density were then used to calculate the Hausner ratio "HR" and compressibility index "CI".
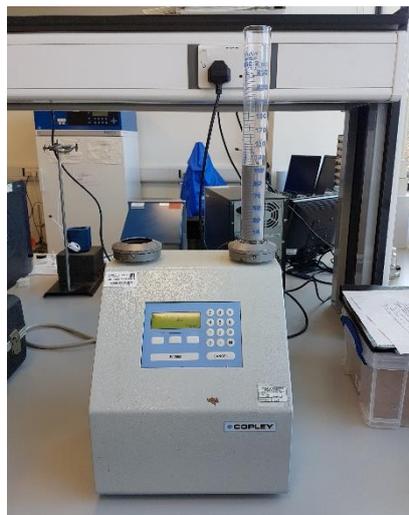
Figure 3. 17 The apparatus of Tapped density equipment

For free flow powder the value of bulk density and tapped density should be close together and the Carr index would be small. A Carr index greater than 25 indicating the poor flowability and cohesive powder while for good flow powder the Carr index would be smaller than 15 (Table 3.4).

$$CI = 100 \times \frac{(\rho_T - \rho_B)}{\rho_T}$$ Equation 3.3

Where CI is Carr Index, V_B is volume of untapped powder and V_T is tapped volume.

The Hausner ratio also could be measured by using the Carr index from following equation:

$$HR = \frac{\rho_T}{\rho_B}$$ Equation 3.4

or

$$HR = \frac{100}{(100 - CI)}$$ Equation 3.5

Where HR is Hausner ratio, ρ_T is Tapped density, ρ_B is Bulk density and CI is Compressibility Index.

Compressibility Index (%)	Scale of Flowability	Hausner Ratio
≤10	Excellent	1.00 – 1.11
11 – 15	Good	1.12 – 1.18
16 – 20	Fair	1.19 – 1.25
21-25	Passable	1.26-1.34
26-31	Poor	1.35-1.45
1.4532-37	Very Poor	1.46-1.59
>38	Awful	>1.60

Table 3. 4 Scale of flowability using the density measurement (47)

3.3.2. Angle of repose

To measure the flowability statically, the angle of repose test was performed. The developed device which is called Mark 4 Powder Research Ltd. AOR Tester as shown in Fig. 3.18 was used.
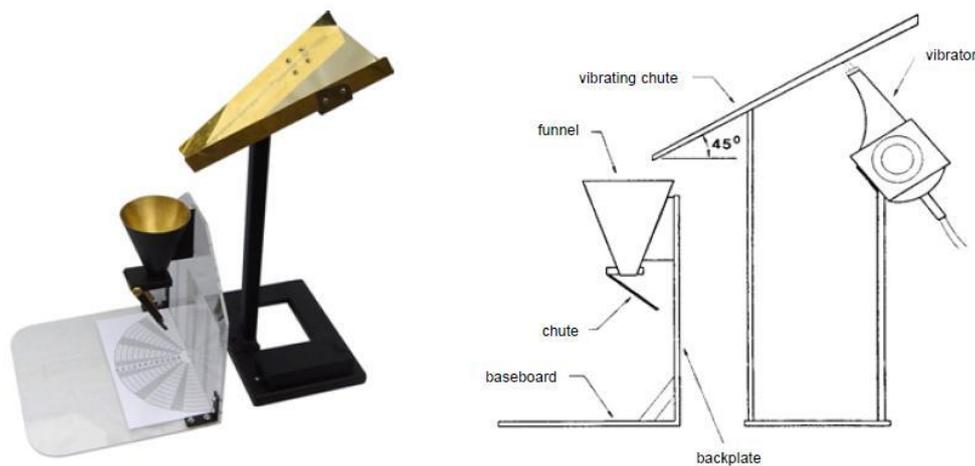
Figure 3. 18 Mark 4 Powder research Ltd. AOR tester

100 gr of sample was weighted and poured into metal beaker. As our powder is free flow it did not need vibrator but for consistency of procedure the powder was poured manually and very slowly (roughly 25 seconds) for each sample. The powders fall through the conical funnel then reached the lower chute and finally the pile of powder was settled on the base (Fig. 3.19).

The slope angle of the conical pile of powder on to the free surface (horizontal base) or the inverse tangent of the ratio of height of pile to half of the base is angle of repose. The test was repeated three times for each sample. The angle also measured by using a digital camera both angle of each side of pile were found and averaged.

25° - 30°	**Excellent flowing**
31° - 35°	Good
36° - 40°	Fair- aid not needed
41° - 45°	Passable- may hang up
46° - 55°	Poor- must agitate
56° - 65°	Very poor
>66°	Very, very poor

Table 3. 5 Classification of flowability using angle of repose (57)
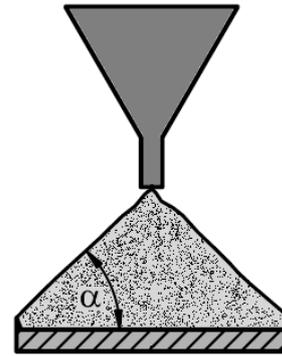
Figure 3. 19 Angle of repose

The scale of flowability in Table 3.5 indicating that smaller angle represents better flowability. The angle of repose depends on the physical properties such as, density, particle size and shape, moisture content (119). The angle of repose greater than 45 degree indicating cohesive powder and for free flow powder the angle would be less than 25 degree.

3.3.3. Dynamic angle of repose (Rotating drum)

Another method was dynamic angle of repose using GranuDrum supplied by Granutools™. It consists of horizontal rotating drum covered on both sides with transparent glass, filled with powder and a camera in front to rotate at different rates. The glass sided drum was loaded of 100g of each powder and rotated at range of 2-4-6-8-10 rpm and a CCD camera collected snapshots and data for each rotating speed. The avalanche angle is the angle of powder surface just before avalanche starts to the horizontal line. The method behind the technique is that, by rotating the drum sample happened to increase the angle of inclination up to unsteady situation from which it will avalanche and the camera capture image of the powder free surface and the movement of avalanches inside the rotating drum (Fig. 3.20).
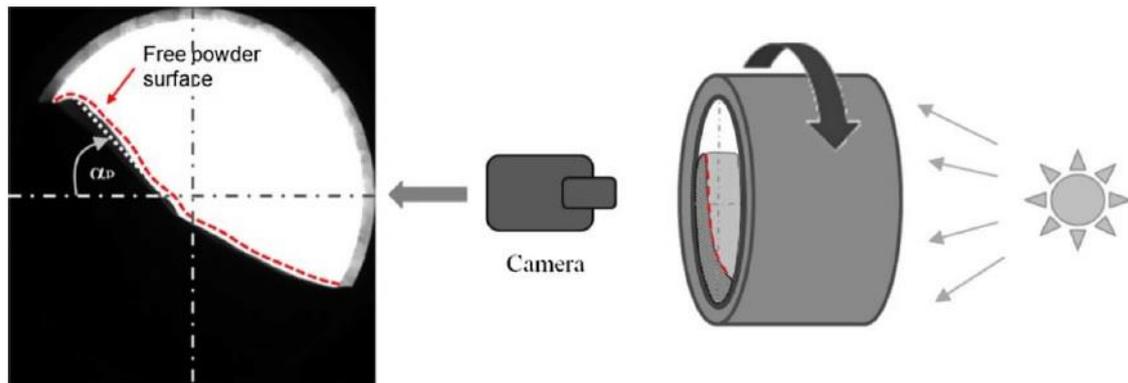
Figure 3. 20 Schematic of avalanche angle measurement

It should be noted that the higher the value of avalanche angle, the worse the powder flowability. A low value of the flowing angle corresponds to a good flowability.

3.3.4. Flowmeter

Powder flow rate was investigated by using the GranuFlow (Granutools ™) which consist of 300 mm stainless steel cylinder and rotating plate with various orifice diameters (Fig. 3.21). 200g of each powder poured with funnel in cylinder and rotating plate with orifice size of 4, 6, 8, 20 and 12 mm positioned under the cylinder. The powder was discharge from smallest orifice and then plate rotated manually to the bigger one and the weight of sample for each orifice were measured. The data analysis software was obtained mass flow rate for each aperture size.
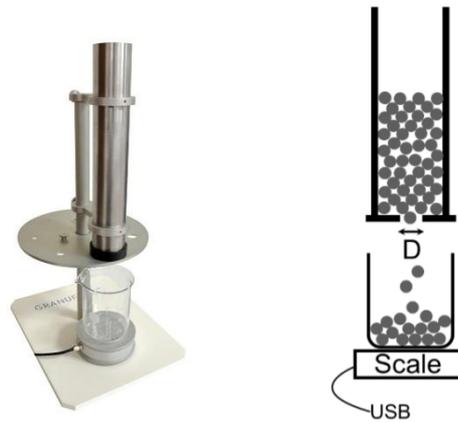
Figure 3. 21 Granuflow and the principle of measuring powder flowrate

Another method to evaluate powder flow rate was using inhouse made powder flowmeter at the university of Leeds to assist the minimum orifice diameter, hopper angle, minimum column height of powder inside the hopper and the critical stress where shows the condition where the powder stop to flow (Fig. 3.22). These results are important regarding to the process of EBM in additive manufacturing, when the powder stored in two hoppers, which are located on both sides of build chamber.
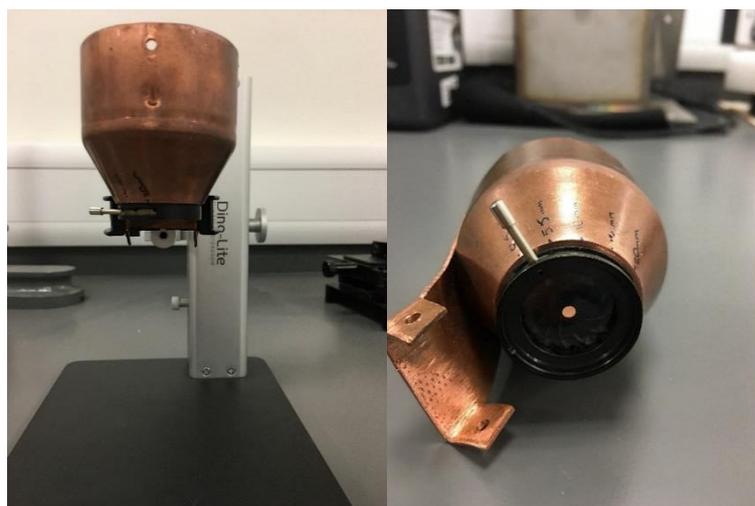
Figure 3. 22 In-house flowmeter (a) whole set-up (b) close-up look at orifice adjustment

The flowmeter consists of hopper with 50 mm diameter, 25 mm height, 30-degree angle and base with adjustable iris shape orifice with opening size from 0 to 20 mm. The experiment was performed in accordance with ASTM B213 standard test method. A 30g of each powder gently poured to hopper while the orifice on the bottom was completely closed, then it was slowly opened at 1mm and allow powder to flow.

3.3.5. FT4 rheometer

Dynamic testing of the metal powders was carried out to determine any difference between the flow behaviour of the powders. The measurements were carried out using a standard FT4 powder rheometer (Freeman Technology Ltd., UK) (Fig. 3.23). The standard test procedure is as follow; the vessel filled with the powders and samples were pre-conditioned the impeller blade (5° helix angle and 23.5 mm diameter) which forces the powder downwards at constant speed of 60 mm/s, towards the bottom of the vessel (25.0 ml), clockwise to gently create a reproducible low stress packing bed, then moves upwards at the same speed. Next the extra powder will be removed from top of the vessel by splitter. The pre-conditioning step removes any packing history and gives rise to the formation of a more uniform powder bed to ensure reproducible data. Following this, dynamic flow properties were will be determined by rotating the blade with chosen helix angle and speed (anti-clockwise) to move vertically to the powder bed.
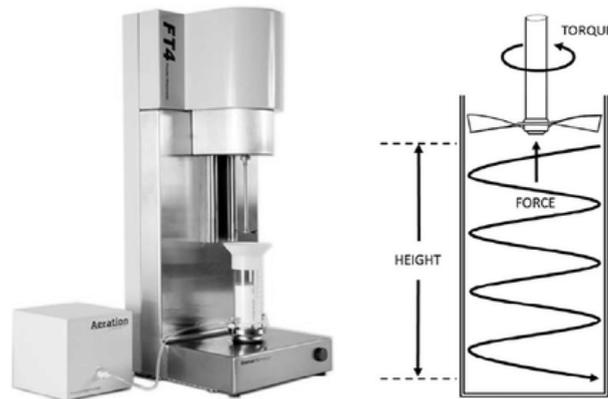
Figure 3. 23 FT4 rheometer tester (71)

A standard protocol for measuring the flowability energy was employed, involving 11 consecutive tests. The first 7 tests are carried out at the same blade speed (100 mm/s), followed by the remaining 4 tests carried out at reducing blade tip speeds (100, 70, 40 and 10 mm/s). Prior to each individual measurement, the powder was again conditioned according to the instrument's methodology. The dynamic testing of the samples was performed in three replicates.

3.3.6. Ring shear cell

The Schulze ring shear tester is improvement of the Jenike tester for measuring flow properties, wall friction and bulk density. All measurements of the both samples, performed by Schulze Ring Shear Cell RST-XS at the University of Leeds. The Schultze shear cell is consisting of bottom annular ring-shaped cell, where the powder is placed and a lid. There are series of radial vanes on lid and on the base, which prevent the powder from slipping during the shearing process. The lid is connected to vertical rod which is applying normal force to make compaction at desire level. The sample bed is subjected to rotating bottom to make

shear stress with angular velocity of ω (Fig. 3.24). For continuously monitoring the procedure there are two tie rods which is connected to the lid of ring cell (71).
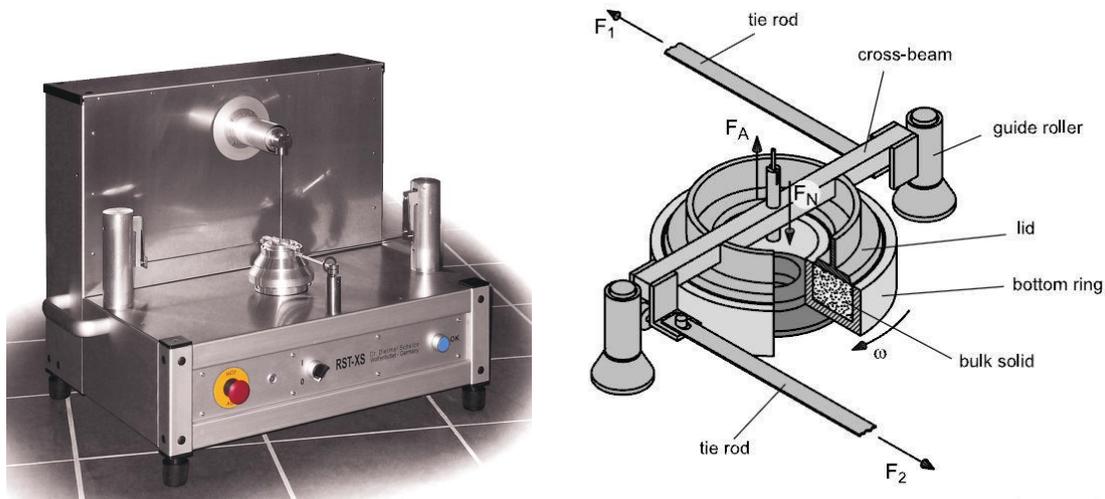
Figure 3. 24 Ring shear cell RST-XS (58)

Then, the sample is sheared with an increasing stress up to the point that the powder start to fail, and consequently starts to flow. The stress at failure is the unconfined yield strength, σ_c, of the material (69). The flow factor is the ratio of the major principal stress applied over the unconfined yield strength of the material at this consolidation stress, as shown in Equation 3.6:

$$ff_c = \frac{\sigma_1}{\sigma_c} \qquad\qquad \text{Equation 3.6}$$

Based on flow factor value Tomas and Schubert (1979) categorised powders as shown in Table 3.6.

ff_c value	Flow behaviour
<1	No flowing
1-2	Very cohesive
2-4	Cohesive
4-10	Easy flowing
>10	Free flowing

Table 3. 6 Classification of powder flow based on flow factor value

3.3.7. Ball indentation

Ball indentation was investigated using the Instron 5566 mechanical testing machine (Instron Corp. USA) with constant strain rate of 0.1 mm/min and maximum load of 10 mN, which kept the testing at quasi-static conditions.

Figure 3. 25 Ball indentation process

The samples were first consolidated in a die by a stainless-steel piston using a 10 N load cell which has a resolution of 0.25 mN (Fig. 3.25a,b).

The properties of glass indenter are given in Table 3.7. According to standardisation of ball indentation of Zafar et al. (79) samples were fed into the die through the sieve method to gives a uniform filling.

Diameter	8 mm
Roundness	>0.99 (ratio width/length)
Bulk density	Mean value 1.53 kg/m^{-3}
Young's modulus	65 Pa
Hardness	>6 GPa
Roughness	0.08 μm

Table 3. 7 Properties of glass indenter (106)

Indentation hardness test were carried out at 10 mN load using a spherical glass indenter of 8 mm diameter. The ball indentation load was chosen in regard to the penetration depth of ball in powder bed to be more than 40% of the indenter radius to give a reliable measure of the yield stress (106). Three repeats were carried out for each test for finding error values. The tests were carried out under ambient conditions, at a temperature of 20-25^0 C and relative humidity of 40-60%.

Ball indentation can provide flow behaviour of powders at low consolidation pressures. However, at these pressures powder flow behaviour is dependent on conditioning and packing configuration of the powder bed.

The XMT technique has been used to analyse the ball indentation process quantitatively and to visualize of radial and axial packing fraction of entire bed, the effect of wall on powder, the effect of indenter size on confinement region and localise packing fraction of powder for loose or at low stress compaction. Detailed study of XMT to investigate how the packing density

could change in different regions of the powder bed as a result of consolidation and indentation processes are presented in Chapter 5.

Chapter 4   Assessing Powder Flowability Characterisation of Different Grades of Titanium Powders

4.1. Introduction

An important factor to characterise the powder flowability in this research is whether the technique could replicate the region of consolidation and shear stress of AM system (<1 kPa). The objective of this chapter is to use common flowability techniques outlined in section 3.2 in order to determine how powder behaves as bulk in various techniques and correlate the powder flowability characteristic with powder spreading. Furthermore, the reliability of the ball indentation technique and the effect of different filling systems (poured and tapped) were carried out and the determination of constraint factor is discussed. As described before, the hardness measurement is related to the unconfined yield stress (Y) by the constraint factor (C). Therefore, the unconfined yield stress measured by standard and low shear cell tests are also reported in this Chapter.

Powder flow properties characterisation have been used to determine the hopper angle, minimum column height of powder inside the hopper, and the critical stress (the condition where the powder stops to flow) for both GA and HDH powders and different methods for their deamination have been discussed. These results are important regarding the process of EBM in additive manufacturing when the powder is stored in two hoppers, which are located on both sides of the build chamber.

4.2 Powder flowability measurement assessed by different techniques

4.2.1 Density and compressibility

Tapped density tester JV 2000 equipment (Copley Sci., UK) at University of Leeds was used in this study for the characterisation of the powder density and compressibility which described in previous chapter (3.3.1). First both samples were weighted and then poured freely into the measuring tapped density cylinder. Then the test has been started with impact load of 5 Hz and the data has been collected every minute.

From the following data bulk density of both samples have been measured, then the cylinder was placed on the tapping machine and tapped for 30 minutes which there has not been any change to the volume afterwards (Fig. 4.1).
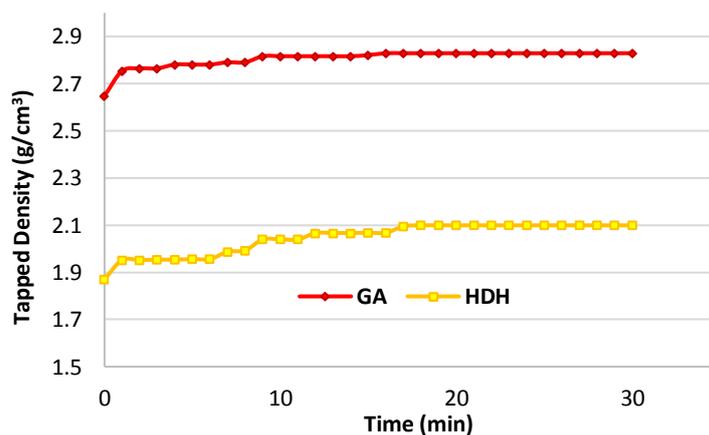
Figure 4. 1 measurement of tapped density as a function of time

Then the volume of both samples has been recorded then the tapped density of both samples has been measured. From both tapped density and bulk density, Carr index and Hausner ratio

were calculated from equations (3.3 and 3.4) and presented in Table 4.1. Each test was repeated 5 times for readability of results.

Powder	Bulk density (g/ml)	Tapped density (g/ml)	Hausner Ratio (H)	Compressibility index (CI) %	Scale of flowability
GA	2.6	2.8	1.07	7.1	Excellent
HDH	1.9	2.1	1.10	10.5	Good

Table 4. 1 Scale of flowability related to tapped density for both samples

It can be seen that the GA powder reached to steady state sooner than HDH powder indicating that spherical GA powder would settle more easily than irregular shape HDH powder. The Compressibility Index for GA was found to be 7.1, and the Hausner Ratio was determined as 1.07, indicating that this powdered sample would be classed as free flowing. HDH powder has a compressibility index of 10.5 which indicates that the powder would still exhibit good degrees of powder flow.

4.2.2 Angle of repose

Another common method to measure powder flowability is angle of repose. To measure this angle both samples have been tested under the ambient lab conditions (same temperature and humidity) and have been done with high consideration to make sure the angle and rate of pouring of powder to the device would be the same for each run. Each sample was tested three times and results were very close as can be seen in Table 4.2. The illustration of angle of repose for both samples are presented in Fig. 4.2.
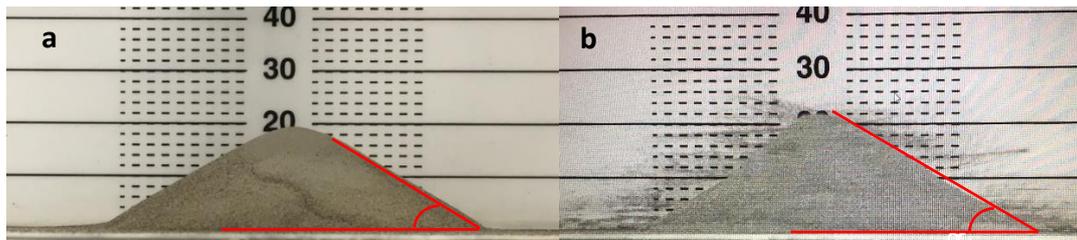
Figure 4. 2 Experimental set up of AOR on (a) GA and (b) HDH samples

The average result shown in Table 4.2 for GA was 27.1° while HDH had angle of 31.5°. Both samples shown good flowing however GA had a smaller angle of repose and been categorized as free flow and therefore have a better flowability compare to HDH which is categorised in easy flowing regime due to more inter-particulate friction or resistance to movement between particles. As can be seen from Fig. 4.2b the HDH powder scatters more due to more adhesion between HDH powders and surface of the angle of repose equipment compare to the GA powders.

	Angle of repose	Scale of flowability
GA	27.1 ± 0.17	Excellent
HDH	31.5 ± 0.35	Good

Table 4. 2 Angle of repose results for both samples

4.2.3 Dynamic angle of repose (Avalanche angle)

To measure avalanche angle 100g of sample was used and the results were collected for each rotating speed as explained in Section 3.3.3. Fig. 4.3 presents the illustration of both powders

just before and after the first avalanche at 2rpm. Each powder was run three times and the average avalanche angle was calculated as 33.4° for GA powder and 46.5° for the HDH powder. The observation of both samples indicates powder HDH formed the higher surface fractal as a result of cohesiveness and inter-particle force due to their shape and surface roughness. Similar to the angle of repose, the HDH powder scatters and sticks to the equipment wall as seen in Fig. 4.3.

GA:

	Angle [°]: 33.4
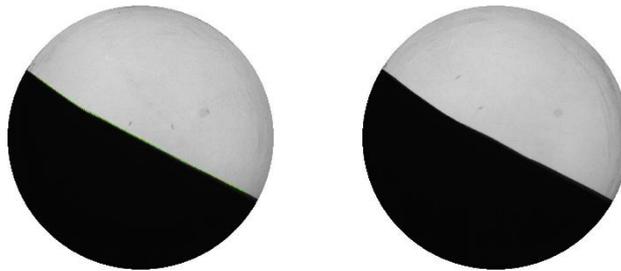
HDH:

	Angle [°]: 46.5
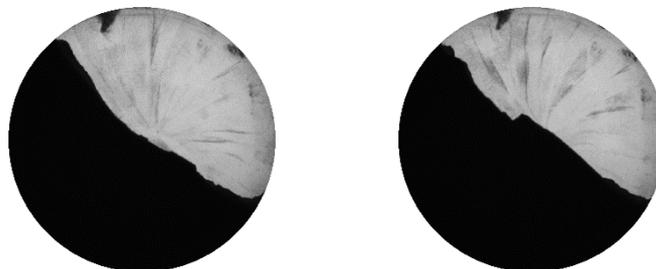
Figure 4. 3 Illustration of surface fractal and avalanche angle for top (GA) and bottom (HDH) powders just before and after avalanche happening

It should be noted that a high the value of avalanche angle indicates to a poor powder flowability.

4.2.4 Powder flowrate

Powder flow rate was investigated by using the GranuFlow (Granutools ™) at the University of Surrey, which consist of 300 mm stainless steel cylinder and rotating plate with various orifice diameters. 200g of each powder was poured with funnel in the cylinder with the orifice sizes of 4, 6, 8, 20 and 12mm. The powder discharge was examined starting from the smallest orifice to the biggest one and the weight of sample for each orifice were measured. The mass flow rate was obtained from the data analysis software for each aperture size. The plot of mass flux versus aperture size presented in Fig. 4.4. Results are the average of three repeats.
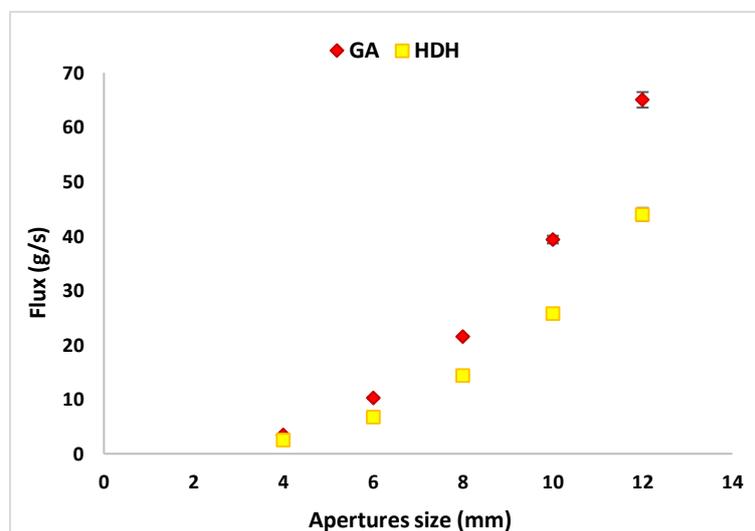
Figure 4. 4 Mass flow rate profile for GA and HDH powders

The mass flow rate of GA increase more with orifice size than the HDH powder, indicating a better flowability of GA powders.

To evaluate powder flow rate under smaller orifice sizes an in-house powder flowmeter was developed at the University of Leeds to identify the minimum orifice diameter for flow (Fig. 4.5). The 30g from each powder was gently poured into the hopper while the orifice on the bottom was completely closed, then it was slowly opened until at 1mm powder started to flow. If orifice hole at the bottom of hopper become visible, then the smallest orifice that enabled the powder flow can be identified, which is commonly known as "flow index" (120). Fig. 4.5 shows that despite of the same flow index (1 mm) for both GA and HDH powders, powder HDH exhibits behaviour similar to rat-holing phenomenon. Which occurs when discharge of powders takes place only in a flow channel located above the outlet and all powder flow from other part of hopper stops.

(a) (b)
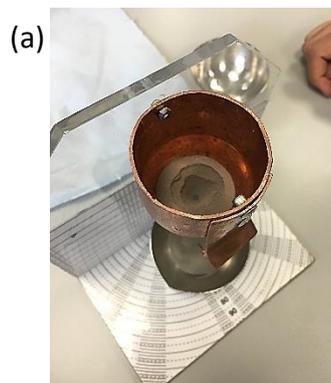
| The flowmeter technique for GA powder indicating that powder discharge easily at 1 mm orifice size. | The flowmeter technique for HDH powder demonstrating powder creating rat hole at the 1 mm orifice size. |
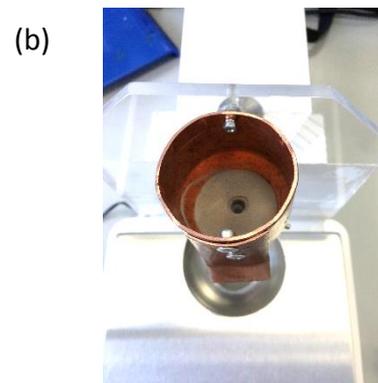
Figure 4. 5 Top-down view of the flow channel formed inside the cylinder at 1 mm orifice for (a) GA powder and (b) HDH powder

4.2.5 FT4 rheometer

Freeman FT4 powder rheometer has been used to determine powder flowability in a dynamic regime. Results have been presented in Fig. 4.6 which shows a sequence of 11 flow tests for both samples. The error bar represents the standard deviation of three repeats. The first seven tests performed at 100 mm/s speed of rotating blade moved vertically through the sample, with conditioning between to form the stability test, followed by the remaining 4 tests at variable blade tip speeds (100, 70, 40, and 10 mm/s).

For HDH powders significantly larger energy, as compared with GA powder, was required to displace the conditioned powder for an individual test. Also, a significant increase in flow energy levels with reducing blade speeds (70, 40, and 10 mm/s) compared with those measured in constant flow rate zone, signifies increasing levels of cohesion and friction within the powder bed. The non-cohesive powders are less sensitive to flow rate changes. GA powder has shown no significant change in flowability energy, which is classified as a stable powder.
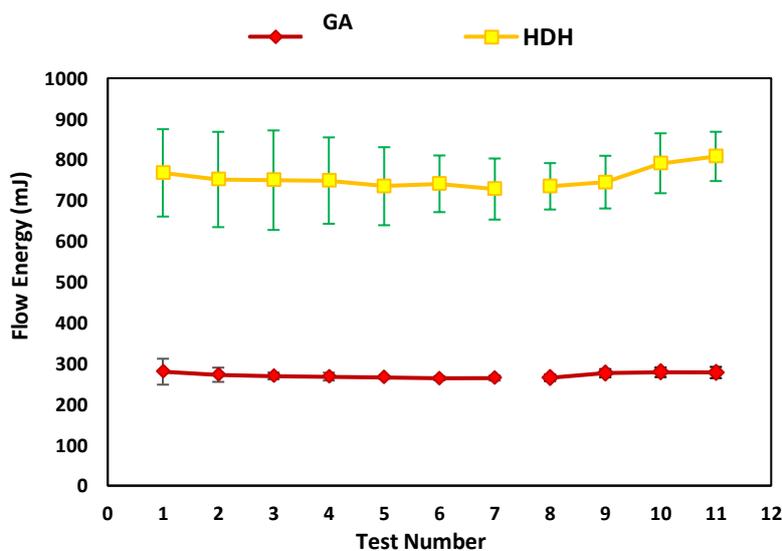
Figure 4. 6 Flow energy measurement at fixed and variable blade tip speed

The dynamic testing of the samples was performed in three replicates. The mean values of the parameters measured with the stability test are presented in Table 4.3. The basic flow energy (BFE) which described in the Section 2.3.2.3 section is presented for the energy required to displace the powder during downward movement of the blade, while the specific energy (SE) which is the energy to move powder upward movement, indicates how the powder will flow in a loosely packed state. The higher values of BFE and SE for HDH powder compare to GA powder indicating a less flowability of HDH powder due to its irregular particle shape and particle interlocking.

Samples	BFE (mJ)	NBFE	SI	FRI	SE (mJ/g)	CBD (g/ml)
GA	264.24 ± 6.28	4.88 ± 0.64	0.95 ± 0.12	1.05 ± 0.02	2.02 ±0.21	2.19 ± 0.29
HDH	728.09 ± 75.01	20.62 ± 2.20	0.95 ± 0.03	1.10 ± 0.01	6.28 ± 0.60	1.41 ± 0.01

Table 4. 3 Parameters used to describe flow behaviour, derived from Freeman FT4 rheometer

Conditioned Bulk Density (CBD) which corresponds to the density of a sample inside the vessel of FT4 after the pre-conditioning step shows that the powder HDH again demonstrates poor packing behaviour as compared to GA powder. Also, higher Normalized Basic Flowability Energy (NBFE) which is equal to the ratio of BEF to the sample mass, once again shows powder HDH demonstrates greater cohesion between the particles and poor flow in a low-stress situation.

4.2.6 Shear cell

4.2.6.1. Schulze ring shear cell RST-XS (Standard)

Typically, the shear test could be divided into two steps: pre-shear and shear steps. The shear velocity is between the range of 0.05 - 30 mm/min. The sample is prepared with optimized consolidation stress and then the failure point for each shear stress value is obtained. Each flow function consists of five yield loci (failure points) which are the points that at each normal stress, the maximum shear stress (shear stress to initialize the flow) is obtained. These yield points could make a roughly straight line that is called yield locus. Once the yield locus is found than the two Mohr's circle can be derived, which yield locus is their tangent. From Mohr's circle the major consolidation stress (σ_1) and corresponding unconfined yield stress (σ_c) can be obtained (Fig. 4.7).
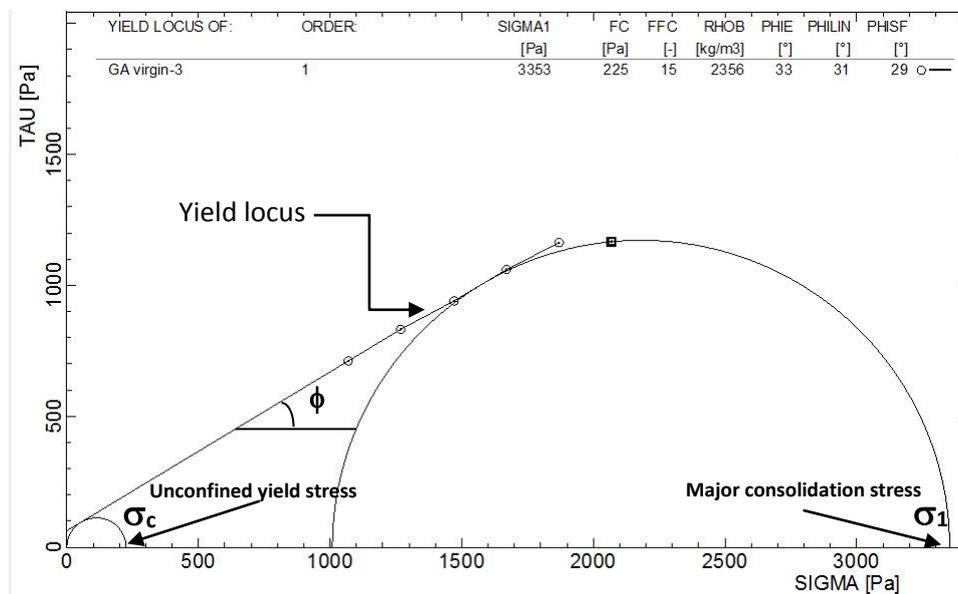
Figure 4. 7 Illustration of the Mohr's circle, major consolidation stress (σ1) and unconfined yield stress (σc), internal angle of friction and yield locus for GA powder

Analysis of shear tests results in a plot of flow function (FFc) which corresponds to ratio between the major consolidation stress (σ_1) and the unconfined yield stress (σ_c) are presented in Fig. 4.8. It should be noted that for the values of major consolidation stress the pressure on powder by its own weight needs to be considered. This is because shearing takes place roughly in the middle of the powder bed, hence half of pressure due to the weight of powder can be added to the major consolidation stress, assuming there is little effect from wall friction. Therefore, 261 Pa for GA powders and 263 Pa for HDH powders, according to the shear cell ring dimension (height) and the powder bulk density has been added to the value of major consolidation stress. The larger FFc value means the better flowability of powder.
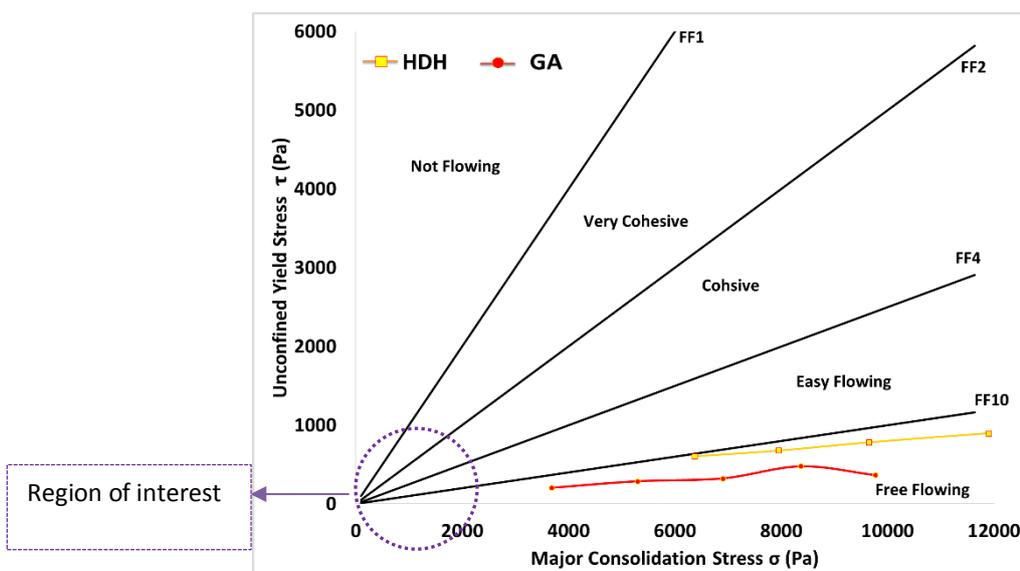
Figure 4. 8 Ring shear test results for both samples GA and HDH (Ti6Al4V)

Also, the internal angle of friction (φ_e), which is caused by particles' contacts against each other could be found from the yield locus points. For sample GA the average internal angle of friction is 32° while it is 43° for HDH. It shows that due to the rougher surface of HDH, the particles tend to interlock more to each other and generate more friction. The flow function

(FFc) at 6109 Pa consolidation which corresponds to the smallest major consolidation for HDH sample, and the average internal angle of friction and wall friction of both samples are presented in Table 4.4. The flow function at this major consolidation stress, which has been found by interpolation, indicates that both powders are in the free flow region.

	GA	HDH
Flow function at 6109 Pa	19.5	10.06
Internal angle of friction (°)	32	43
Wall Friction (°)	11	14

Table 4. 4 Powder flow properties driven from standard shear cell results

However, the region of interest for AM application while powder is going through very low consolidation stress still needs to be obtained.

4.2.6.2. Schulze ring shear cell RST-XS.s (Low consolidation)

The flow properties of powders at lower consolidation stress were determined with the use of a relatively new shear cell ring RST-XS.s at the University of Surrey. These tests were performed at low pre-shear stresses which normally are not achievable with standard shear cells, to examine the flow behaviour in a low-stress range. The powder flow function as a plot of the unconfined yield strength versus the major principal consolidation stress is presented in Fig. 4.9.
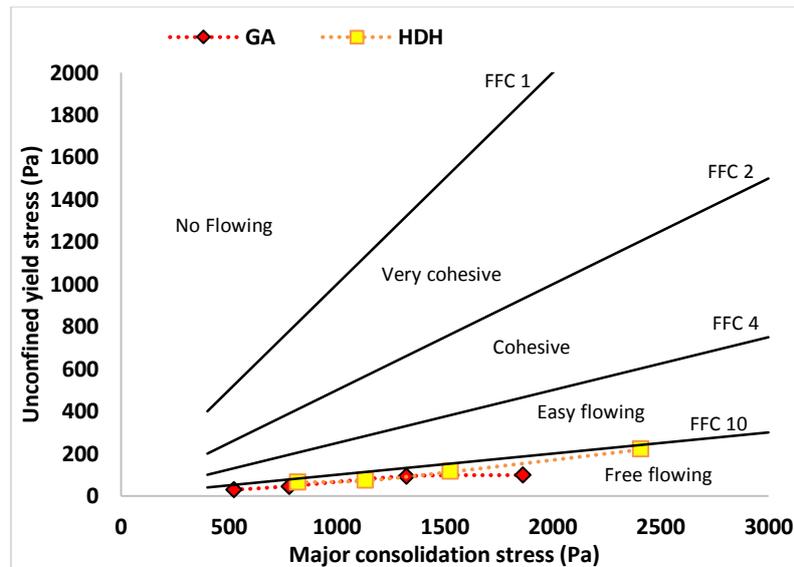
Figure 4. 9 Ring shear RST-XS.s test results for both samples GA and HDH (Ti6Al4V)

Fig. 4.9 shows that at low consolidation stress (<2 kPa) the HDH powder flow behaviour improves and gets closer to the GA powders. It should still be noted the minimum consolidation stress which gives reliable results for GA powder was around 521 Pa after adding the weight of the powder to the major consolidation stress extracted by shear cell software. It is calculated as a 261Pa (weight of the sample) plus the 260 Pa (major consolidation stress) from the shear cell. The same process was repeated for HDH powders (adding the 263 Pa weight of sample to 558 Pa from shear cell). Results from Table 4.5 indicate that at 821 Pa major consolidation stress (the smallest stress for HDH powders and interpolated for GA powder), the flow function is 16.64 for GA and is 12.9 for HDH (categorised as a free-flowing for both powders). Therefore, powder flowability with lower consolidation stress (under 500Pa) still needs to be found.

	GA	HDH
Flow function at 821 Pa	16.64	12.9
Internal angle of friction (°)	32	44

Table 4. 5 Powder flow properties driven from low-stress shear cell results

4.2.7 Ball indentation

In order to determine powder flowability at low stresses (≤ 0.5 kPa), the ball indentation technique was used to investigate the hardness of both samples by using the Instron 5566 mechanical testing machine (Instron Corp. USA) with a constant strain rate of 0.1 mm/min and maximum load of 10 mN which kept the testing at quasi-static conditions. Fig. 4.10 shows a setup of ball indentation which is consists of the ball indenter with high precision spherical glass ball indenters (8mm) by Sigmund Linder GmbH (type M) which was fixed to the top of the loading rod using super glue, a stationary anvil, and the die made of stainless steel with an inner diameter of 20 mm.
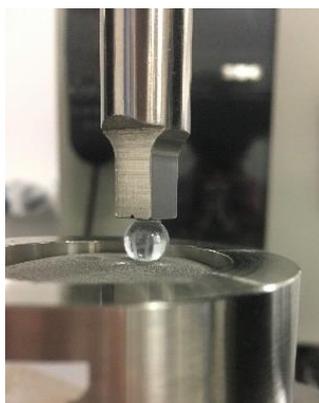
Figure 4. 10 Experimental set up of ball indentation

4.2.7.1. Effect of various consolidation pressure on hardness and packing fraction

Hassanpour and Ghadiri, (2007) introduced a method to evaluate the bulk powder hardness. However, this method was not used for AM powder with a high grade of flowability. According to the standardisation of ball indentation by Zafar et al. (106) samples were fed into the die through the sieved method for a uniform filling. Then the surface was scraped by a piece of paper to give the smooth and flat powder bed.
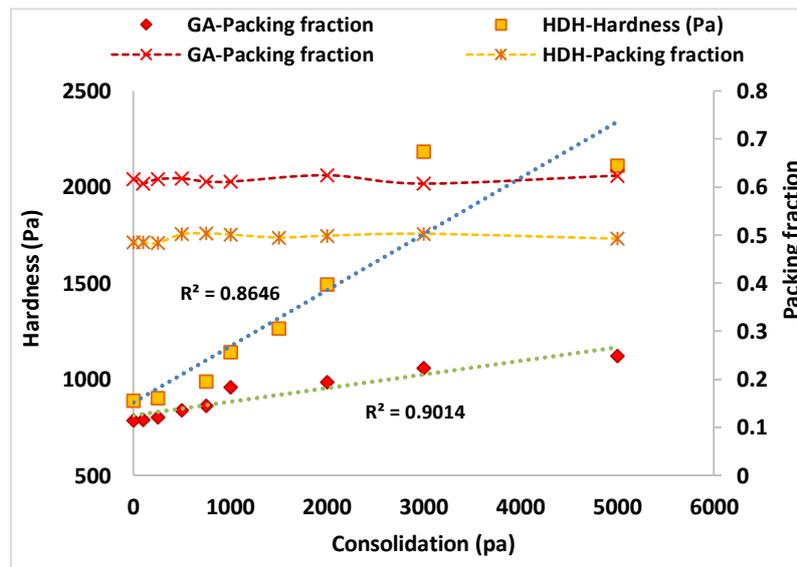
Figure 4. 11 Hardness and packing measurement of GA and HDH samples by using ball indentation

In this work, the first test was carried out without any consolidation (0 Pa) (just scraping) and an indentation hardness test was conducted at 10 mN load with a constant strain rate of 0.1 mm/min using a spherical glass indenter of 8 mm diameter. For the rest of the tests, the powder bed was scraped and uniaxially compacted to a range of (100-5000 Pa) consolidation pressures. Ball indentation test was then carried out on the compressed powder bed using 10

mN indentation loads to assess the hardness of the powder bed. It should be noted in contrary to the shear cell tester, for the ball indentation test, the hardness measurement is carried out on the surface of consolidated powders, hence the effect of powder weight could be minimized and can be discounted from the value of consolidation stress. The tests were carried out under ambient conditions. The average values of hardness for both samples of GA and HDH are shown in Fig. 4.11.

Comparison between indentation hardnesses obtained for HDH and GA over a range of consolidation pressures, indicates that the hardness of both samples increases linearly with an increase of consolidation pressure which shows the powder with higher consolidation has a greater resistance to the indentation. Since the densification of powders subjected to compaction is influenced by inter-particle friction (Yu and Hall, 1993), the higher hardness means less flowability of the powder. The hardness of HDH powder at the higher pre-consolidation pressure is much greater than the GA sample. This might be due to the shape of the sample and the interlocking of particles and powder friction.

Also, the packing fraction ranges for both samples are independent of the range of pre-consolidation pressure and it is relatively constant except for a small change at very low consolidation. However, the GA sample with spherical particles has higher packing fraction than HDH with irregular shape.

4.2.7.2. Effect of tapping on hardness and packing fraction

To characterise the effect of filling and stress history of powder on packing fraction and hardness, the samples were first tapped in a die by using Tapped Density tester JV 2000 equipment (Copley Sci., UK) to settle the powder by mechanically raising the die and allowing

it to drop the specific distance of 3 +/- 0.2 mm under its own weight at a various taps values (3-5-10-30-50 and 100) for both samples, then indentation tests were carried out with 10mN load on the tapped samples. The results are presented in Fig.4.12.
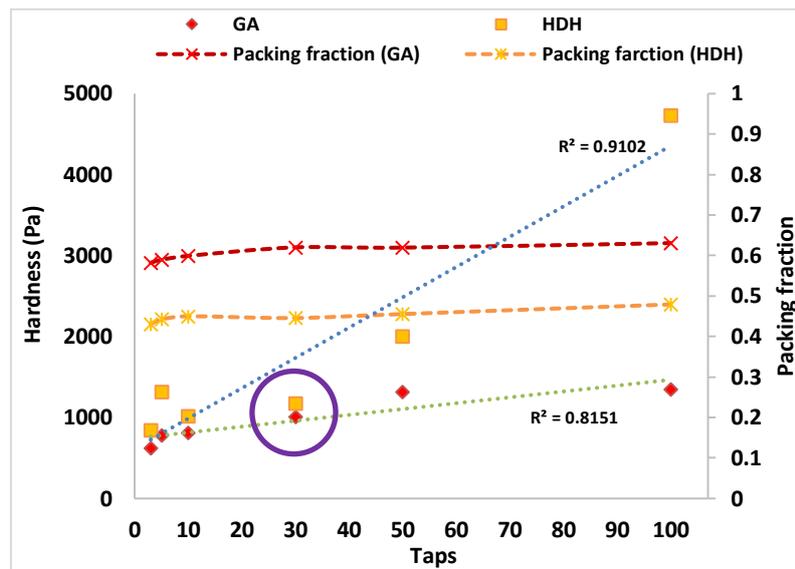
Figure 4. 12 The effect of number of tapping on hardness and packing fraction of GA and HDH powders

For a free flow powder such as GA, the ability to settle and inter-particulate interaction are less significant hence tapping could have less significant influence on the hardness. However, for less flowable powder like HDH, there are greater interactions and greater difference between hardness before and after tapping, especially over 50 taps. For HDH powder, the packing fraction is increased slightly higher than GA, which was also noticeable from compressibility measurements, where HDH showed higher degree of CI than GA.

4.2.7.3. Effect of various consolidation on hardness and packing fraction for 30 tapped samples

To minimize the effect of filling and stress history of powder and to achieve exact condition and reduce the number of affecting variables on powder bed, samples were tapped at 30 times and then characterised for hardness and packing fraction analysis using ball indentation technique with various consolidation stress, as shown in Fig. 4.13. This is because up to 30 taps the hardness measurement for both samples are close as shown in the previous section.
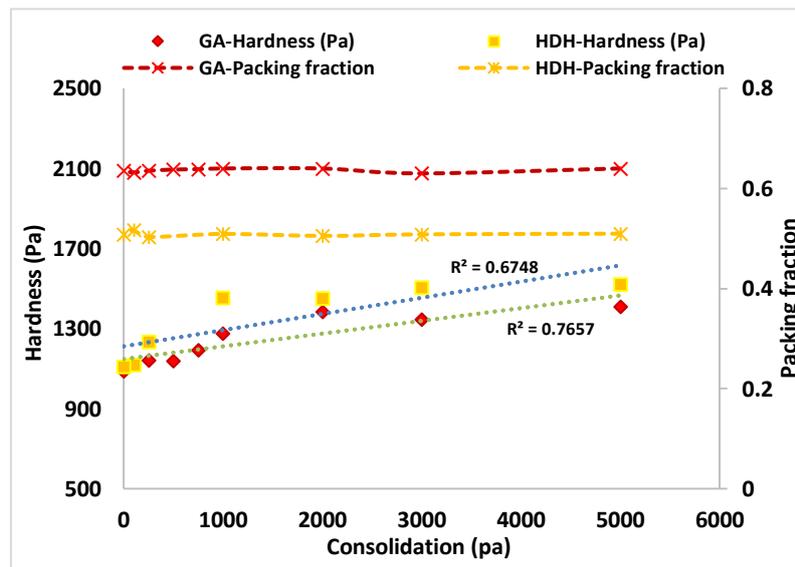
Figure 4. 13 Hardness and packing measurement of GA and HDH on 30 tapped samples

It can be seen from Fig. 4.13 that hardness increases slightly for both samples at various consolidation pressure for tapped samples in comparison with Fig. 4.11 on loose pack samples. The reason is, that for the loose (no tapping before compaction) powders rearrange due to their weight and physical properties therefore when powders undergo compaction, with constant pressure, the powder bed became more consolidated, and hardness will

increase. On the other hand, the tapped samples rearranged the particles and they could reach the critical packed state and therefore the consolidation would not affect the powder bed.

Again, the packing fraction ranges for both samples are independent of the range of pre-consolidation pressure and it is relatively constant. However, the GA sample with spherical particles having larger packing fraction than HDH with irregular shape (same as loose powders in previous section).

These phenomena are needed to study in detail and the results of ball indentation process at three different stages of loose, compacted and indented were characterised by using XMT and the results are presented in the next chapter.

4.2.7.4. Analysis of yields stress from hardness

To calculate the yield stress from indentation hardness, for solid materials Tabor (1951) proposed that the hardness is directly related to yield stress by applying the constraint factor (C). For powders C values would depend on single-particle properties such as particle shape, surface roughness, and inter-particle friction. In order to determine the yield stress from the ball indentation technique, it is important to establish the value of constraint factor of both GA and HDH powders to be able to characterise the powder flowability and find flow function. The constraint factor can be calculated by using Equation 2.4 where the C is the ratio of the hardness over the unconfined yield stress at the same consolidation stress.

	Constraint factor (C) for untapped ball indentation	Constraint factor (C) for tapped ball indentation
GA	19.7	27.2
HDH	16.6	21.2

Table 4. 6 Comparison of the constraint factor (C) of both powders calculated from hardness and yield stress from two different shear cells (standard-low)

To measure the C value from shear cell results, the hardness and calculated unconfined stress at 750 Pa consolidation for untapped and tapped samples have been used. The last two data points from low stress shear cell have been chosen and the ball indentation data between those two values have been used to interpolate the unconfined stress. The C value for GA was then calculated as 19.7 for untapped ball indentation results and 27.2 for tapped ball indentation. To calculate the C value for HDH the same procedure was used, and results are presented in Table 4.6.

GA
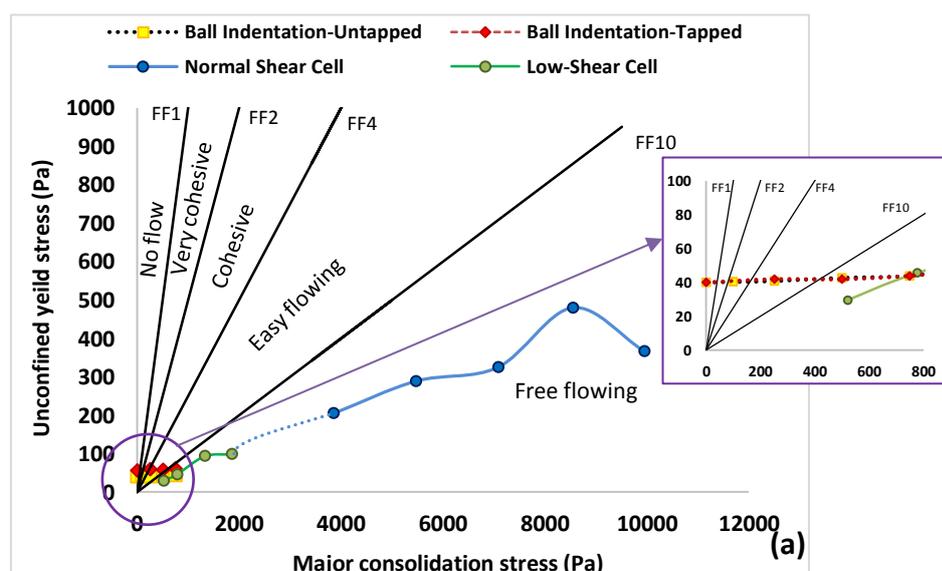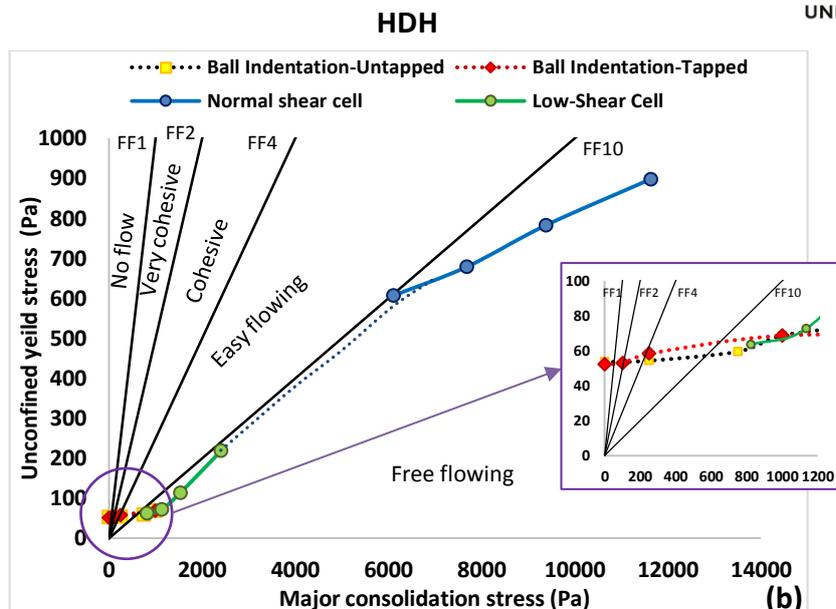
Figure 4. 14 Flow function of (a) GA and (b) HDH samples driven from shear cell and ball indentation techniques

Fig. 4.14a shows the unconfined yield strength values from the ball indentation measurements (untapped and tapped) at major principal stresses of 0, 0.1, 0.25, 0.5, 0.75, 1.0, 2.0, 3.0, and 5.0 kPa, along with the unconfined yield strength measurements carried out in the shear cell for both low and standard shear stress. The dashed line between two shear cell results were assumption values of unconfined yield stress for the range of 2000Pa to 4000Pa which there have not been any results but indicating that these two techniques could be correlated well with each other.

The indentation technique has shown an increase in unconfined yield strength at lower consolidation levels in comparison to values that presented from the low shear tests. Although most of the results suggest that powder GA is in an easy-free flowing region.

Fig. 4.14b presents the unconfined yield stress of HDH powders for ball indentation techniques (untapped, tapped) and for both standard and low shear stress. Again, the indentation technique shows higher flow function at lower consolidation levels. The flow function values for both powders at low stress are presented in Table 4.7.

	Flow function (ffc)	
Consolidation stress (Pa)	GA	HDH
100	2.4	1.9
250	6.1	4.6
750	17.1	12.6

Table 4. 7 Values of ffc for both powders at low stress region

It should be noted that in order to understand the bulk scale behaviour of powder, single particle interactions also must be considered. For two particles in contact at loose bulk stage, the interaction is dominated by capillary, electrostatic and van der Waals forces (58). In the absence of moisture and for uncharged powder the dominant force is restricted to the van der Waals force and the magnitude of it depends on the particle size, shape, surface roughness and surface energy of powders.

As particle size decreases, the amount of surface area per unit mass increases, and surface-energy forces have a greater influence on bulk powder flow characteristics.

The ratio between inter-particle attractive force and weight (called the granular Bond number (Bo) which quantifies inter-particle cohesion as the ratio of cohesion force (or adhesion force for dissimilar particles) to the particle weight due to gravity (Eq. 4.1).

$$Bo = \frac{F_{Adhesion}}{W}$$ Equation 4.1

Where $F_{Adhesion}$ can be measured by knowing the interfacial surface energy of the two particles in contact.

Particles with higher cohesion forces relative to their weight (*Bo* > 1) are considered cohesive whereas particles with lower cohesion forces relative to their weight (*Bo* < 1) are consider non-cohesive (135).

For powders used in this work, the calculated Bo for Ti6AL4V powders is much higher than 1 (135), hence one could infer that the flowability of powder at very low or near zero consolidation stresses is mainly dictated by the Bo number. In detail study of powder surface properties would help to better understand the powder behaviour at very low stress levels, which could be the subject of further investigations.

4.2.8. Summary of powder flowability techniques

As it stated before from numerous literatures the powder flowability cannot be confirmed using only single measurement technique.

Therefore, the results of seven different flowability techniques to determine the scale of flowability of both powders are presented in Table 4.8.

	GA	HDH
Hausner ratio	1.07	1.10
Compressibility index (CI) %	6.2	9.5
Static angle of repose	27.1	37.6
Dynamic angle of repose	33	46
Internal angle of friction	32	43
Wall Friction (°)	11	14
Flowrate (gr/s) at 12mm aperture	65	44
BFE (mJ)	264.2	728.1
Standard shear cell flow function at 6109 Pa	19.5	10.06
Low shear cell flow function at 821 Pa	11.35	8.79
Ball indentation flow function at 821 Pa	18.15	13.22
Scale of flowability	Excellent	Good
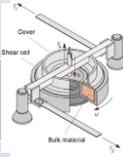
Table 4. 8 Comparison on of different flowability tests for both samples

4.3. Powder flow properties characterisation

Powder flow properties are specific characteristics which would contribute to the flow behaviour of specific powders (5). Examples of flow properties include density, wall friction, hopper angle, minimum column height of powder inside the hopper and the critical stress where shows the condition where the powder stop to flow.

Jenike (50) established the stress equations to characterise powder flow properties and developed his method to design hopper angle and hopper opening size with following steps size:

The effective angle of internal friction (φ_e) and angle of wall friction (φ_x) which have been driven from shear cell technique (Table 4.4) is used to calculate the maximum hopper angle (θ_p) from the mass flow diagram for conical hopper (17). To achieve the mass flow, which all particle is in motion during the discharge there is relationship between angle of wall friction, internal angle of friction for specific powder and hopper angle (Fig. 4.15).
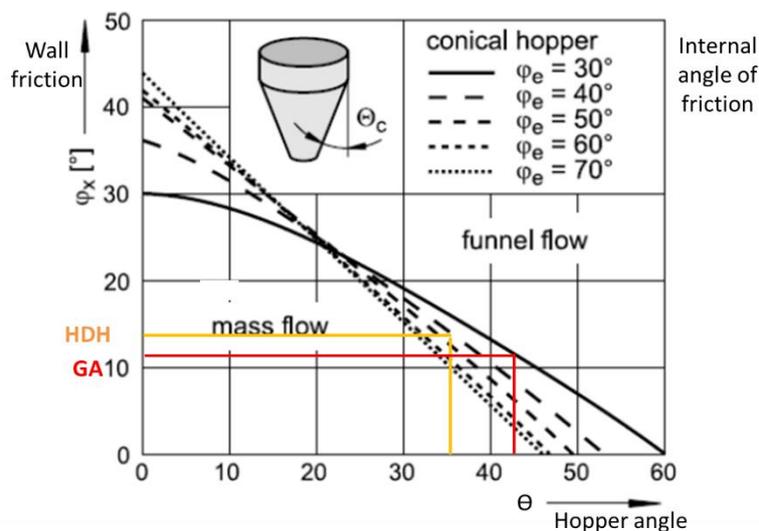
Figure 4. 15 Mass flow diagram for conical hopper (17)

Maximum hopper slope to have a mass flow from diagram is equal to:

$$\text{Hopper } \theta_{GA} = 42°$$

$$\text{Hopper } \theta_{HDH} = 35°$$

Also, Jenike introduced the hopper flow factor "ff", which is ratio of compacting stress in hopper to the stress developed in powder (Eq. 4.2).

$$\frac{\sigma_{Compacting\ stress\ in\ hopper}}{\sigma_{Stress\ developed\ in\ powder}} = ff \qquad \text{Equation 4.2}$$

The higher value of "ff" means less flowability of powder since high compacting stress means higher compaction. The flow factor depends on nature of wall material, slope of hoper and flowability characteristic properties of powder (51).

Jenike plotting angle of wall friction versus calculated hopper angle to provide the diagrams for an easy determination of "ff" values for both conical and wedge shape hopper for different values of internal angle of friction ((φ_e) of 30, 40, 50, 60 and 70.). In case of our experiments, diagrams of conical hopper for internal angle of friction of ($\varphi_e = 30°$) for GA and ($\varphi_e = 40°$) for HDH have been used Fig.4.16.
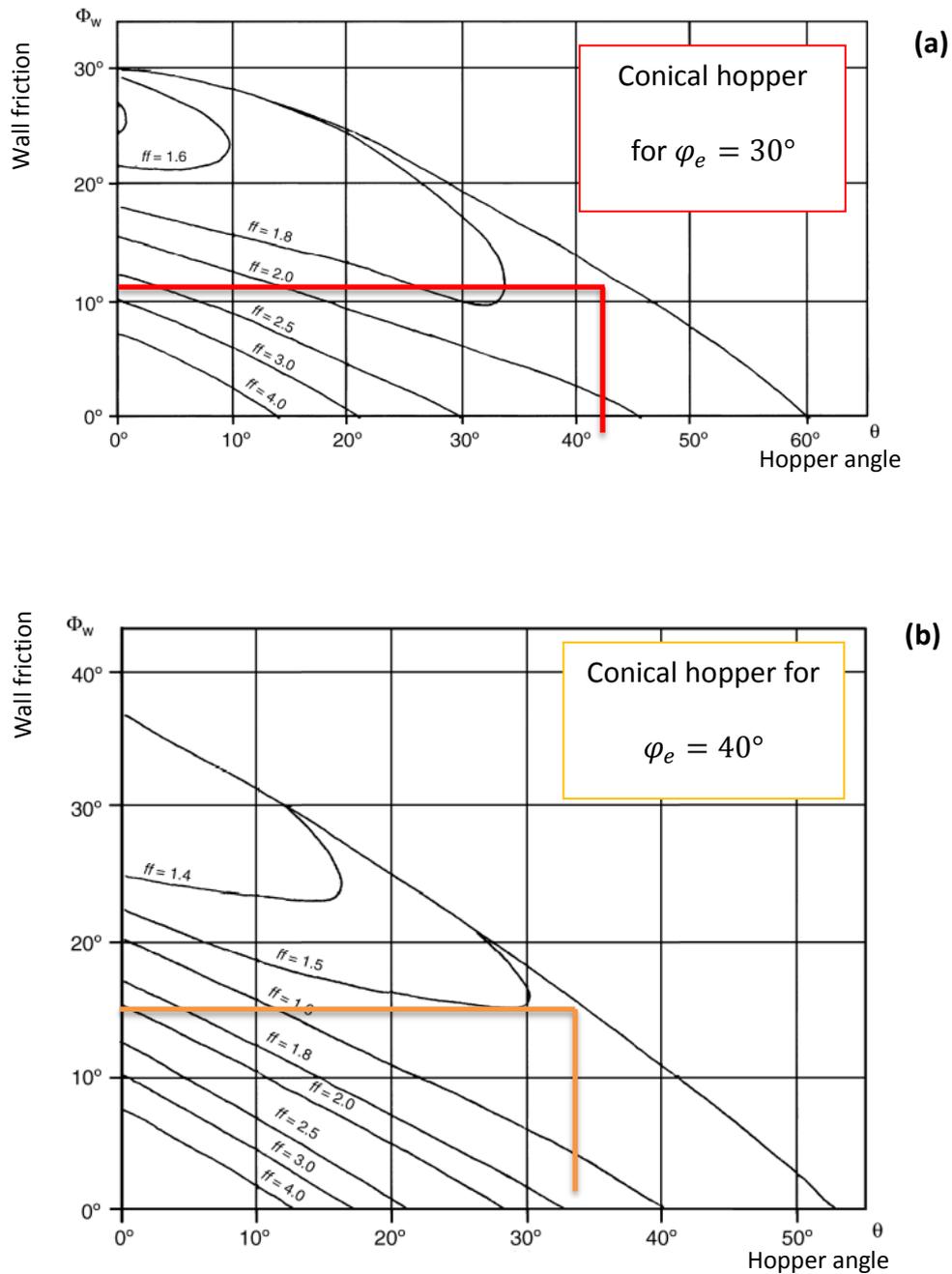
Figure 4. 16 Hopper flow factor values for conical channels, (a) for internal angle of friction of 30 (GA). (b) for internal angle of friction of 40 (HDH) (17)

From previous diagram, it was found that to ensure the mass flow of GA powder, the limiting value of hopper angle would be $\theta = 42°$. The value of the hopper half angle was reduced by a safety margin of 2–3° to θp = 12°. Then entering the diagram of conical hopper with effective

104

angle of friction 30°, giving hopper flow factor "ff" 2.0. same procedure was considered for

HDH powder.

$$(GA) \text{ flow factor from table: } ff = 2.0$$

$$(HDH) \text{ flow factor from table: } ff = 1.6$$

Therefore, analytical results to design of hopper which includes internal angle of friction, wall

friction, density, hopper angle and flow factor of both samples were presented in Table 4.9.

	φ_e (°)	φ_x (°)	ρ ($\frac{kg}{m3}$)	θ (°)	ff
GA	32	11	2356	42	2.0
HDH	43	14	1841	35	1.6

Table 4. 9 Analytical results to design the hopper

Therefore, by knowing the flow factor, both critical applied stress "$\sigma_{critical}$" and minimum

size of hopper would be measured. The critical applied stress shows the limiting condition of

powder for flow where the unconfined stress is equal the stress develop in powder (Eq. 4.3).

$$\frac{\sigma_{Consolidation}}{ff} = \sigma_{Unconfined} \qquad \text{Equation 4.3}$$
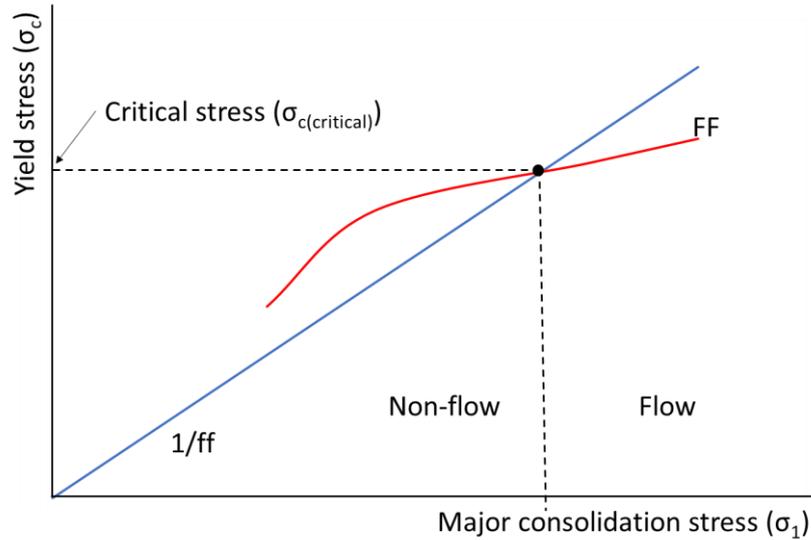
Figure 4. 17 Criterion of flow and non-flow regarding to critical applied stress

The critical applied stress is determined from the intersection of line of $(\frac{1}{ff})$ and the line of

flow function (Fig. 4.17). Flow function line can be determined both from low shear cell and

ball indentation techniques for untapped and tapped methods and compared. The shear cell

results are not covered lower consolidation pressure (0-500 Pa), however, the line of flow

function was extrapolated and presented in Fig.4.18.

106
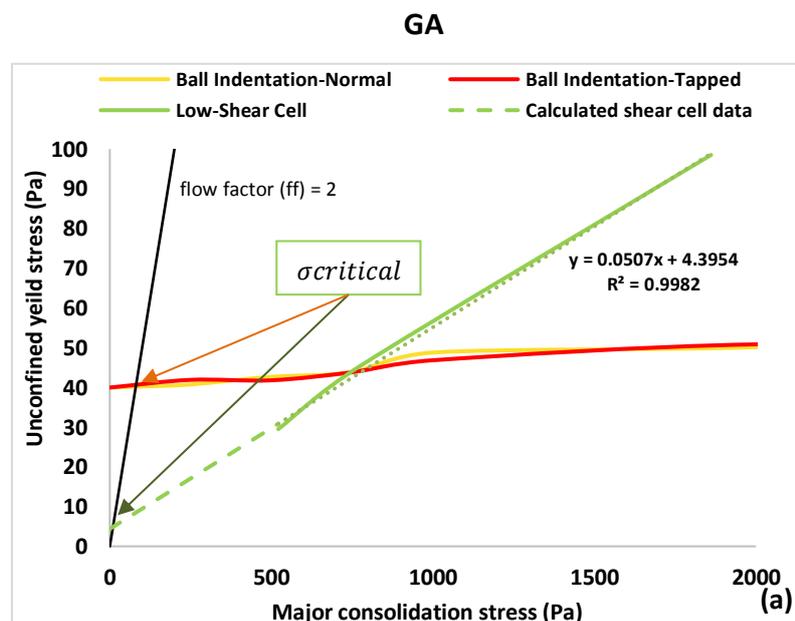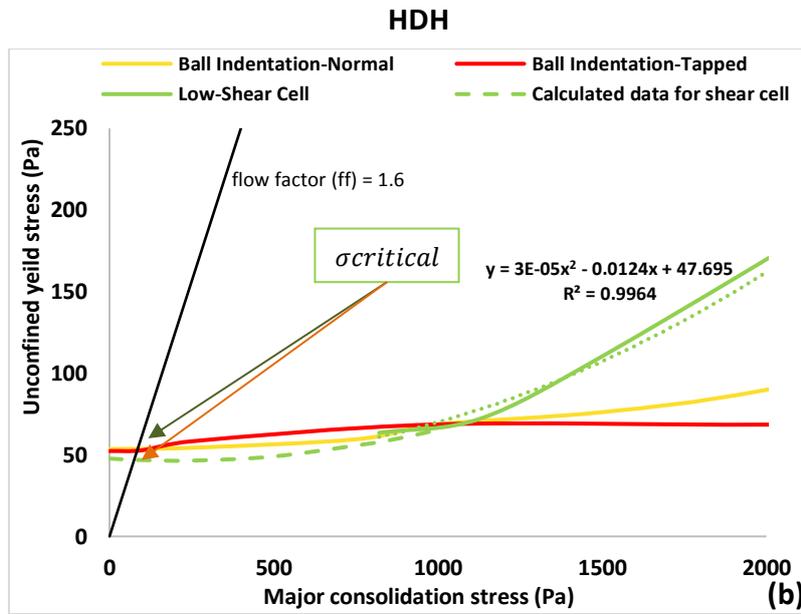
Figure 4. 18 Evaluation of Critical Applied Stress from flow function for both (a) GA and (b) HDH

The minimum diameter of opening for conical hopper to avoid arching is then calculated using

values of critical applied stress, hopper angle and bulk density of powder (Eq. 4.4).

$$D_{min} = \frac{H(\theta_p)\sigma_{critical}}{\rho_B g}$$ Equation 4.4

$$H(\theta_p) = 2.0 + \frac{\theta_p}{60}$$ Equation 4.5

where H is a function of hopper angle and g is the gravitational acceleration constant (Eq.

4.5).

Depending on the critical stress and average bulk density of samples, the minimum column

height of powder on hopper which the powder will flow were measured (Eq. 4.6).

$$H_{min} = \frac{\sigma_{critical}}{\rho_B g}$$ Equation 4.6

The results for both powders are presented in Table 4.10.

			$\sigma_{critical}$ (Pa)	D_{min} (mm)	H_{min} (mm)
GA	Ball indentation	Untapped	40	2.5	88.3
		Tapped	41	2.5	90.5
	Low shear cell		6	0.3	13.2
HDH	Ball indentation	Untapped	53	3.1	116.2
		Tapped	52	3.1	114.0
	Low shear cell		47	2.8	103.0

Table 4. 10 Calculated values of critical applied stress, the minimum hopper opening size and minimum height of powder for GA and HDH powders in a conical hopper

The results from Table 4.10 show that regarding which technique to driven the flow function line, all calculated values of $\sigma_{critical}$, hopper opening size and height of powder inside the hopper would be different. Although all techniques indicated that the HDH powder has the higher critical applied stress compare to GA indicating that the HDH powders need the larger outlet diameter on the hopper to prevent a cohesive arch from developing, and the easier flow is for GA powder.

Also, it appears that the flow function resulted from the low shear cell for GA powders underestimates the value of critical stress and therefore, it could affect the calculation of minimum orifice diameter. It was shown from Section 4.2.4 that minimum orifice diameter for GA powders was 1mm.

4.4 Powder spreadability

Powder bed density or packing fraction of the bed is one of the main factors that influences the melting process, powder solidification and as a result the quality of the final part (6). Usually, free flow powder produces high packing bed density inside the EBM chamber resulting in the fully dense parts (121). Drummer et al. (122) summarised few important aspects regarding powder properties for high-quality powder bed with the minimum void between particles for polymers; (i) high sphericity (>0.6), (ii) small surface area to volume ratio, (iii) wide range of size distribution (10-120µ), (iv) small Hausner ratio (<1.25). Morphological analysis which are presented in Section 3.2.1. indicated that both powders have reached the threshold for having good packing efficiency regarding their sphericity (GAΨ_{50}=0.9, HDHΨ_{50}=0.7), their size distribution, and the values of Hausner ratio (HRGA=1.07, HRHDH=1.10).

To experimentally measure the quality of the powder bed, the spreading rig setup was designed and used to measure the values of powder bed density for two types of powders (GA and HDH) (Fig. 4.19). This study has been carried out by a Master by Research student (Ms Fatemeh Talebi, 2021), at the University of Leeds (123).

The rig consisted of the build plate (Lb:115mm, Wb:65 mm), which is connected to a software to achieve the different spreading velocities, and the stationary blade which is adjusted vertically to optimize a desirable gap size.

Blad

Build plate
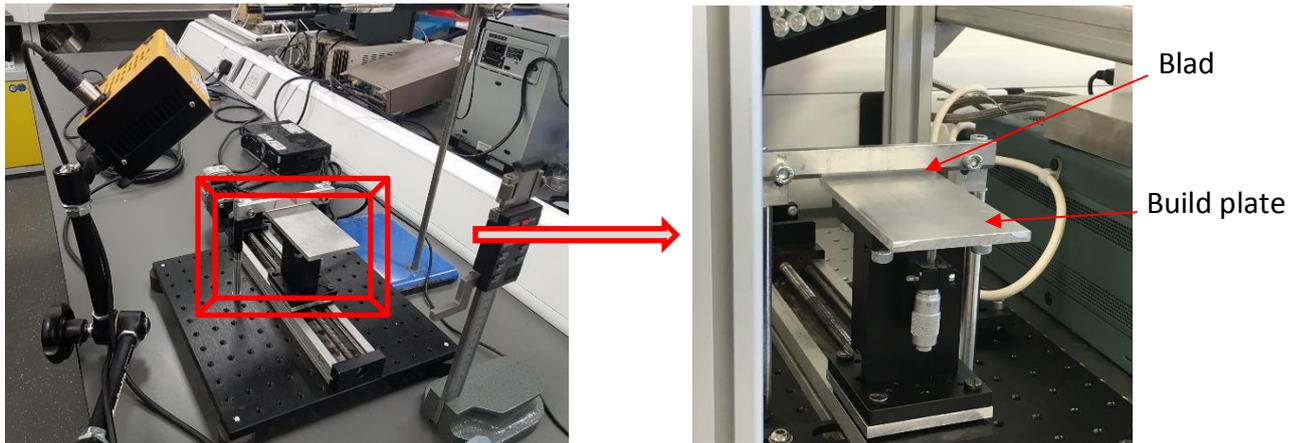
Figure 4. 19 Rig set up of spreading process

To characterise the powder bed density, the powder was weighted and poured in front of the blade though the funnel to create a heap. The gap between blade and bed were measured by using "feeler gauge" and then bed started moving at 50 mm/s of spreading velocity. A layer of powder was spread over the bed and excessive powder was collected at the end of bed. The remaining powder on the bed were used to measure for its weight and its volume. The powder bed density was calculated by using Equation (4.7):

$$\rho_b = \frac{m_{powder\ bed}}{V_{Powder\ bed}} \qquad \text{Equation (4.7)}$$

Where, ρ_b is packing bed density, $m_{powder\ bed}$ is the mass of spread layer on the powder bed and $V_{Powder\ bed}$ is the volume of powder calculated by taking the area of the spread layer using Image J, multiply by the gap size.

This study was carried out at different gap sizes and different blade speeds (123), however, to correlate the powder flowability techniques presented in this chapter with the

spreadability measurement, the highest gap size (508 µm) and slowest blade speed (50 mm/s) were chosen as they generated the highest powder bed density. Changes in these parameters (gap size and blade speed) outside the above mentioned range resulted into undesirable packing densities, hence were omitted for this study.

Results for both samples are presented in Fig. 4.20.
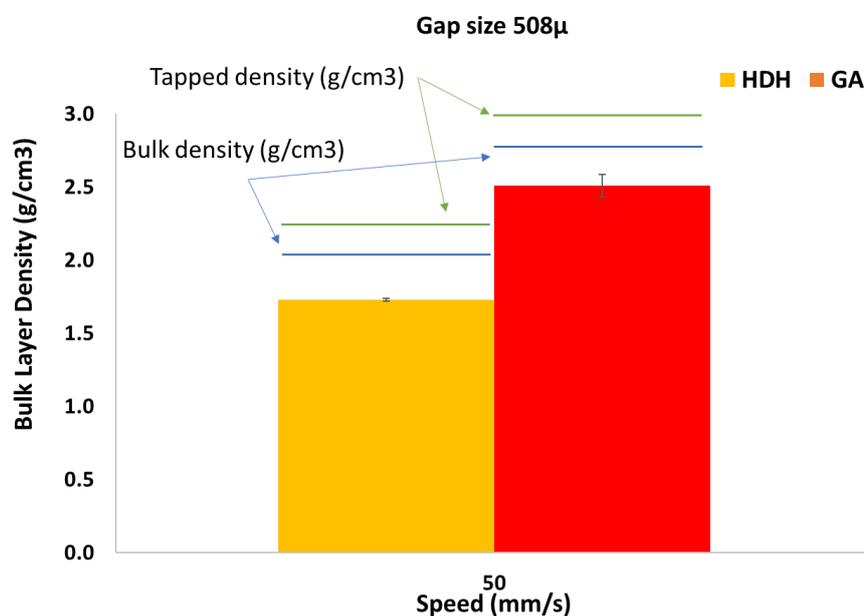
Figure 4. 20 Comparison of powder bed density with apparent and tapped density for (a) GA and (b) HDH

According to Chatham et al. the packing density generated by the spreading process should be equal to the bulk density of the powder, although a more dense packing arrangement for the given size and morphological properties corresponds to the tapped density values of those powders.

Fig. 4.20 shows the bulk layer density (packing fraction) of both GA and HDH samples. The results indicate that HDH powder shows quantitatively lower packing density in comparison

to GA powder. The irregular shape of powder HDH leads to a looser rearrangement of particles, lessening the packing density. Nevertheless, both powders have not reached their bulk density and are far from their tapped density values. This might be a result of the blade properties. According to Haeri et al. the counter-rotating roller has been found better spreader than the blade which producing a denser powder bed (4). The blade spreading mechanism induces the dragging of particles and moves them from one place to another over the bed surface (121).

The spreading results is correlated with the angle of repose (static and dynamic), powder flowmeter, and low shear cells evaluation of powder flowability. While all these techniques indicate that both powders are flowable but GA powder has better flowability compared to HDH powder. On the other hand, some techniques such as FT4 underestimate the flowability of HDH powder and has shown there is a significant difference between the two powders.

The ball indentation technique has shown acceptable results regarding measuring the critical applied stress for both powders, showing GA powder has better flowability than the HDH powder, while suggesting at very low stress (less than 100 pa), both powders behave in a cohesive manner.

It should be mentioned that the powder packing behaviour during consolidation and ball indentation can affect the measurements which will be analysed in the next Chapter.

4.5 Conclusion

Powder flowability is determined using seven different measurement methods, i.e. compressibility index, hall flowmeter, angle of repose, Hausner ratio, avalanche angle,

powder rheology, and shear tests. The powders are tested under static and dynamic conditions and from low to high-stress regions. Relatively similar powder flow properties are observed for all different techniques, except powder rheology, which indicate that, despite having a good flowability of both powders, GA powders shows slightly better flowability compare to HDH powder. However, the flow behaviour at stress levels below 500 Pa, which is closer to the stress level encountered during spreading, can only be measured using the ball indentation technique. Results from the ball indentation technique shows that at low stress (<0.5 kPa) the flow factor decreased significantly, and powder were categorised as cohesive, with HDH powder being more cohesive than GA powder. It should be stated that the critical stress, which is driven from both ball indentation and shear test techniques, indicate that minimum orifice diameter calculated from ball indentation is a more reliable method than shear cell test.

Furthermore, the correlation between powder flow characteristics and the spreading results are investigated which shows that spread GA powder has a higher packing density compare to HDH powders. The irregular shape of powder HDH can lead to a looser rearrangement of particles and reducing the packing density.

Chapter 5
X-ray Microtomography Analysis of Ball Indentation Process

5.1. Introduction

The ball indentation method could be a suitable approach to characterise powder flowability in correlation to the conditions of powder spreading, however, despite a number of reported papers, there is a lack of understanding of the powder packing behaviour during the indentation process. In this chapter the time lapse XMT has been used to characterise the ball indentation of powders. The packing behaviour of powders during the process of filling (loose), consolidation (compacted) and ball indentation (indented) have been studied. This study will be led to deeper understanding of ball indentation method and therefore could be useful in further developing the technique.

5.2. Experimental procedure

5.2.1. Methodology

To investigate the packing density for loose and compacted powder and replicate the powder bed geometry of ball indentation in 3D representation, the XMT (MicroXCT, Xradia Versa 410) at the University of Leeds was used.

The experimental rig included a die (10mm internal and 20 mm external diameter cylindrical with 15mm depth), a piston (10mm diameter), a ball indenter (4mm diameter) made of glass and a set of weights to allow a range of consolidation stress to be tested. The die and the

piston were made of poly (methyl methacrylate) in order to ensure minimal attenuation of X-ray during capturing of projection slides for the rig (Fig. 5.1).
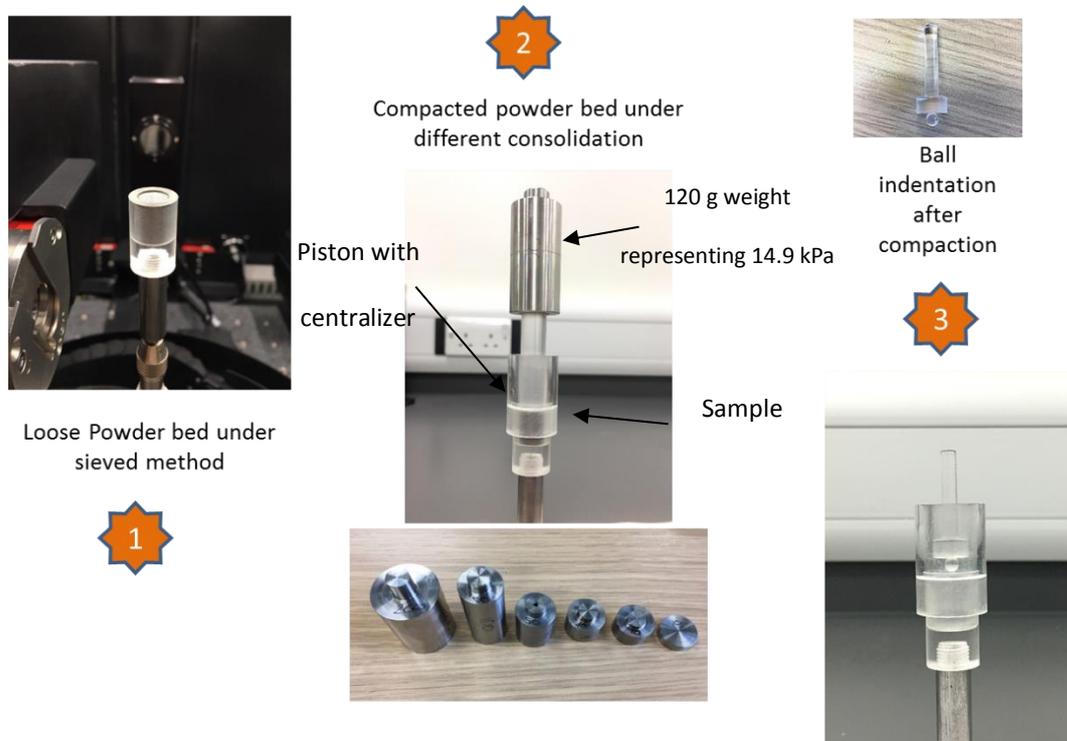
Figure 5. 1 Sample preparation for three stages of indentations during X-ray micro tomography

Initially the die was fully filled with powder GA (3.10 g) and HDH (2.50 g) with the "sieved method". In the sieved method, the sample was passed through a sieve that the mesh size was 5 times the D_{50} of the samples ($5xD_{50}$) directly above a funnel on top of the die to get the uniform loose randomly packed powder bed (79). Then it was mounted on the rotating sample stage with a high level of care (Fig. 5.2a). Then the same setting of X-ray photon power of 140kV and current setting of 70μA from Table 3.3 were used to acquire series of projection images as sample was rotating. The magnification or final voxel size in reconstruction of

volume is dependent on the distance between the X-ray source and sample holder which is set to 7.4 μm.

The first scan was performed on the initial state of loose particles, where their rearrangements could be affected by their properties such as shape, weight and particle-particle and particle-wall friction.

Then second scan was performed after mounting the piston with 120 g weight at the top applying a pressure equal to 14.9 kPa. In this study a relatively high consolidation stress was used because during ball indentation the weight of in situ ball indentation set up (sliding rod attached to the ball) would be relatively large and that would have led to an excessive penetration if a low consolidation stress was used. Also, to minimize any undesirable particle disturbance due to the moment of sample holder, the piston was placed on the sample while it was inside the X-ray device.

For the last scan, the load was removed, and the ball indenter was placed carefully on top of the powder bed, then it was lowered under its own weight (1.01g equal to 9.9mN). For each of the three different stages of "loose, compaction and indentation", the X-ray micro tomography settings were kept constant to ensure similar resolution and region of interest.

All the tests were measured at a constant temperature of 25°C inside the chamber with relative humidity of (40%).
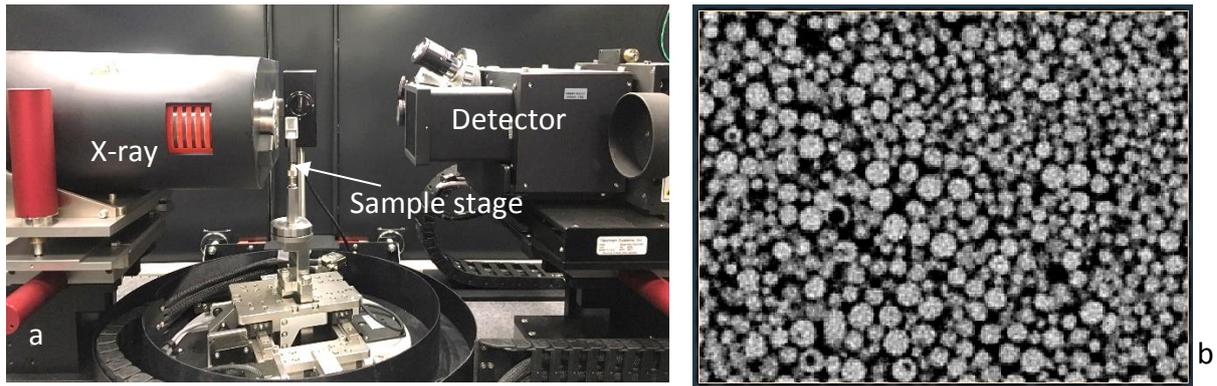
Figure 5. 2 XMT (a) set up, (b) reconstructed image of sample GA

5.2.2. Data analysis

The 3D reconstructed volume of the whole sample was characterised by the Avizo® software. Initially, images were subjected to sharpening and edge detecting filter to remove a substantial level of noise while preserving the edge of each particle (Fig. 5.3a). Then to separate the individual particles from the void (Fig. 5.3b) the images were segmented manually into binary format based on the distribution of greyscale of each pixel value. To identify different phases of particles and voids filled by the air, in radiograph images of XMT, the variation of X-ray absorption is indicated by different greyscale intensities which can be seen in voxel intensity histogram (124) that are related to physical density and atomic mass of the object.

(a) ■ Void between particle (b)

□ Particles

HDH

Applying sharpening and edge

detection filter before segmentation

GA
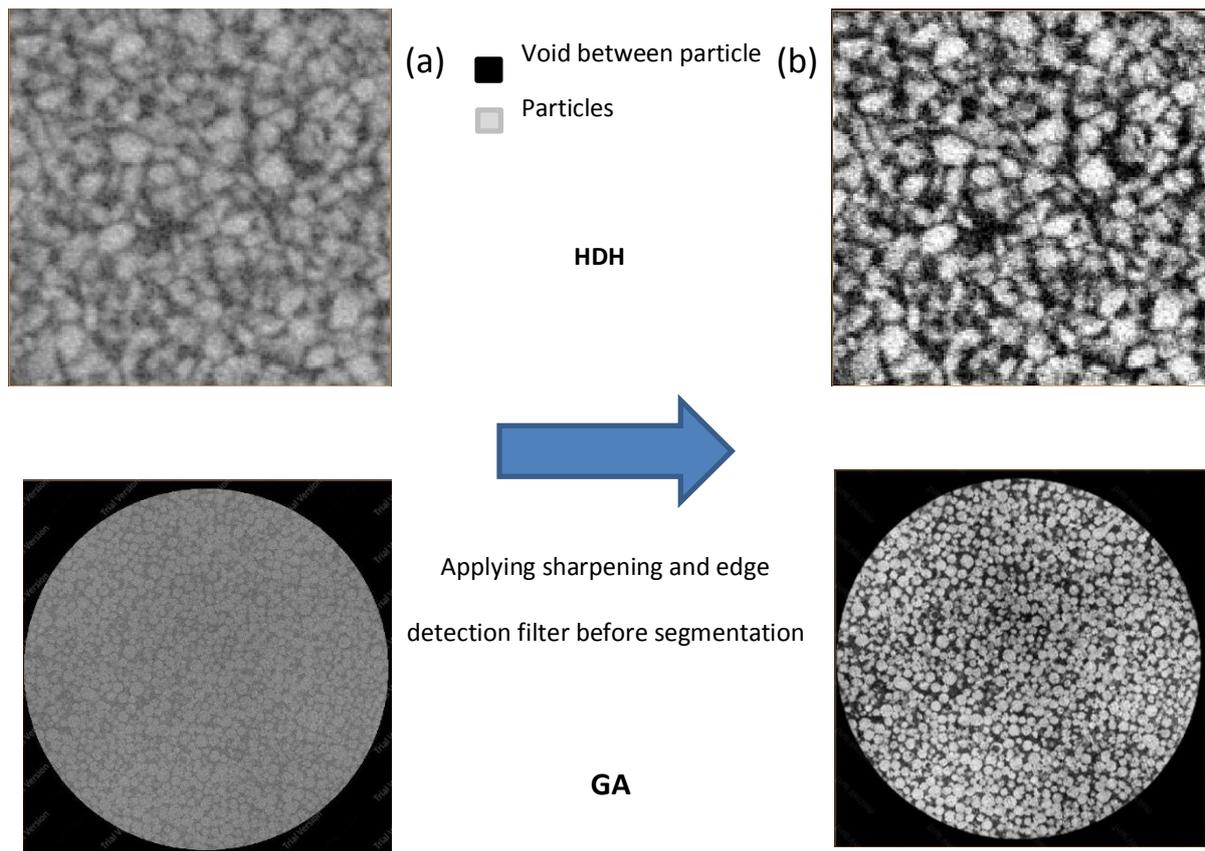
Figure 5. 3 (a) Before and (b) after sharpening filter on sample HDH and GA

User dependency is the basic limitation of thresholding technique. To make sure that the range of binary segmentation is correct, the quantitative results should be comparable with known parameters (e.g. density) obtained by different methods. To ensure accuracy of determination of individual particles with their internal details and their edges, the whole sample packing density fraction given by the software (Eq. 5.1) after binarization was compared with the calculated packing density fraction of powders from its volume (from height of sample in the die), weight and true density (39) (Eq. 5.2). Then the range was chosen by considering the error ($\pm$ 0.001 gr/cm^3)

PF $_{density}$ from Avizo software = $\dfrac{Volume\ accupied\ by\ partcles\ after\ thresholding}{Volume\ of\ whole\ sample}$ Equation 5.1

PF $_{density}$ from calculation = $\dfrac{Density\ measured\ by\ weight\ and\ volume\ of\ sample}{Material\ density\ (single\ particle\ \ true\ density)}$ Equation 5.2

5.3. Result and discussion

To calculate the "packing fraction" for loose, compacted and indented samples, the pixels area occupied by particles were obtained for each projection slide and used for the calculation of the total packing fraction.

Fig. 5.4 shows the X-ray image of loose state of the powders filled by the sieving method (79) followed by the compacted and indented powder bed for both samples. It can be observed that the indenter penetrated more into the compacted HDH powders which could indicated to a less consolidated state as compared to that of GA powders.
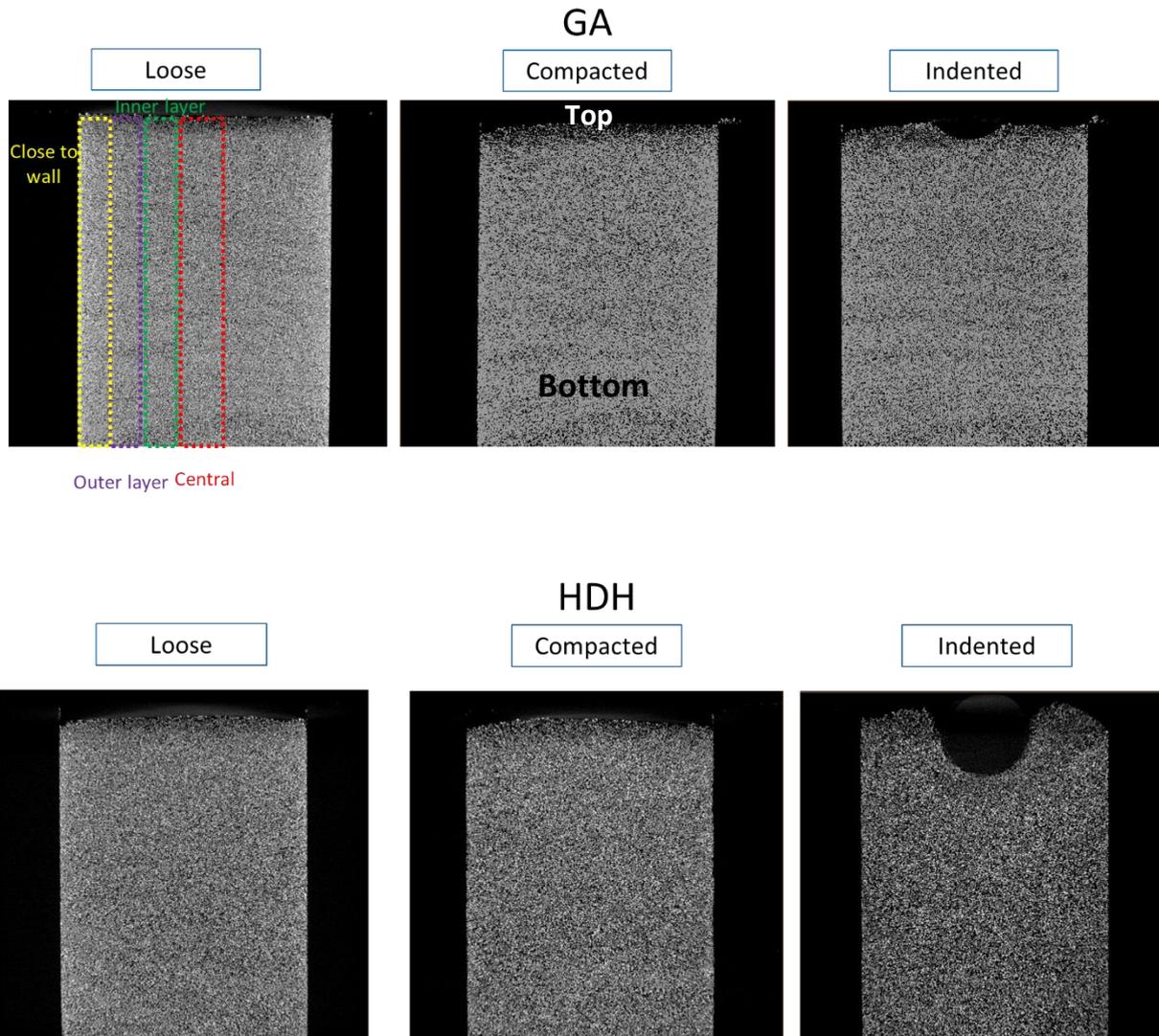
Figure 5. 4 2D Axial greyscale slide through the 3D volume for each test (Loose-Compacted-Indented) of GA and HDH powders

The regions of interest for the quantitative comparison of packing density both radial (central, inner, outer and wall sections) and axial (top to bottom sections) through the bed have been chosen for all three stages (loose, compacted and indented) (Fig. 5.5). The radial sections have the same width and length (1110 and 850 μm, respectively) going from top to bottom around 8015 μm. Each zone is the average of 4 separated section. Each section has been chosen from the same point at three stages of experiments. The boundary box of each section has been exactly the same in 3 axes (x, y and z) and the central zone is exactly the under the ball to

cover the plastic deformation zone. All average packing fraction values for each section are presented in Fig. 5.6.
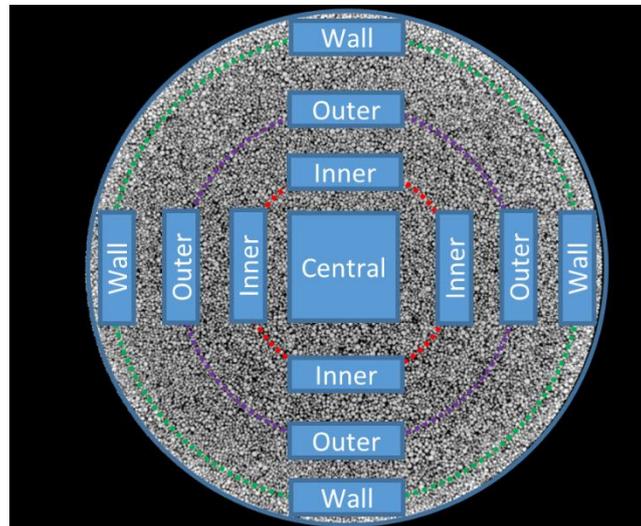
Figure 5. 5 2D Cross section slide of HDH powder with region of interest

The overall average packing fraction (percentage) as well as those of individual radial sections for loose, compacted and indented states are compared for both samples in Fig. 5.6. It can be seen that HDH has lower overall packing fraction than GA for all three states. However, for both samples the packing fraction of the loose stage increases from the central section towards the wall. This variation reduces after the compaction stage for both samples, where a reduction of the packing density is observed near the wall after the compaction (more significant reduction for HDH than GA) as opposed to other sections where an increase in packing fraction is seen. After indentation, the packing density reduces in all regions for GA powders, while this reduction is only observed around the wall for the HDH powders.

Overall, the GA powders have a higher packing fraction than HDH powders due to their size, shape, and surface roughness. Specially at loose stage which powders do not undergo of

compaction, GA particles with higher sphericity and aspect ratio tend to get higher packing fractions (125, 126). While the HDH particles with irregular shape would tend to interlock and entrap more air leading to smaller packing percentage. Hence, they could tend to have more block movement when they are being indented which could result in smaller or no changes in the packing fraction. This could resemble a behaviour of powders with a critical state of consolidation.
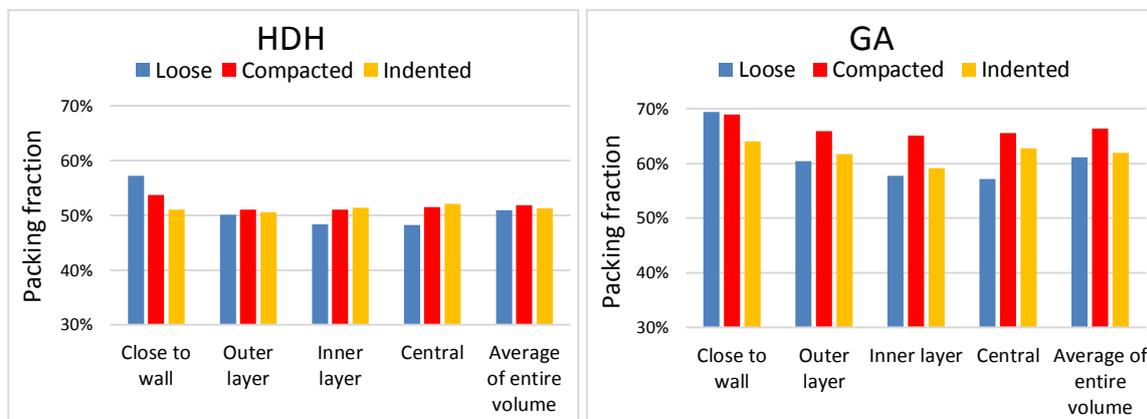
Figure 5. 6 HDH and GA Powders packing fraction for loose, compacted and indented samples

The frictional interaction between the particles and particles and the wall could affect the packing pattern of the powders. If the particle-wall friction is smaller than that of particle-particle, during loose-packing, particles are settled easier near the walls according to their nature (size and shape), hence the packing fraction becomes higher close to the wall, while in the middle section the interlock of particles results in less packed density fraction. This observation has been reported by previous researchers using destructive experimental approach (embedding the compact in resin and slicing) (127) as well as computer simulation (128). In order to test this hypothesis for GA and HDH powders, the "coefficient of sliding friction" (CoF) between particle-particle and particle wall was experimentally measured for

both samples (129). For particle-particle CoF measurement, a mono layer of particles was adhered to two surfaces (Perspex, same material as the die and piston) (Fig. 5.7), placed on top of each other and tilted until the sliding angle was detected (Fig. 5.8).
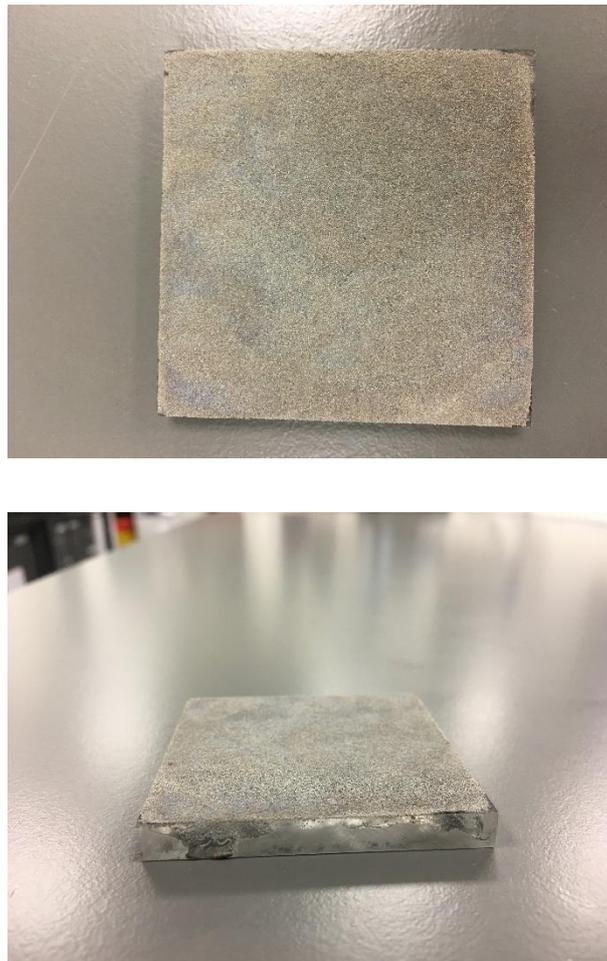
Figure 5. 7 Image of prepared sample of GA adhered to surface for measuring CoF

For the measurement of particles and wall CoF, the same process is applied but a plane lower surface is used instead of that of adhered particles. The results of CoF for both particle-particle and particle-wall are calculated by Eq. 5.3 and 5.4 and presented in Table 5.1. Each test repeated until the STD did not change significantly. This was achieved after 10 repeats.

$$\alpha \;=\; \sin^{-1}\frac{H_S}{L_S} \qquad\qquad \text{Equation 5.3}$$

$$COF = \tan\alpha \qquad\qquad \text{Equation 5.4}$$

Where α is the sliding angle, H_S is the height of tilted surface layers and L_S is length of surface layer.
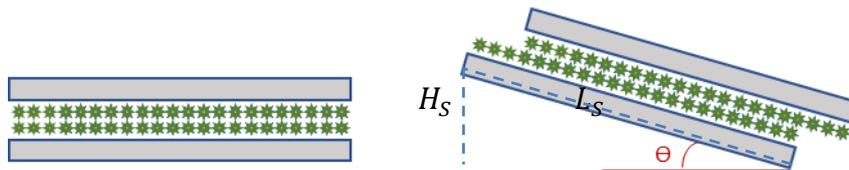
Figure 5. 8 Schematic diagram for measuring CoF between particle-particle

It can be observed that indeed the particle-wall CoF is lower than that of particle-particle for both samples, hence leading to a higher packing towards the wall according to the aforementioned theory. These results are correlating well with internal angle of friction of both samples extracted by shear cell results.

	Coefficient of sliding friction (μ)	
	Powder-Powder	**Powder-Wall**
HDH	0.87 ± 0.038	0.25 ± 0.009
GA	0.47 ± 0.062	0.19 ± 0.019

Table 5. 1 Sliding friction of both samples

The axial variation of the packing density has also been analysed for both samples. In particular, the axial variation for central section (around indentation point) and that of wall

zone are shown in Fig. 5.9 for both samples (axial variation of other zones can be found in supplementary data). For GA powders as presented in Fig 5.9a, it can be noticed that the trends of axial variation of packing densities are very similar, all the way from top to the bottom, for all three stages. At loose stage powders rearrange due to their weight and physical properties for which a trend is formed. When powders undergo compaction, with constant pressure on the bed, the packing density increases, but keeps a similar axial trend as that of the loose stage. Once the compaction pressure is removed and indentation stage takes place, it can be observed that the packing fraction is reduced but here again with the same trend as those of compaction and loose stages, except near the top, just below the indenter, where there is further reduction in packing fraction due to the dilation of powder to accommodate shear under the indenter. It should be noted, after removal of compaction pressure, before the indentation stage take place, there could be a degree of elastic recovery for the powder bed (130, 131) which could also contribute to the reduction in packing density.

Fig. 5.9b shows the axial variation of packing density for GA at the three stages in the zone close to the wall. It can be observed that GA powders have high packing density near the wall at loose stage due to their small powder-wall friction (as described earlier) but with little reduction after the compaction stage followed by further reduction after the indentation. Here, the axial trend in packing fraction is not entirely similar for the three stages, unlike the central zone. It is interesting to note that there is a significant drop of packing fraction close to the bottom section for all stages, as particles became less packed in the bottom-corner of the die. This phenomenon can be observed for HDH powder as well (Fig. 5.9d).

Fig. 5.9c shows the axial packing fraction for HDH powders in the central section at loose and compacted stages. Similar trends for axial packing fraction are observed for loose and

compacted stages, while for the indentation stage, where overall HDH exhibits no significant change in packing fraction, there is a degree of rearrangement of particles which leads to different axial trend compared to the loose and compacted stages. As opposed to GA powders, HDH powders did not show the dilation of powder (reduction in packing fraction) under the indenter suggesting the powders could be under a critically packed state presumably due their irregular shape (Fig. 5.9c). It should also be noted that the indenter has penetrated more into HDH (2.6 mm) as compared to GA powders (1.4 mm) and this might also be affecting the observed packing behaviour for the HDH powders.

It should be noted that the critical packed state determines whether powder tends to retain the same void fraction during shear deformations. In dense (over consolidated) powders the bed reaches the critical state as a result of dilation, while in loose packing it tends to reach the critical state after a volumetric contraction.

Fig. 5.9d lays out the packing density of HDH powders in the zone close to the wall. The packing fraction reaches to the highest level at the loose stage and shows more significant reduction after the compaction. There is a sudden drop in packing density at all stages near the bottom corner, with somewhat a higher extend as compared to GA powders.

Dilation under the indenter
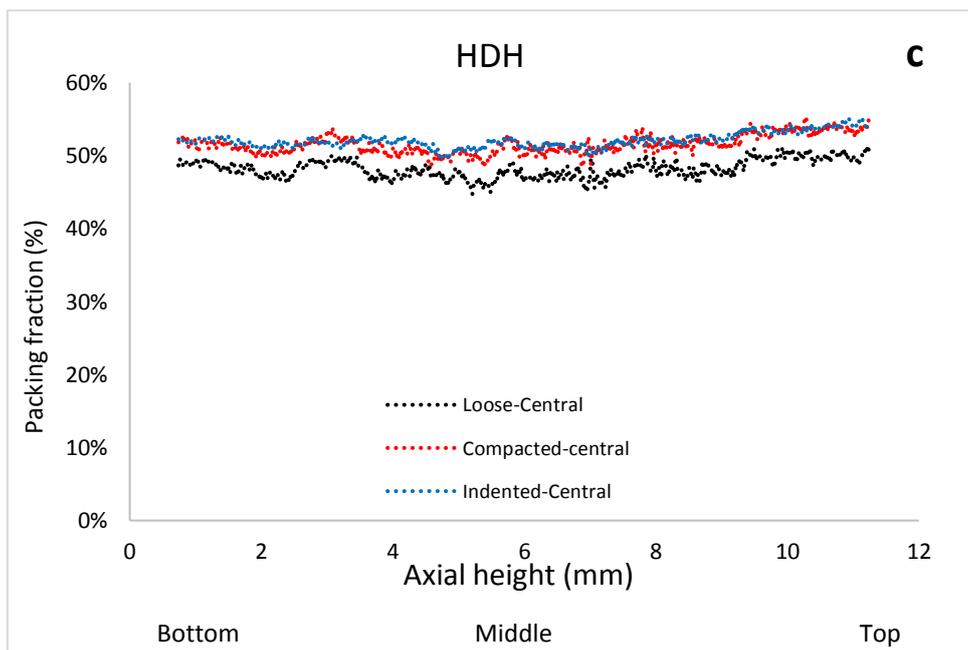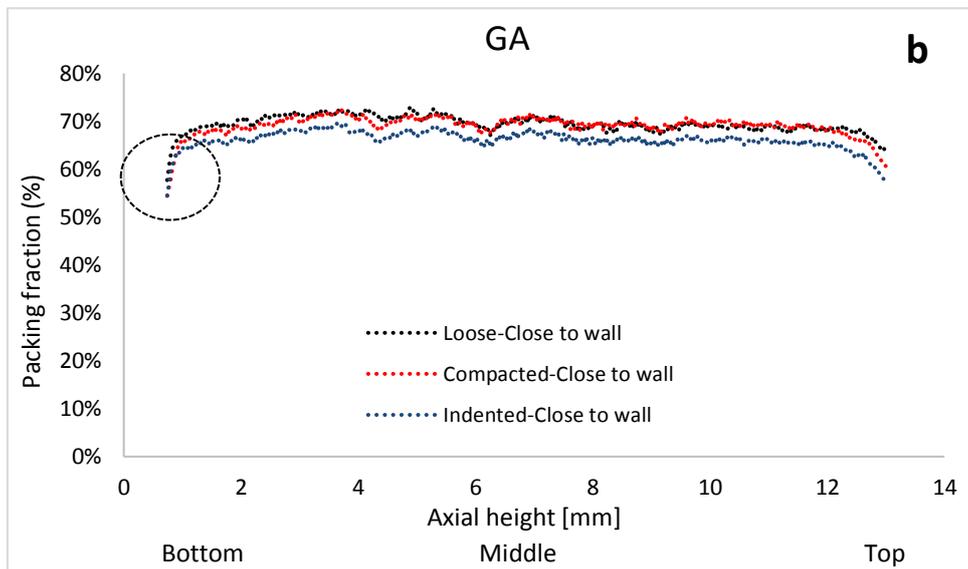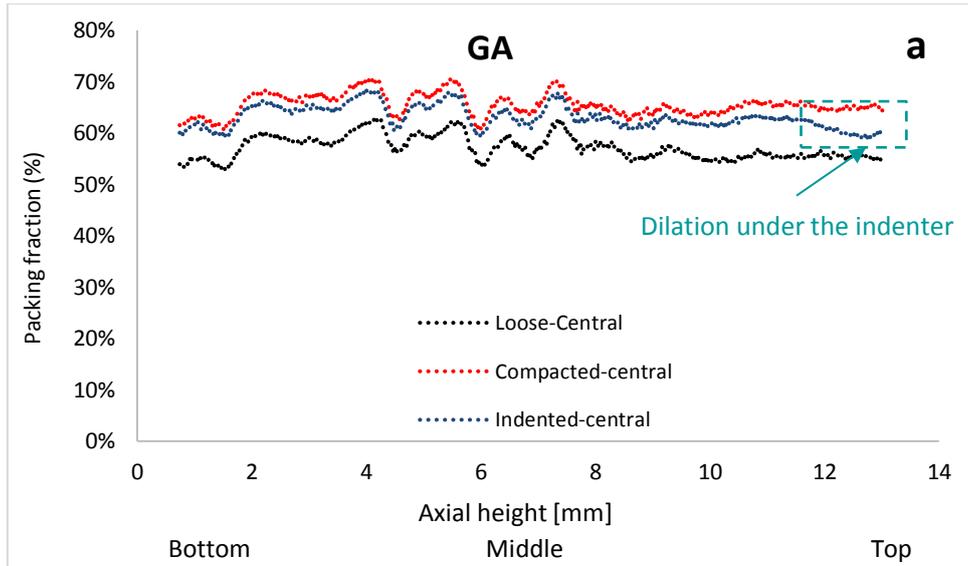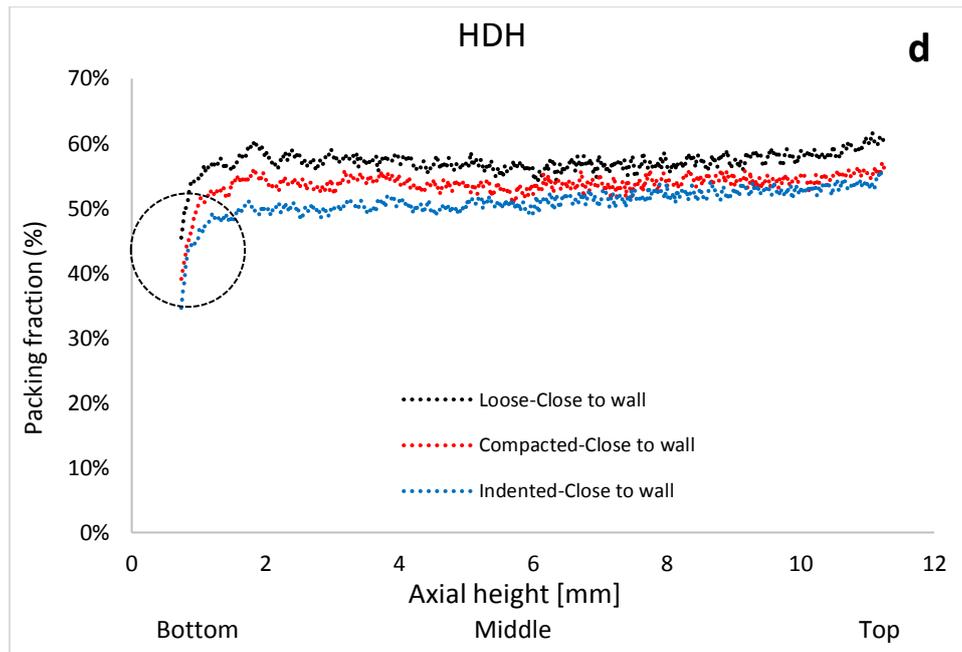
Figure 5. 9 Axial packing fraction for GA powder in (a)central zone, (b) wall section and for HDH powder in (c) central, (d) wall zone at "loose-compacted- indented" stages

The above analyses show that at loose stage, GA powder in the central zone has the same packing fraction as the HDH powder close to the wall zone (ca 57%), indicating that for loose or very low compaction stages, the radial position of indent would significantly influence the powder bed hardness measurement. This is due to the difference between the particle-particle and particle-wall frictions for the two powders investigated in this study. Furthermore, the trend of packing fraction under the indentation zone could be an indication of critical state of the powder compaction for the HDH powders as opposed to GA. This could have significant influence on the value of constraint factor for the calculation of powder yield stress (79, 89) from hardness measurement which is mainly due to the particle re-arrangements under the indentation zone as affected by the particle shapes and coefficient of frictions.

The study in this work demonstrates the different packing behaviours of the two grades of Ti6Al4V which is caused by their different morphologies. This morphology differences would have an influence on the spread layer quality during the AM process which could have impact on the quality of final product. Overall HDH powders have less packing fraction after consolidation compared to GA, which would result in smaller bed hardness. However, irregular particles (HDH) would have less freedom due to the interlocking phenomenon which reduces their individual mobility. Hence, they could tend to have more block movement when they are being indented which could result in smaller or no changes in the packing fraction.

5.4. Conclusion

The purpose of this chapter was to characterise internal visualization of the filling, compaction and ball indentation processes of powders by XMT. in order to develop better understanding of the powder packing behaviour and effect of consolidation pressure and ball indentation on powder bed.

Quantitative analysis of powder packing fraction was carried out both radially (central, inner, outer and wall sections) and axially (top, middle, and bottom sections) through the bed for filling, compaction and ball indentation stages for both samples. The overall results showed that the HDH powder has lower packing fraction than GA due to their shape and surface roughness, however for both samples, there is an increase of the packing fraction of the filling (loose) stage from the central section towards the wall, due to a lower particle-wall CoF than that of particle-particle.

In the central zone, after the compaction stage, the packing density increases for both samples, however, for GA powder after removal of compaction pressure, there could be a degree of bed expansion presumably due to the elastic recovery for the powder bed. During indentation, GA powders also shown slight reduction in their packing fraction just under the indenter due to the dilation of powder to accommodate shear. However, for the indentation stage the HDH powders did not show a dilation under the indenter, suggesting the powders could be under a critically packed state, presumably due their irregular shape.

Chapter 6   Conclusions and Future Works

6.1. Introduction

In this chapter, an overview of the main conclusions of this thesis is given, followed by suggestions for further research in the field, which were inspired from the work carried out in this thesis.

6.2. Conclusions

The overall aim of this PhD study was to experimentally characterise single and bulk powder properties of two samples of Ti6Al4V powders, produced by different production routes, with varying shapes and sizes and to discover the appropriate test method which could predict the flow behaviour with relevance to powder spreading in AM. For this purpose, the powder's physical properties, including particle size distribution, shape, and density were characterised using the XMT and laser diffraction techniques. The shape analysis has revealed that the GA powders have nearly spherical shape while the HDH has rather irregular shape with surface asperities. The analysis of equivalent diameter has shown that there is a slight difference between the volume equivalent and area equivalent sphere diameters for both powders due to the existence of internal pores and presence of concave/hollow particles for GA powders which could adversely affect the quality of final AM products.

As part of this study, the flowability of both samples was characterised using static and dynamic angle of repose, and measurement of powder compressibility using Hausner ratio and Carr index, rotating drum, flowmeter, and FT4 rheometer. Also, the ring shear cell test was used to measure the shear strength of both powders at a different range of consolidation loads (low to high) and some specific details of powder characteristics such as internal angle

of friction, angle of wall friction. The ball indention process was used to determine the unconfined yield stress at low consolidation levels of both powders. All techniques except ball indentation and FT4 indicated that the two powders behave under free to easy flowing categories and GA powder has slightly better flowability compare to HDH powder. The variance between these two powders' flowability is related to the effect of morphology of the particles. However, the difference between the flow behaviour of the two powders is shown to be more significant using the measurements form the FT4 rheometer, i.e. the BFE values of 264.2 and 728.1 mJ for GA and HDH, respectively, indicating that HDH demonstrates greater cohesion and worse flow under low-stress conditions than GA powder. A comparison between different techniques demonstrated the difficulty of measuring powder bulk behaviour such as flowability by using only one technique.

The ball indentation technique is able to measure powder bed hardness (later to infer the unconfined yield stress) for low consolidation stress (<0.5 kPa) which is not achievable by the low shear cell measurement. However, the unconfined yield stress measured by low shear cell results has been used to determine the value of constraint factor (C) for both powders at the lowest possible consolidation stress, i.e.750 Pa. The C value is then assumed to be constant for the range of lower stresses (0-500 PA) used in ball indentation.

Two different procedures of ball indentation have been followed. In the first procedure, the powder was filled using the usual sieve method, suggested by previous researchers. To minimize the effect of the stress history of powder and to achieve exact conditions and reduce the number of affecting variables on the powder bed, in the second procedure the samples were tapped 30 times and then characterised for the hardness measurements. The overall

results show that the hardness of both samples increases linearly with an increase of consolidation pressure indicating that the powder with higher consolidation has a greater resistance to the indentation and flow. The unconfined yield strength results from the ball indentation technique show a notable decrease of both powders' flow at low stresses, categorising them under cohesive regime. The GA powder certainly would not be considered as a cohesive powder based on all measurements except ball indentation which shows relatively high unconfined yield stress (which is often associated with cohesive powders) at low consolidation stress. Therefore, at very low or near zero consolidation stresses the main affecting factor for behaving of powders are the Bo number.

In addition, to further assess the ball indentation technique for free flow powders the time-lapse XMT, and the packing behaviour of powders during the process of filling (loose), consolidation (compacted) and ball indentation (indented) have been studied. Quantitative analysis of powder packing fraction at radial (central, inner, outer, and wall sections) and axial (top, middle, and bottom sections) positions through the bed for the three stages of filling, compaction, and ball indentation, showed that the HDH powder has lower packing fraction than GA due to their shape and surface roughness. However, for both samples, there is an increase of the packing fraction from the central section towards the wall for the filling (loose) stage, due to a lower particle-wall CoF than that of particle-particle. At compaction stage, the packing density increases for both samples, however, GA powder showed that after removal of compaction pressure, there could be a degree of bed expansion presumably due to the elastic recovery for the powder bed. During indentation, GA powders also shown slight reduction in their packing fraction just under the indenter due to the dilation of powder to accommodate shear. However, HDH powders presumed to be under critically packed state

and did not show a dilation under the indenter, suggesting the higher cohesion between powders, presumably due to their irregular shape. It has been observed that for loose or possibly very low compaction stages, the indention position can have significant influence on the value of hardness for both powders, which is mainly due the differences in their particle shapes and coefficient of frictions.

Understanding these phenomena help to address the effect of various morphologies on the powder bed quality, which is the important factor for the quality of the final products. It shows that GA powder with higher flowability has a quantitatively higher packing density compare to HDH powders. The irregular shape of powder HDH leads to a looser rearrangement of particles and lessening the packing density. Furthermore, the correlation between powder flow characteristics and the spreading results shows that spread GA powder has a higher packing density compare to HDH powders.

6.3. Recommended future work

Based on the work carried out in this PhD, a number of recommendations for the advancement of research in the field of powder spreadability in regard to AM process, are made below:

- Full characterisation of different powders with different natures from different feedstocks in order to understand their performance during additive manufacturing processing steps, e.g. delivery and spreading for 3D printing application.

Full characterisation of powder surface properties such as roughness utilising the existing techniques such as surface profiling by atomic force microscopy (AFM), non-contact surface

profiling by optical methods, surface imaging by scanning electron microscopy and nano-indentation.

- XMT could also be employed to obtain the in-situ characterisation of spreading process and powder bed packing fraction. Many key phenomena could be revealing by real-time monitoring of spreading process and in situ observations play a vital role in the development of the bed and blade.

- It would be a great addition to the knowledge in powder flowability for characterise each powder flowability technique to use in-situ XMT to analyse the behaviour of powders inside of each technique.

Reference

1. Attaran, M., 2017. The rise of 3-D printing: The advantages of additive manufacturing over traditional manufacturing. *Business Horizons*, *60*(5), pp.677-688.

2. Pereira, T., Kennedy, J.V. and Potgieter, J., 2019. A comparison of traditional manufacturing vs additive manufacturing, the best method for the job. Procedia Manufacturing, 30, pp.11-18.

3. Spierings, A. B., Voegtlin, M. and Bauer, T., 2016. Powder flowability characterisation methodology for powder-bed-based metal additive manufacturing. Progress in Additive Manufacturing, 1 (1), pp. 9-20.

4. Haeri, S., Wang, Y., Ghita, O. and Sun, J., 2017. Discrete element simulation and experimental study of powder spreading process in additive manufacturing. Powder Technology, 306, pp.45-54.

5. Prescott, J.K. and Barnum, R.A., 2000. On powder flowability. Pharmaceutical Technology, October 2009.

6. Rosas, A.M., 2012. Characerization and parametric study of the flow properties of cohesive powders at temperatures up to 850⬜ C. University of Denmark, DTU.

7. Sutton, A.T., Kriewall, C.S., Leu, M.C. and Newkirk, J.W., 2017. Powder characterisation techniques and effects of powder characteristics on part properties in powder-bed fusion processes. Virtual and physical prototyping, 12(1), pp.3-29.

8. Tong, J., Bowen, C.R., Persson, J. and Plummer, A., 2017. Mechanical properties of titanium-based Ti–6Al–4V alloys manufactured by powder bed additive manufacture. Materials Science and Technology, 33(2), pp.138-148.

9. Geldart, D., Abdullah, E.C., Hassanpour, A., Nwoke, L.C. and Wouters, I.J.C.P., 2006. Characterization of powder flowability using measurement of angle of repose. China Particuology, 4(03n04), pp.104-107.

10. Hausner, H.H., 1981. Powder characteristics and their effect on powder processing. Powder Technology, 30(1), pp.3-8.

11. Peterson, J.E. and Small, W.M., 1994. Evaluation of metal powders using Arnold density meter and Hall flowmeter. Powder metallurgy, 37(1), pp.37-41.

12. Freeman, R., 2007. Measuring the flow properties of consolidated, conditioned and aerated powders—a comparative study using a powder rheometer and a rotational shear cell. Powder Technology, 174(1-2), pp.25-33.

13. Schulze, D., 1996. Measuring powder flowability: a comparison of test methods-part I. Powder and Bulk Engineering, 10, pp.45-61.

14. Krantz, M., Zhang, H. and Zhu, J., 2009. Characterization of powder flow: Static and dynamic testing. Powder Technology, 194(3), pp.239-245.

15. Hassanpour, A. and Ghadiri, M., 2007. Characterisation of flowability of loosely compacted cohesive powders by indentation. Particle & Particle Systems Characterization, 24(2), pp.117-123.

16. Wang, C., Hassanpour, A. and Ghadiri, M., 2008. Characterisation of flowability of cohesive powders by testing small quantities of weak compacts. Particuology, 6(4), pp.282-285.

17. Shunyu Liu, Yung C. Shin, Additive manufacturing of Ti6Al4V alloy: A review, Materials & Design, Volume 164,2019,

18. Geer, S., Bernhardt-Barry, M.L., Garboczi, E.J., Whiting, J. and Donmez, A., 2018. A more efficient method for calibrating discrete element method parameters for

simulations of metallic powder used in additive manufacturing. Granular Matter, 20(4), pp.1-17.

19. Srivatsan, T.S. and Sudarshan, T.S. eds., 2015. Additive manufacturing: innovations, advances, and applications. CRC Press.

20. Ning, F., Cong, W., Qiu, J., Wei, J. and Wang, S., 2015. Additive manufacturing of carbon fiber reinforced thermoplastic composites using fused deposition modeling. Composites Part B: Engineering, 80, pp.369-378.

21. L. E. Murr, E. Martinez, K. N. Amato, S. M. Gaytan, J. Hernandez and D. A. Ramirez. (2012) Fabrication of metal and alloy components by additive manufacturing: examples of 3D materials science Journal of Materials Research and Technology, 1 pp. 42-49.

22. Campbell, I., Diegel, O., Kowen, J. and Wohlers, T., 2018. Wohlers report 2018: 3D printing and additive manufacturing state of the industry: annual worldwide progress report. Wohlers Associates

23. Yi, X., Tan, Z.J., Yu, W.J., Li, J., Li, B.J., Huang, B.Y. and Liao, J., 2016. Three dimensional printing of carbon/carbon composites by selective laser sintering. Carbon, 96, pp.603-607.

24. Zhang J, Song B, Wei Q, Bourell D, Shi Y. A review of selective laser melting of aluminum alloys: Processing, microstructure, property and developing trends. Journal of Materials Science & Technology. 2019 Feb 1;35(2):270-84.

25. Li, P., Warner, D.H., Fatemi, A. and Phan, N., 2016. Critical assessment of the fatigue performance of additively manufactured Ti–6Al–4V and perspective for future research. International Journal of Fatigue, 85, pp.130-143

26. Lewandowski, J.J. and Seifi, M., 2016. Metal additive manufacturing: a review of mechanical properties. Annual review of materials research, 46.

27. Murr, L.E., Gaytan, S.M., Ramirez, D.A., Martinez, E., Hernandez, J., Amato, K.N., Shindo, P.W., Medina, F.R. and Wicker, R.B., 2012. Metal fabrication by additive manufacturing using laser and electron beam melting technologies. Journal of Materials Science & Technology, 28(1), pp.1-14.

28. F. Suska, G. Kjeller, P. Tarnow, E. Hryha, L. Nyborg, A. Snis. (2016) Electron beam melting manufacturing technology for individually manufactured jaw prosthesis: a case report. J. Oral Maxillofac. Surg., 74 pp. 1706.e1-1706.e15

29. Roy, N.K. and Cullinan, M.A., 2015, August. μ-SLS of Metals: Design of the powder spreader, powder bed actuators and optics for the system. In Solid Freeform Fabrication Conference (pp. 134-155).

30. Berretta, S., Ghita, O. and Evans, K.E., 2014. Morphology of polymeric powders in Laser Sintering (LS): From Polyamide to new PEEK powders. European Polymer Journal, 59, pp.218-229.

31. Ziegelmeier, S., Christou, P., Wöllecke, F., Tuck, C., Goodridge, R., Hague, R., Krampe, E. and Wintermantel, E., 2015. An experimental study into the effects of bulk and flow behaviour of laser sintering polymer powders on resulting part properties. Journal of Materials Processing Technology, 215, pp.239-250.

32. Shaheen, M.Y., Thornton, A.R., Luding, S. and Weinhart, T., 2019. Discrete particle simulation of the spreading process in additive manufacturing. In 8th International Conference on Discrete Element Methods, DEM 2019: MS-03: Open-source development (pp. 263-263). University of Twente.

33. Cicala, G., Latteri, A., Del Curto, B., Lo Russo, A., Recca, G. and Farè, S., 2017. Engineering thermoplastics for additive manufacturing: A critical perspective with experimental evidence to support functional applications. Journal of applied biomaterials & functional materials, 15(1), pp.10-18.

34. Deckers, J., Vleugels, J. and Kruth, J.P., 2014. Additive manufacturing of ceramics: a review. Journal of Ceramic Science and Technology, 5(4), pp.245-260.

35. Hao, Y.L., Li, S.J. and Yang, R., 2016. Biomedical titanium alloys and their additive manufacturing. Rare Metals, 35(9), pp.661-671.

36. McCracken, C.G., Motchenbacher, C. and Barbis, D.P., 2010. REVIEW OF TITANIUM-POWDER-PRODUCTION METHODS. International journal of powder metallurgy, 46(5).

37. Kaivosoja, E., Tiainen, V.M., Takakubo, Y., Rajchel, B., Sobiecki, J., Konttinen, Y.T. and Takagi, M., 2013. Materials used for hip and knee implants. In Wear of Orthopaedic Implants and Artificial Joints (pp. 178-218). Woodhead Publishing.

38. Liu, Z., Huang, C., Gao, C., Liu, R., Chen, J. and Xiao, Z., 2019. Characterization of Ti6Al4V powders produced by different methods for selective electron beam melting. Journal of Mining and Metallurgy B: Metallurgy, 55(1), pp.121-128.

39. Chen, G., Zhao, S.Y., Tan, P., Wang, J., Xiang, C.S. and Tang, H.P., 2018. A comparative study of Ti-6Al-4V powders for additive manufacturing by gas atomization, plasma rotating electrode process and plasma atomization. Powder technology, 333, pp.38-46.

40. Sun, P., Fang, Z.Z., Zhang, Y. and Xia, Y., 2017. Review of the methods for production of spherical Ti and Ti alloy powder. Jom, 69(10), pp.1853-1860.

41. Narra, S.P., Wu, Z., Patel, R., Capone, J., Paliwal, M., Beuth, J. and Rollett, A., 2020. Use of Non-Spherical Hydride-Dehydride (HDH) Powder in Powder Bed Fusion Additive Manufacturing. Additive Manufacturing, 34, p.101188.

42. Ciowiki (2021) Additive Manufacturing (AM). Available at: https://cio-wiki.org/wiki/Additive_Manufacturing_(AM)#google_vignette (Accessed: 14 April 2021)

43. Sun, Y.Y., Gulizia, S., Oh, C.H., Doblin, C., Yang, Y.F. and Qian, M., 2015. Manipulation and characterization of a novel titanium powder precursor for additive manufacturing applications. Jom, 67(3), pp.564-572.

44. Ma, Y., Evans, T.M., Philips, N. and Cunningham, N., 2020. Numerical simulation of the effect of fine fraction on the flowability of powders in additive manufacturing. Powder Technology, 360, pp.608-621.

45. Chen, H., Chen, Y., Liu, Y., Wei, Q., Shi, Y. and Yan, W., 2020. Packing quality of powder layer during counter-rolling-type powder spreading process in additive manufacturing. International Journal of Machine Tools and Manufacture, p.103553.

46. Hausner, H.H., 1967. Friction conditions in a mass of metal powder. Polytechnic Inst. of Brooklyn. Univ. of California, Los Angeles.

47. Carr, R.L., 1965. Evaluating flow properties of solids. Chem. Eng., 18, pp.163-168.

48. Podczeck, F. (2012). Method of the practical determination of the mechanical strength of tablets from empiricism to science. Int J Pharm, 436 (1-2), pp. 214-232

49. Emery, E.M., 2008. Flow properties of selected pharmaceutical powders (Doctoral dissertation).

50. Traina, K., Cloots, R., Bontempi, S., Lumay, G., Vandewalle, N. and Boschini, F., 2013. Flow abilities of powders and granular materials evidenced from dynamical tap density

51. Leadbeater, C.J., Northcott, L. and Hargreaves, F., 1968. Some properties of engineering iron powders. In Iron Powder Metallurgy (pp. 72-121). Springer, Boston, MA.

52. Abdullah, E. C., & Geldart, D., 1999. The use of bulk density measurements as flowability indicators. Powder Technology, 102(2), pp. 151-165.

53. Zocca, A., Gomes, C.M., Mühler, T. and Günster, J., 2014. Powder-bed stabilization for powder-based additive manufacturing. Advances in Mechanical Engineering, 6, p.491581.

54. Tang, H.P., Qian, M., Liu, N., Zhang, X.Z., Yang, G.Y. and Wang, J., 2015. Effect of powder reuse times on additive manufacturing of Ti-6Al-4V by selective electron beam melting. Jom, 67(3), pp.555-563.

55. Yang, A., Sliva, A., Banerjee, R.N., Dave, N. and Pfeffer, R., 2005. Dry particle coating for improving the flowability of cohesive powders. Powder Technology, 158, pp.21–33.

56. Schmid M, Amado F, Levy G, Wegener K (2013) Flowability of powders for selective laser sintering (SLS) investigated by round Robin test. In: High value manufacturing: advanced research in virtual and rapid prototyping, pp 95–99

57. Geldart, D., Abdullah, E.C., Hassanpour, A., Nwoke, L.C. and Wouters, I.J.C.P., 2006. Characterization of powder flowability using measurement of angle of repose. China Particuology, 4(03n04), pp.104-107.

58. Schulze D. Flow properties of powders and bulk solids. 2006–2011.

59. Xu, W., Xiao, S., Lu, X., Chen, G., Liu, C. and Qu, X., 2019. Fabrication of commercial pure Ti by selective laser melting using hydride-dehydride titanium powders treated by ball milling. Journal of Materials Science & Technology, 35(2), pp.322-327.

60. Wu, C.Y. and Cocks, A.C.F., 2004. Flow behaviour of powders during die filling. Powder Metallurgy, 47(2), pp.127-136.

61. Jiang, Y., Matsusaka, S., Masuda, H. and Qian, Y., 2009. Development of measurement system for powder flowability based on vibrating capillary method. Powder Technology, 188(3), pp.242-247.

62. Mellin, P., Lyckfeldt, O., Harlin, P., Brodin, H., Blom, H. and Strondl, A., 2017. Evaluating flowability of additive manufacturing powders, using the Gustavsson flow meter. Metal powder report, 72(5), pp.322-326.

63. Sun, Y., Aindow, M. and Hebert, R.J., 2018. Comparison of virgin Ti-6Al-4V powders for additive manufacturing. Additive Manufacturing, 21, pp.544-555.

64. Kaye, B.H., Gratton‐Liimatainen, J. and Faddis, N., 1995. Studying the avalanching behaviour of a powder in a rotating disc. Particle & particle systems characterization, 12(5), pp.232-236.

65. Rastogi, S. and Klingzing, G.E., 1994. Characterizing the rheology of powders by studying dynamic avalanching of the powder. Particle & particle systems characterization, 11(6), pp.453-456.

66. Liao, C.C. and Tsai, C.C., 2020. Behavior of density-induced segregation with multi-density granular materials in a thin rotating drum. Granular Matter, 22(3), pp.1-9.

67. Gu, H., Gong, H., Dilip, J.J.S., Pal, D., Hicks, A., Doak, H. and Stucker, B., 2014. Effects of Powder Variation on the Microstructure and Tensile Strength of Ti6Al4V Parts

Fabricated by Selective Laser Melting. Presented in 25th Annual International Solid Freeform Fabrication Symposium. pp. 470-483

68. Zafar, U., Hare, C., Calvert, G., Ghadiri, M., Girimonte, R., Formisani, B., Quintanilla, M.A.S. and Valverde, J.M. 2015. Comparison of cohesive powder flowability measured by Schulze Shear Cell, Raining Bed Method, Sevilla Powder Tester and new Ball Indentation Method. Powder Technology, 286, pp. 807-816.

69. Schulze, D. (2007), Powders and Bulk Solids: Behaviour, Characterization, Storage and Flow, Springer, 1st Edition, Germany.

70. Wei, W.H., Wang, L.Z., Chen, T., Duan, X.M. and Li, W., 2017. Study on the flow properties of Ti-6Al-4V powders prepared by radio-frequency plasma spheroidization. Advanced Powder Technology, 28(9), pp.2431-2437.

71. Freeman, R., 2007. Measuring the flow properties of consolidated, conditioned and aerated powders—a comparative study using a powder rheometer and a rotational shear cell. Powder Technology, 174(1-2), pp.25-33.

72. Freeman, R. and Fu, X., 2008. Characterisation of powder bulk, dynamic flow and shear properties in relation to die filling. Powder Metallurgy, 51(3), pp.196-201.

73. Dihoru, L.V., Smith, L.N. and German R.M. 2003. Experimental analysis and neural network modeling of the rheological behaviour of powder injection moulding feedstocks formed with bimodal powder mixtures. Powder Metallurgy, 43(1), pp. 31-36.

74. Søgaard, S., Bryder, M., Allesø, M. and Rantanen, J., 2012, April. Characterization of powder properties using a powder rheometer. In Proceedings of Electronic Conference on Pharmaceutical Sciences (Vol. 2).

75. Clayton, J., 2014. Optimising metal powders for additive manufacturing. Metal Powder Report, 69(5), pp.14-17.

76. A Hassanpour, M Ghadiri. (2007). Characterisation of flowability of loosely compacted cohesive powders by indentation. Particle & Particle Systems Characterization 24 (2), 117-123

77. Atkins, A.G. and Tabor, D., 1965. Plastic indentation in metals with cones. *Journal of the Mechanics and Physics of Solids*, *13*(3), pp.149-164.

78. Wang, C., Hassanpour, A. and Ghadiri, M., 2008. Characterisation of flowability of cohesive powders by testing small quantities of weak compacts. Particuology, 6(4), pp.282-285.

79. U. Zafar, C Hare, A. Hassanpour, M. Ghadiri. (2017). Ball indentation on powder beds for assessing powder flowability: Analysis of operation window. Powder Technology 310, 300-306

80. Du Plessis, A., Yadroitsev, I., Yadroitsava, I. and Le Roux, S.G., 2018. X-ray microcomputed tomography in additive manufacturing: a review of the current technology and applications. 3D Printing and Additive Manufacturing, 5(3), pp.227-247.

81. Heim, K., Bernier, F., Pelletier, R. and Lefebvre, L.P., 2016. High resolution pore size analysis in metallic powders by X-ray tomography. Case Studies in Nondestructive Testing and Evaluation, 6, pp.45-52.

82. Bernier, F., Tahara, R. and Gendron, M., 2018. Additive manufacturing powder feedstock characterization using X-ray tomography. Metal Powder Report, 73(3), pp.158-162.

83. Cunningham, R., Narra, S.P., Montgomery, C., Beuth, J. and Rollett, A.D., 2017. Synchrotron-based X-ray microtomography characterization of the effect of processing variables on porosity formation in laser power-bed additive manufacturing of Ti-6Al-4V. Jom, 69(3), pp.479-484.

84. Chawanji, A.S., Baldwin, A.J., Brisson, G. and Webster, E., 2012. Use of X‑ray micro tomography to study the microstructure of loose‑packed and compacted milk powders. Journal of microscopy, 248(1), pp.49-57.

85. McDonald, S.A. and Withers. P.J., 2013. Effect of punch shape on granular flow and rearrangement during powder compaction studied by X-ray microtomography. 7th World Congress on Industrial Process Tomography, WCIPT7, 2-5 September 2013, Krakow, Poland

86. McDonald, S.A., Schneider, L.C.R., Cocks, A.C.F. and Withers, P.J., 2006. Particle movement during the deep penetration of a granular material studied by X-ray microtomography. Scripta materialia, 54(2), pp.191-196.

87. McDonald, S.A., Motazedian, F., Cocks, A.C.F. and Withers, P.J., 2009. Shear cracking in an Al powder compact studied by X-ray microtomography. Materials Science and Engineering: A, 508(1-2), pp.64-70.

88. Stavrou, A.G., 2020. Assessing powder flowability at low consolidation stresses (Doctoral dissertation, University of Surrey).

89. Pasha, M., Hare, C., Hassanpour, A. and Ghadiri, M., 2015. Numerical analysis of strain rate sensitivity in ball indentation on cohesive powder Beds. Chemical Engineering Science, 123, pp.92-98.

90. Schubert, H., 1984. Capillary forces-modeling and application in particulate technology. Powder Technology, 37(1), pp.105-116.

91. Castellanos, A., 2005. The relationship between attractive interparticle forces and bulk behaviour in dry and uncharged fine powders. Advances in Physics, 54(4), pp.263-376.

92. Buysman, P.J. and Peersman, G.A.L., 1967. Stability of ceilings in a fluidized bed. In Proceedings of the International Symposium on Fluidization. Netherlands Univeristy Press Amsterdam.

93. Seville, J.P.K. and Clift, R., 1984. The effect of thin liquid layers on fluidisation characteristics. Powder Technology, 37(1), pp.117-129.

94. Formisani, B., Girimonte, R. and Pataro, G., 2002. The influence of operating temperature on the dense phase properties of bubbling fluidized beds of solids. Powder Technology, 125(1), pp.28-38.

95. Johanson, K., 2014. Personal Communication. Material Flow Equipment, LLC, 7010 NW 23rd Way, Suite A, Gainesville, FL 32653 USA.

96. Tardos, G.I., McNamara, S. and Talu, I., 2003. Slow and intermediate flow of a frictional bulk powder in the Couette geometry. Powder Technol., 131, pp. 23–39.

97. Vock, S., Klöden, B., Kirchner, A., Weißgärber, T. and Kieback, B., 2019. Powders for powder bed fusion: a review. Progress in Additive Manufacturing, pp.1-15.

98. W. Gao, Y. Zhang, D. Ramanujan, K. Ramani, Y. Chen and C.B. Williams. (2015) The status, challenges, and future of additive manufacturing in engineering. Comput. Aided Des., 69, pp. 65-89

99. A. W. Jenike, (1967) Powder Technol. 1, 237–244.

100. W.A. Gray, (1972) Proc. 1st Int. Conf on the Compaction and the Consolidation of Particulate Matter, Brighton, UK, pp.99-105.

101. Packing of fine powders subjected to tapping A.B. Yu School of Materials Science and Engineering, The Universiry of New South Wales, PO Box I, Kensington, NSW 2033

(Australia) J.S. Hall CSIRO Division of Mineral and Process Engineering, PO Box 312, (Received May 27, 1993; in revised form September 20, 1993)

102. Bao, N., Shen, L., Feng, X., Lu, X. and Yanagisawa, K., 2004. Shape and size characterization of potassium titanate fibers by image analysis. Journal of materials science, 39(2), pp.469-476.

103. Fu, X., Dutt, M., Bentham, A.C., Hancock, B.C., Cameron, R.E. and Elliott, J.A., 2006. Investigation of particle packing in model pharmaceutical powders using X-ray.

104. Hou, H. and Sun, C.C., 2008. Quantifying effects of particulate properties on powder flow properties using a ring shear tester. Journal of pharmaceutical sciences, 97(9), pp.4030-4039.

105. Bumiller, M., Carson, J. and Prescott, J., 2002, July. A preliminary investigation concerning the effect of particle shape on a powder's flow properties. In World congress on particle technology (Vol. 4, pp. 21-25). Sydney Australia.

106. Podczeck, F. and Mia, Y., 1996. The influence of particle size and shape on the angle of internal friction and the flow factor of unlubricated and lubricated powders. International Journal of Pharmaceutics, 144(2), pp.187-194.

107. Yu, W., Muteki, K., Zhang, L. and Kim, G., 2011. Prediction of bulk powder flow performance using comprehensive particle size and particle shape distributions. Journal of pharmaceutical sciences, 100(1), pp.284-293.

108. Sofou, A., Evangelopoulos, G. and Maragos, P., 2005. Soil image segmentation and texture analysis: a computer vision approach. IEEE Geoscience and Remote Sensing Letters, 2(4), pp.394-398.

109. Veta, M., Huisman, A., Viergever, M.A., van Diest, P.J. and Pluim, J.P., 2011, March. Marker-controlled watershed segmentation of nuclei in H&E stained breast cancer

biopsy images. In 2011 IEEE international symposium on biomedical imaging: from nano to macro (pp. 618-621). IEEE.

110. Wang, Y., Lin, C.L. and Miller, J.D., 2016. 3D image segmentation for analysis of multisize particles in a packed particle bed. Powder Technology, 301, pp.160-168.

111. Wang, Y., Lin, C.L. and Miller, J.D., 2015. Improved 3D image segmentation for X-ray tomographic analysis of packed particle beds. Minerals Engineering, 83, pp.185-191.

112. Lin, C.L. and Miller, J.D., 2010. Advances in X-ray computed tomography (CT) for improved coal washability analysis. In International Coal Preparation Congress, 2010 Conference Proceedings (pp. 888-897). Society for Mining, Metallurgy & Exploration Inc., Englewood, CO.

113. Shi, Y. and Yan, W.M., 2015. Segmentation of irregular porous particles of various sizes from X-ray microfocus computer tomography images using a novel adaptive watershed approach. Géotechnique Letters, 5(4), pp.299-305.

114. Fonseca, J., Sim, W.W., Shire, T. and O'sullivan, C., 2014. Microstructural analysis of sands with varying degrees of internal stability. Géotechnique, 64(5), pp.405-411.

115. Lin, C.L. and Miller, J.D., 2005. 3D characterization and analysis of particle shape using X-ray microtomography (XMT). Powder Technology, 154(1), pp.61-69.

116. Merkus, H.G., 2009. Particle size measurements: fundamentals, practice, quality (Vol. 17). Springer Science & Business Media.

117. Liu, Z., Huang, C., Gao, C., Liu, R., Chen, J. and Xiao, Z., 2019. Characterization of Ti6Al4V powders produced by different methods for selective electron beam melting. Journal of Mining and Metallurgy, Section B: Metallurgy, 55(1), pp.121-128.

118. Cunningham, R., Narra, S.P., Montgomery, C., Beuth, J. and Rollett, A.D., 2017. Synchrotron-based X-ray microtomography characterization of the effect of

processing variables on porosity formation in laser power-bed additive manufacturing of Ti-6Al-4V. Jom, 69(3), pp.479-484.

119. McGlinchey, D., 2009. Characterisation of bulk solids. John Wiley & Sons.

120. Zakhvatayeva, A., Hare, C. and Wu, C.Y., 2019. Suction filling of pharmaceutical powders. Powder Technology, 355, pp.438-448.

121. Chatham, C.A., Long, T.E. and Williams, C.B., 2019. A review of the process physics and material screening methods for polymer powder bed fusion additive manufacturing. *Progress in Polymer Science*, *93*, pp.68-95.

122. Drummer, Dietmar, Martha Medina-Hernández, Maximilian Drexler, and Katrin Wudy. "Polymer powder production for laser melting through immiscible blends." *Procedia engineering* 102 (2015): 1918-1925.

123. Talebi, F., 2021. Characterisation of spreadability behaviour of Ti6Al4V powders for Additive Manufacturing (Master dissertation, University of Leeds (School of Chemical and Process Engineering)).

124. Kak, A.C. and Slaney, M., 2001. Principles of computerized tomographic imaging. Society for Industrial and Applied Mathematics.

125. Gray, W.A., 1968. Packing of solid particles.

126. York, P., 1978. Particle slippage and rearrangement during compression of pharmaceutical powders. Journal of Pharmacy and Pharmacology, 30(1), pp.6-10.

127. Michrafy, A., Dodds, J.A. and Kadiri, M.S., 2004. Wall friction in the compaction of pharmaceutical powders: measurement and effect on the density distribution. Powder Technology, 148(1), pp.53-55.

128. He, Y., Evans, T.J., Yu, A.B. and Yang, R.Y., 2017. DEM investigation of the role of friction in mechanical response of powder compact. Powder Technology, 319, pp.183-190.

129. Alizadeh, M., Hassanpour, A., Pasha, M., Ghadiri, M. and Bayly, A., 2017. The effect of particle shape on predicted segregation in binary powder mixtures. Powder Technology, 319, pp.313-322.

130. Armstrong, N.A. and Haines-Nutt, R.F., 1974. Elastic recovery and surface area changes in compacted powder systems. Powder Technology, 9(5-6), pp.287-290.

131. Berggren, J., Frenning, G. and Alderborn, G., 2004. Compression behaviour and tablet-forming ability of spray-dried amorphous composite particles. European journal of pharmaceutical sciences, 22(2-3), pp.191-200.

132. Ghadiri, M., Pasha, M., Nan, W., Hare, C., Vivacqua, V., Zafar, U., Nezamabadi, S., Lopez, A., Pasha, M. and Nadimi, S., 2020. Cohesive powder flow: Trends and challenges in characterisation and analysis. *KONA Powder and Particle Journal*, *37*, pp.3-18.

133. Nadimi, S. and Fonseca, J., 2019. Image based simulation of one-dimensional compression tests on carbonate sand. *Meccanica*, *54*(4), pp.697-706.

134. Angelidakis, V., Nadimi, S. and Utili, S., 2021. SHape Analyser for Particle Engineering (SHAPE): Seamless characterisation and simplification of particle morphology from imaging data. *Computer Physics Communications*, *265*, p.107983.

135. Yan, Y., Chibowski, E. and Szcześ, A., 2017. Surface properties of Ti-6Al-4V alloy part I: Surface roughness and apparent surface free energy. *Materials Science and Engineering: C*, *70*, pp.207-215.

Supplementary data
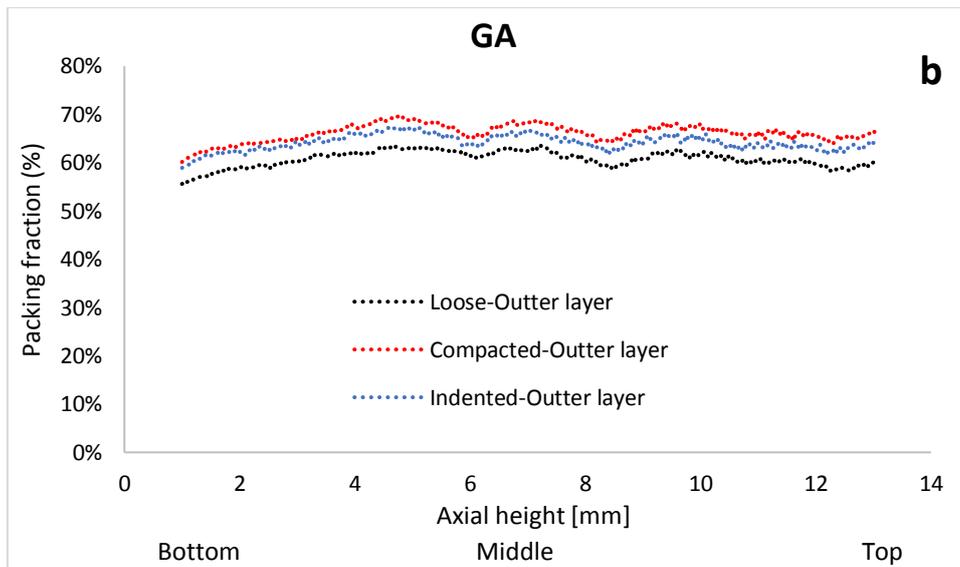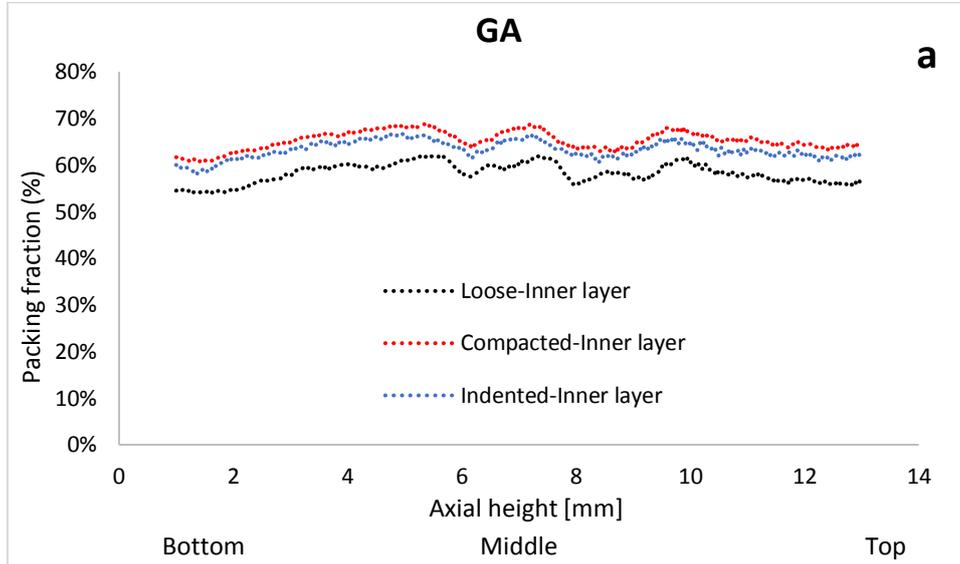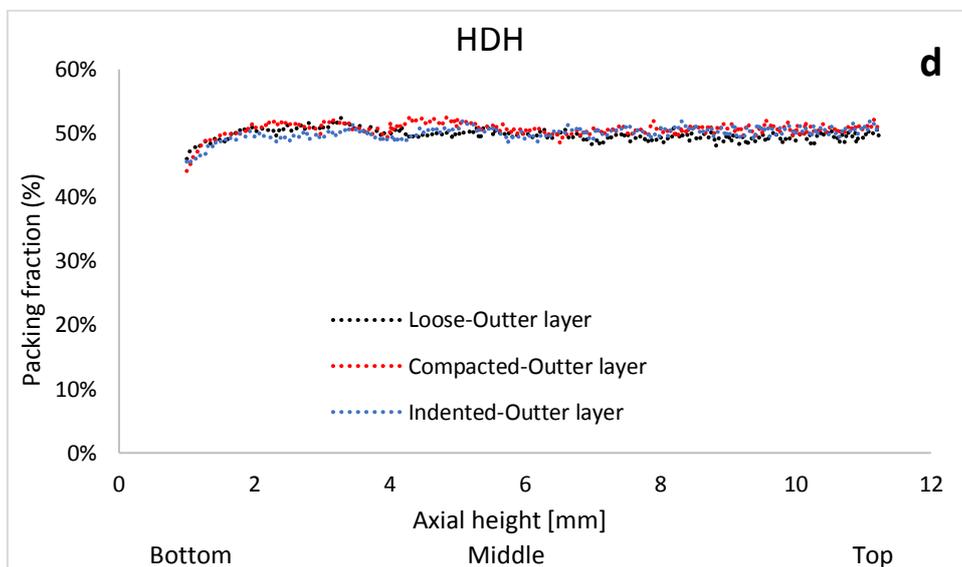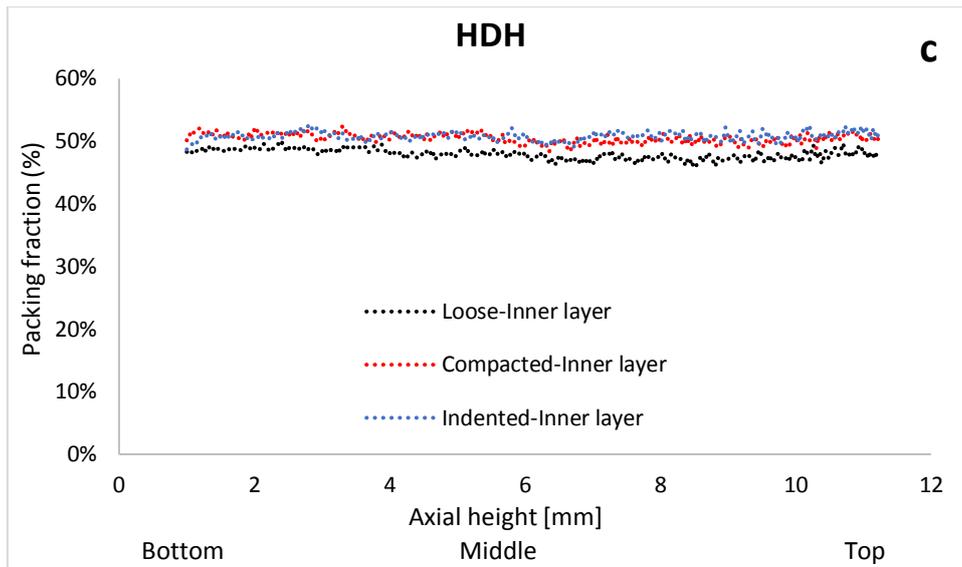
Axial packing fraction for GA powder in (a) inner layer, (b) outer layer and for HDH powder in (c) inner layer, (d) outer layer at "loose-compacted- indented" stages